A HYBRID SEGMENTATION APPROACH USED IN THE COMPUTER DIAGNOSTIC SYSTEM FOR MALIGNANT MELANOMA

By

SUYI SHAO

A DISSERTATION PRESENTED TO THE GRADUATE SCHOOL
OF THE UNIVERSITY OF FLORIDA IN PARTIAL FULFILLMENT
OF THE REQUIREMENTS FOR THE DEGREE OF
DOCTOR OF PHILOSOPHY

UNIVERSITY OF FLORIDA

1994

ACKNOWLEDGMENTS

I would like to express my sincere gratitude to my advisor Dr. John Staudhammer and my supervisor Dr. Ralph R. Grams for their guidance, supervision, and encouragement throughout the preparation of the dissertation. Thanks are also due to Dr. Stanley Y. Su, Dr. Antonio A. Arroyo and Dr. Fazil T. Najafi for their valuable comments and constructive suggestions during the review of the dissertation.

I gratefully acknowledge Dr. Ron White and the technical staff in NASA Life Science for their support and appreciate the continuous long-term support of NASA.

I also wish to thank my parents, my husband and my son for their constant love, support and encouragement.

TABLE OF CONTENTS

Abstract of Dissertation Presented to the Graduate School of
the University of Florida in Partial Fulfillment of the
Requirements for the Degree of Doctor of Philosophy

A HYBRID SEGMENTATION APPROACH USED IN THE COMPUTER DIAGNOSTIC SYSTEM FOR MALIGNANT MELANOMA

By

SUYI SHAO

April 1994

Chairman: Dr. John Staudhammer
Major Department: Electrical Engineering

The objective of this study is to develop a hybrid segmentation approach used in the computer diagnostic system for malignant melanoma. The approach has three stages: (1) PEDBOR; (2) LVDSO quantization; (3) mapping.

In Stage I, a new algorithm, called Pixel-Feature-Controlling Edge Detection Based On Regularization (PEDBOR), is used to remove noise and detect edges simultaneously. It is based on the regularization model, but has several critical improvements. The improvements are: (1) simple optimization method, which allows employing additional knowledge about the physical nature of edges to control the regularization procedure; (2) a data driven threshold function, which avoids the difficulty of setting a threshold; (3) classification of pixels based on both magnitude and orientation of the image gradient; and (4) new line process functions set for different types of pixels based on desired line process function properties, which makes the whole regularization

adaptively controlled by pixel features. These empower the PEDBOR algorithm to operate without setting parameters and result in a well-posed and well-conditioned process that is robust to noise. By using PEDBOR in Stage I, both noise removed images and edge images with high quality can be obtained. They provide good references for Stage II and Stage III.

In Stage II, a quantization method using iterative largest-variance-direction-split-optimization (LVDSO) in the histogram domain of the color space is applied to the noise removed image. It is fast. In the quantization, an oversegmenting parameter is used to avoid the difficulty of setting an exact parameter and to resolve the problem of inconsistencies.

Stage III is a mapping procedure. It uses the edge image from Stage I as the reference of true regions, and uses the segmented image from Stage II as the reference of true edges to remove false edges and false regions.

Experimental results indicate that the final segmentation images have high quality, that is, they are uniform, compact, dissimilar and consistent, and have accurate and continuous boundaries.

CHAPTER 1
INTRODUCTION

1.1 Motivation

Malignant melanoma is a common and deadly dermatologic disease. Based on statistics released by the American Cancer Society in 1991 [Fri 91], malignant melanoma is the eighth most frequently diagnosed cancer (See Fig. 1-1). In that year, there were 30,000 new cases of malignant melanoma and 6500 deaths from the disease. Figs. 1-2 and 1-3 give two statistics. The first one shows the lifetime risk for an individual American in different years. From this we can see that currently among 105 new babies, one will develop malignant melanoma. The second figure shows the incidence rate and death rate of malignant melanoma in different years. The curve tells us that the incidence rate is increasing exponentially and the death rate is climbing linearly. Although the death rate has also continued to increase, survival percentage has doubled from 40% in 1940s to 80% in 1980s. The increase in survival is entirely attributed to early diagnosis. Therefore an early and correct diagnosis is very important. To establish an early diagnosis, many visual features of malignant melanoma, such as color, size, border, shape, elevation, surface characteristics of the surrounding skin, and the evolution history of these features, need to be analyzed. Fig. 1-4 shows two pictures of a malignant melanoma. The left one is the initial phase picture, and right one corresponds to the tumor phase. Fig. 1.5 indicates the typical evolution of a melanoma. It diagrams melanoma's features: shapes, sizes, and color distributions, in the different phases. These features, however, are often poorly defined and lack consistency in feature identification; they are not reliably identified by different observers, even by experienced dermatologists. To increase the consistency of the

diagnosis and to provide a diagnostic tool for many users so that they could evaluate their skin lesions conveniently and consistently, a computer diagnostic system is needed.

The diagnostic system is an image-analysis-based knowledge base system working under PC Windows environment. Fig. 1-6 shows the functional system diagram of the system. Its information sources are color pictures from scanners or cameras. The system first isolates disease lesions by using an image segmentation technique. Based on the segmentation results, a group of high level analyses is carried out to extract the visual features of the lesion. Then these features are classified into conceptual feature patterns by the pattern analyzer. Finally, the feature pattern triggers corresponding rules in the rule base to make a clinical decision.

In such a system, image segmentation is the most important step. High quality segmentation results will better define visual features of pictures, thus providing a complete and consistent model for any further analysis. By using an ensemble of features, one can obtain higher levels of confidence than the inherent accuracy of any one feature. Thus, we can increase the confidence in classification of images which possibly contain malignant melanoma. High quality segmentation should result in uniformity, compactness, dissimilarity regions, as well as accurate and continuous boundaries from noisy images. Automatic image analysis for the detection of malignant melanoma depends to a large extent on the approach for segmenting suspect lesion regions.

The image segmentation in the system is also the most difficult step because (1) many control parameters need to be determined and it is impossible to choose a set of parameters that are suitable for all areas of the image; (2) the control parameters interact in complex ways and are difficult to model mathematically; (3) the variations of skin lesion images cause the parameters and computations of segmentation quality to change for every image, and (4) various types of noise introduce various kinds of unpredictable false elements into the images. At present, no general methods have been found that perform adequately across the diverse types of imagery encountered in suspected

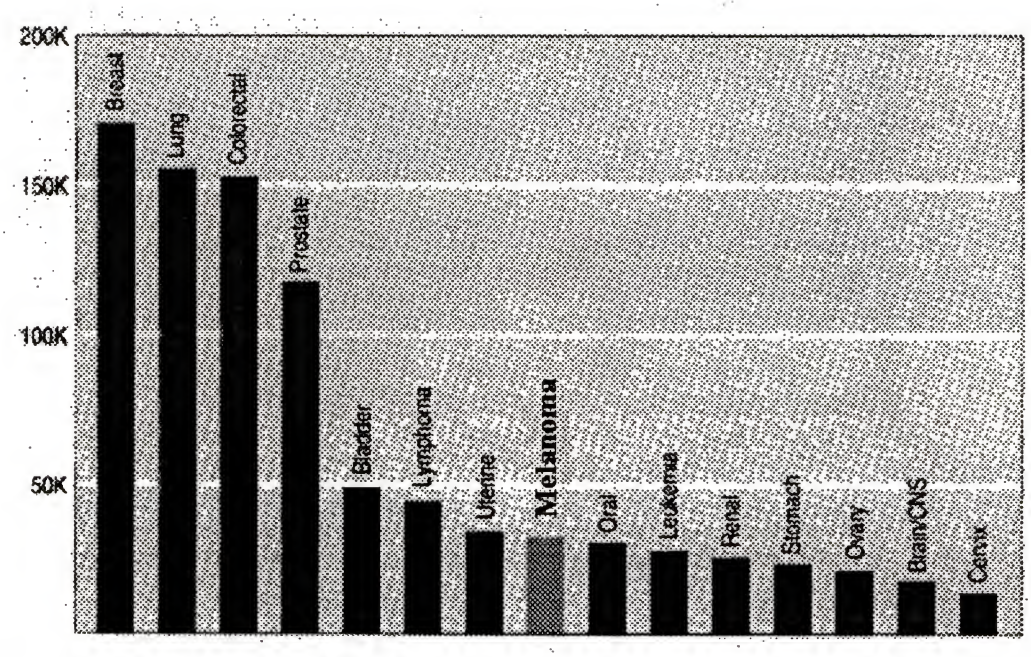

Fig. 1-1 Diagnosed Cancer Frequency Curve in U. S. A. in 1991

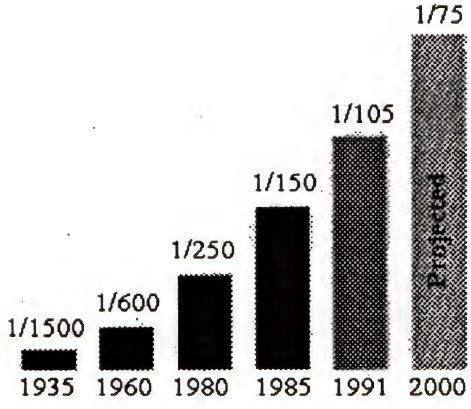

Fig. 1-2 The Lifetime Risk for an Individual American to Develop Malignant Melanoma

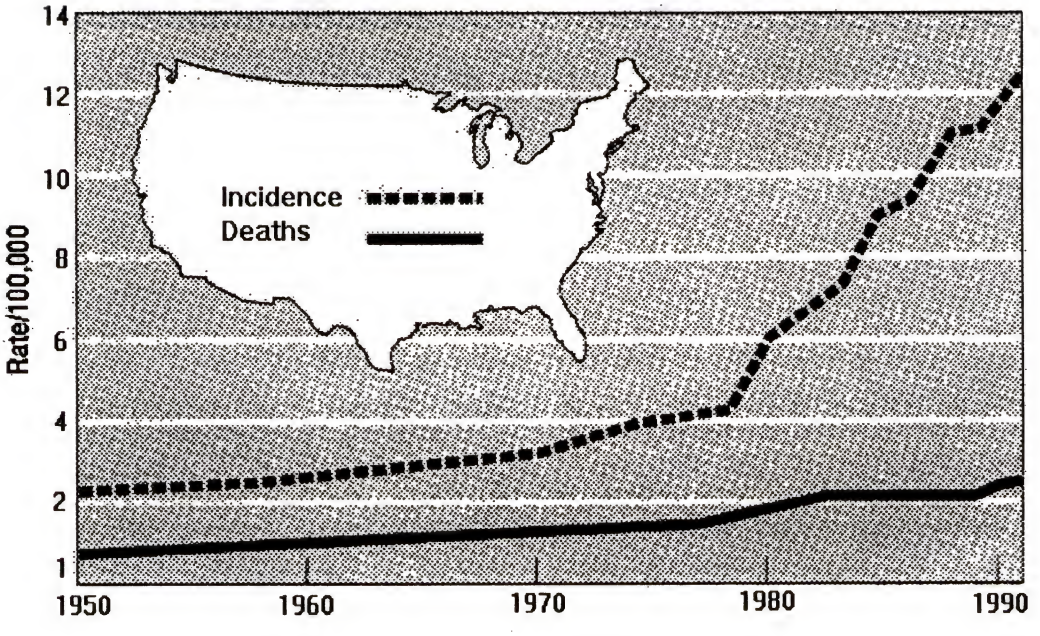

Fig. 1-3 Death Rate and Incidence Rate of Malignant Melanoma

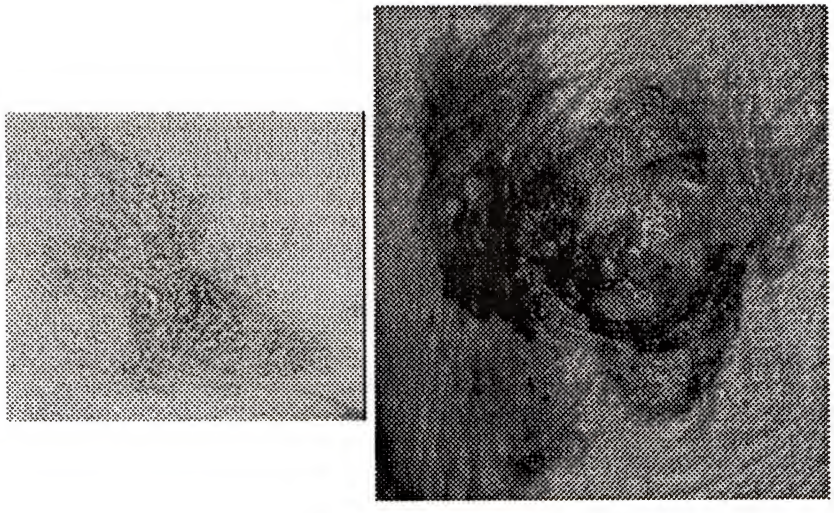

Fig. 1-4 Pictures of a Malignant Melanoma
The left one shows the initial phase.
The right one shows tumor phase.

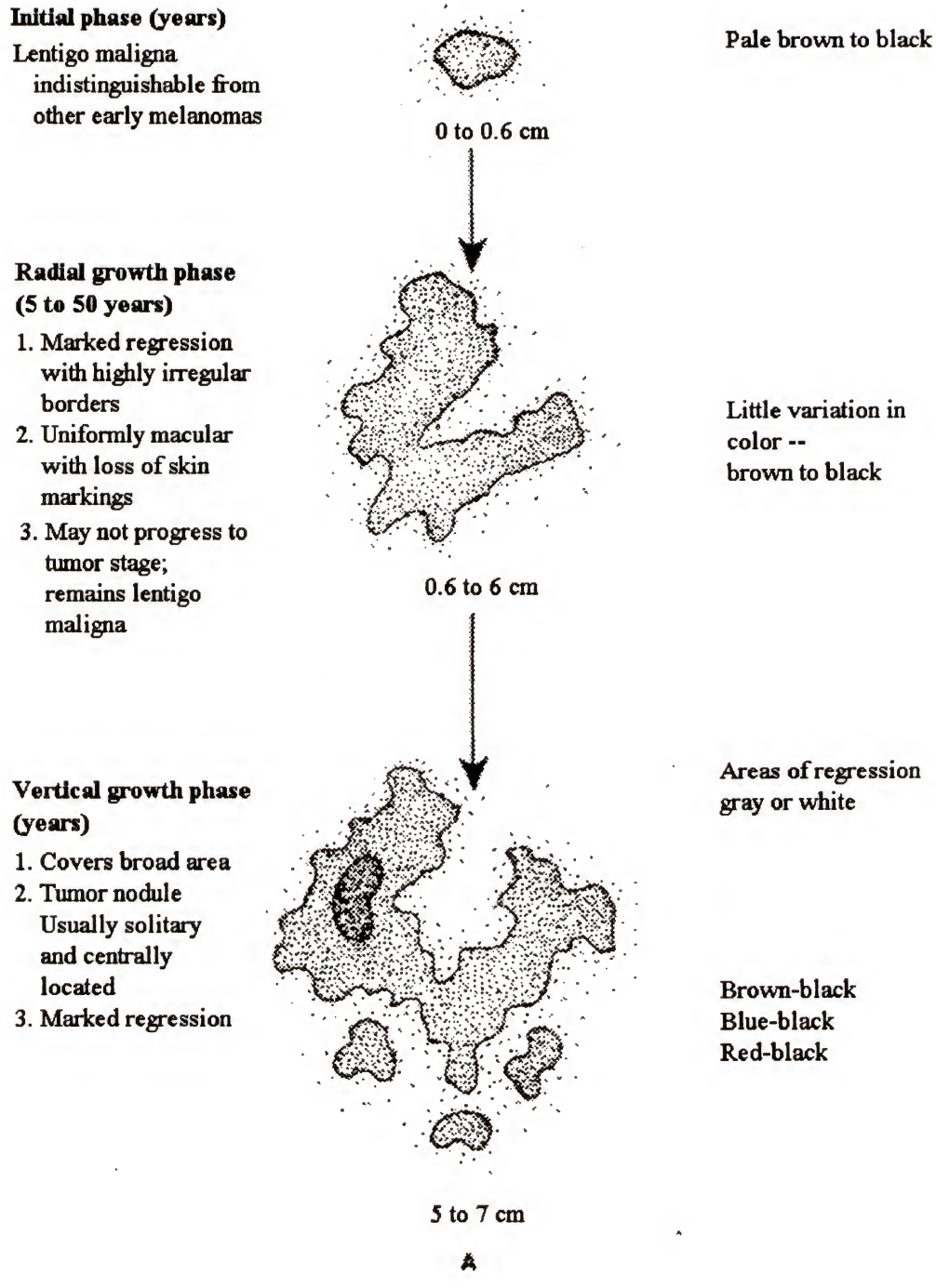

Fig. 1-5 Visual Features of Malignant Melanoma

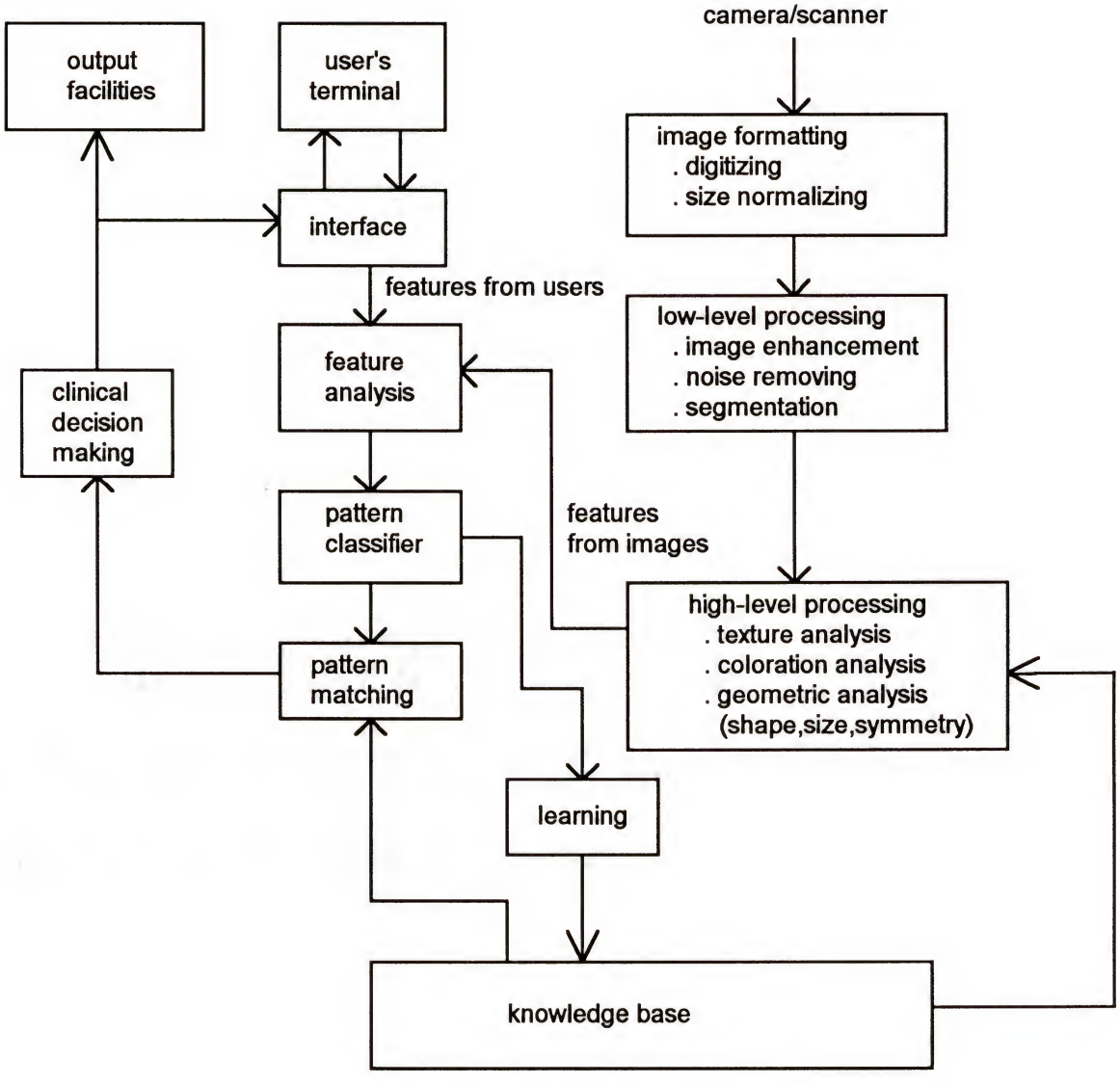

Fig. 1-6 The Flow Chart of the System

melanoma pictures and no algorithms have been found which resolve all difficulties satisfactorily.

The importance and difficulties of the image segmentation present a challenge for developing a suitable segmentation approach for the system. The word "suitable" means that the segmentation approach for the system must satisfy the following requirements:

1. It must be universally suitable to the class of application images without difficulty for user input of processing parameters.
2. It must have high performance, that is, be robust to noise and generate high quality segmentation results in a reasonable time.

1.2 Objective

Thus we face two problems. First is the development of an approach that satisfies the requirements listed above. Second is the determination of how well that approach works. That is, does the newly developed procedure produce correct and consistent results at a high performance level? The goal of this dissertation is to address both of these problems.

The specific objectives of this study are as follows:

1. Develop a new approach satisfying the requirements.
2. Implement the approach.
3. Compare the proposed approach experimentally with other accepted approaches to show that the performance of the proposed approach quantitatively and qualitatively outperforms these established procedures.

1.3 Dissertation Organization

The dissertation consists of two parts: Part I -- literature review, and Part II -- the developed approach. Part I reviews the literature on some segmentation approaches. Chapter 2 reviews basic segmentation algorithms and Chapter 3 presents advanced

segmentation procedures. Chapter 4 summarizes the main problems of these approaches. Part II describes the approach developed in this work, which is a hybrid segmentation approach. Chapter 5 introduces the basic regularization theory from which a new algorithm used in the first stage of the hybrid segmentation approach is developed. The three chapters after Chapter 5 describe three stages of the hybrid segmentation approach developed in this dissertation. Then experimental results are presented in Chapter 9, which evaluate the developed approach and illustrate its ability to segment malignant melanoma. The final chapter summarizes this study and suggests directions for future research.

PART I

LITERATURE REVIEW

Introduction

Image segmentation is typically the first key step and also the most difficult step in processing an image. The primary function of image segmentation is to extract objects of interest from any background present in an image by partitioning the image into homogenous regions, each of which is then processed further. Region homogeneity could be in the sense of intensity, texture, or surface type. In segmenting malignant melanoma, we typically segment on intensity in color space. Over the last decades many researchers have developed excellent segmentation approaches. Powerful algorithms have been used in practice. Performance of segmentation algorithms/approaches is usually evaluated for the following performance measures:

. Uniformity---regions should be uniform or homogeneous;

. Compactness---regions should be simple and without small holes;

. Dissimilarity---adjacent regions should be significantly different;

. Boundaries should be continuous and accurate .

As shown in Fig 2-1, segmentation techniques can be classified as either statistical or non-statistical ones. Under them, there are three basic schemes: edge/boundary based, region based, and shape-based segmentation.

The statistical segmentation techniques use statistical measures and analyses in image segmentation. Generally speaking, statistical segmentation approaches are less sensitive to noise than non-statistical ones since the statistical segmentation techniques employ information of an area instead of an individual point, and the noise can be adequately characterized in statistical terms and be imbedded in the statistical test procedures.

Edge based segmenters segment images by (1) using edge detection techniques to find edges in an image, (2) connecting edges to form closed contours by using some connection algorithms, and (3) mapping contours to regions. The key step in this kind of segmenters is to find true edges. Region based segmenters segment an image by grouping 'similar' pixels to form region patches. The variations among the region based segmentation techniques lie in the grouping schemes and the definitions of the similarity. Shape based segmenters use morphological operators with certain shape structures in noise removing, edge detection and region reshaping.

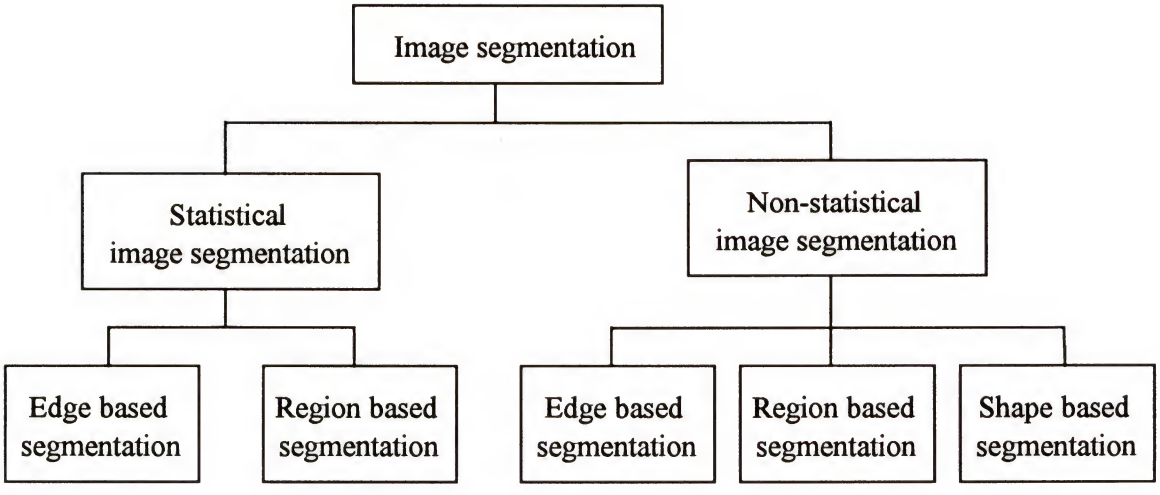

Fig. 2-1 Segmentation Technique Classification

CHAPTER 2
BASIC SEGMENTATION ALGORITHMS

2.1. Edge Based Segmentation

In edge based segmentation, edge detector procedures are the most important ones since edges from the edge detectors are the basic elements of the boundaries of objects, or of the regions which are to be segmented. The most popular classical edge detectors are derivative edge detectors which can be classified as first order derivative edge detectors and second order derivative edge detectors [Gon 87]. Both of these processes are non-statistical ones.

2.1.1. First Order Derivative Edge detectors

The first order derivative edge detectors label a pixel as an edge pixel if the amplitude of its gradient, dG(i, j), is larger than a threshold, T. Thus the edge pixel set, E, is defined as

$$E = \{\text{pixel}_{edge}(x,y),\ (x,y) \in \frac{\partial f(x,y)}{\partial x}\cos\Omega + \frac{\partial f(x,y)}{\partial y}\sin\Omega \geq T\} \qquad (2\text{-}1)$$

This idea has been implemented by Roberts, Prewitt, Sobel and Frei-Chen as follows. Let $F=\{f_1, f_2, \ldots, f_9\}$ be a vector containing the pixel values of a 3*3 neighborhood shown in Fig. 2-2(a); $W_i=\{w_{i1}, w_{i2}, \ldots w_{i9}\}$ be the vector representing the mask shown in Fig. 2-2 (b);

$$W = \sqrt{\sum_{i=1}^{m}(w_i' F)^2}\ . \qquad (2\text{-}2a)$$

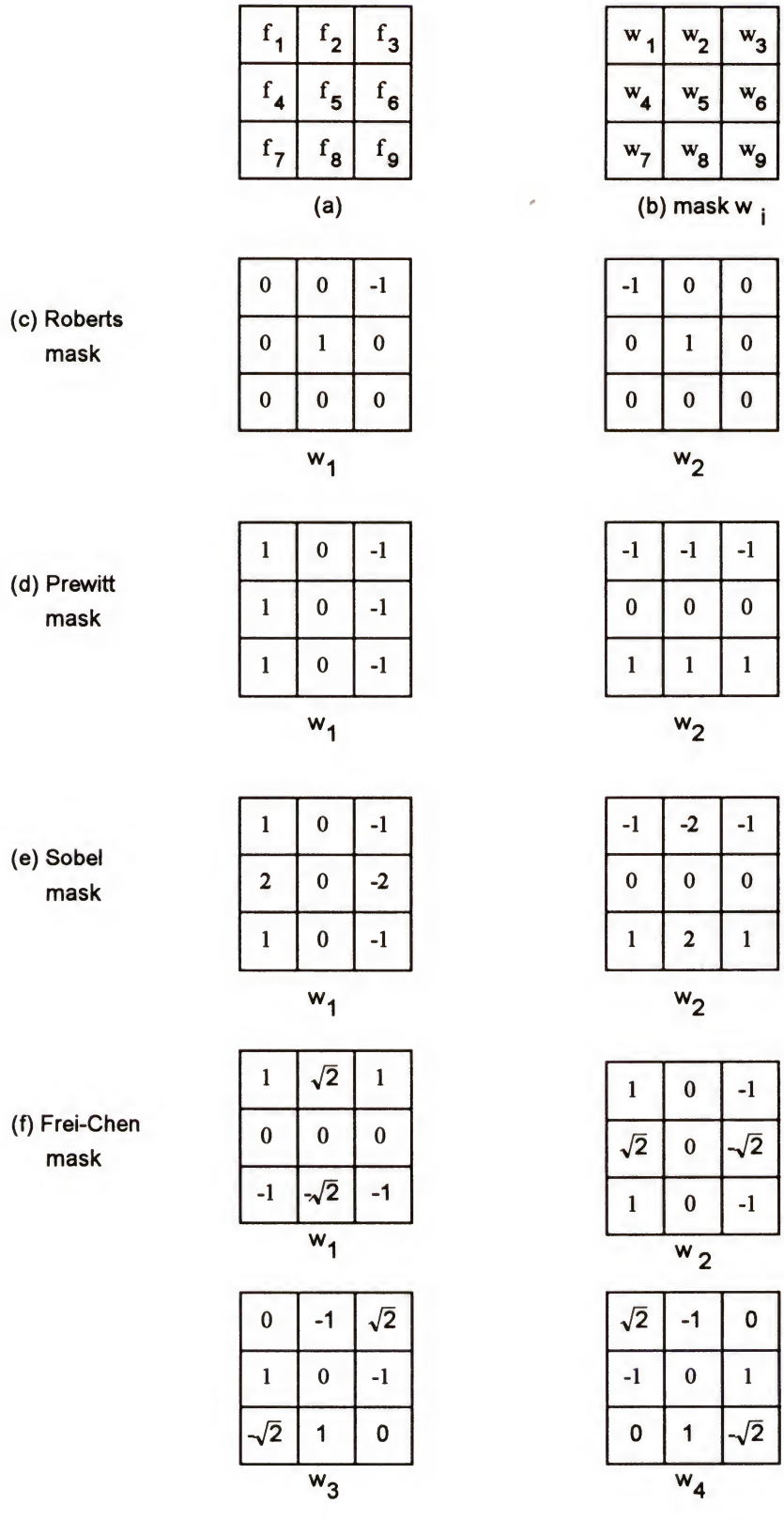

Fig. 2-2 The operator of the first order derivative edge detector

Thus

$$f_5 \text{ is } \begin{cases} \text{an edge pixel} & \text{if } W > T \\ \text{a non-edge pixel} & \text{otherwise} \end{cases} \qquad (2\text{-}2b)$$

The larger the T, the less sensitive the edge detector is to indicating that an edge exists. The differences among the schemes attributed to Roberts, Prewitt, Sobel and Frei-Chen lie in the values of W_i and m (see Fig. 2-2) [Rob 65][Pre 70][Gon 87][Fre 75]. These first order derivative edge detectors are the simplest to implement.

Any edge detectors involving derivatives are necessarily very sensitive to noise. To handle noisy cases, noise removal processing is needed before edge detection. Noise removing can be done by many kinds of linear low-pass filters and non-linear filters. Linear filters include moving average filters, Gaussian filters, Butterworth filters and Homomorphic filters. An example of a non-linear filter is the median filter. Canny [Can 83] has shown that, in 1-D, the optimal filter, according to his criterion, is a linear combination of four exponentials, which can be well approximated by a first derivative of a Gaussain. He has used a filter combined by such filters with varying size and orientations, first convolving it with the original images and then thresholding, to detect edges of 2-D images.

The edges from the first order edge detectors are typically thick and not closed, since they indicate individual pixels as being 'an edge point'. A group of adjacent edge pixels will form a boundary, an edge segment, of a region in the image. What we need is a definite boundary, a curve representing the edge of a region, not a set of disjoint points which may form clumps and thus indicate a thick region for the separation curve. This means further thinning and connecting are required. The threshold value, T, and filter size will greatly affect edge detection quality.

2.1.2. Second Order Derivative Edge Detectors

Second order derivative edge detectors locate edges of non-noisy images by noting the zero crossing of the second order directional derivative. That is, the edge pixel set is:

$$E = \{\text{pixel}_{\text{edge}}(x, y), \quad (x, y) \in \Re\} \tag{2-3a}$$

$$\begin{aligned}\Re = \{ \; & -\nabla^2 f(x^+, y^+) \gtrless 0 \text{ and } -\nabla^2 f(x^-, y^-) \lessgtr 0 \\ & \text{or } -\nabla^2 f(x^+, y^+) \gtrless 0 \text{ and } -\nabla^2 f(x^+, y^-) \lessgtr 0 \\ & \text{or } -\nabla^2 f(x^+, y^+) \gtrless 0 \text{ and } -\nabla^2 f(x^-, y^+) \lessgtr 0 \; \}\end{aligned} \tag{2-3b}$$

$$\nabla^2 = \frac{\partial^2}{\partial^2 x} + \frac{\partial^2}{\partial^2 y} \tag{2-3c}$$

To handle noise cases, a Gaussian filter with size λ may be used [Mar 80.] Marr and Hilderth first undertook Laplacian operation on a Gaussian filter to form a rationally symmetrical Laplacian of Gaussian (LoG) mask. Then they used the LoG mask instead of the Gaussian filter for convolution with images. Marr and Hilderth's contribution led to one of the most popular edge detectors, the LoG edge detector. The LoG edge detector generates closed and one-pixel wide edges. The main problems associated with the LoG edge detector are as follows: (1) For some edge patterns, the detectors with some range of λ will generate zero crossings at reflection points rather than at real edge points, that is the zero crossing does not always correspond to real edge points; (2) There exists a shift between zero crossing and actual edge position because of the interaction between nearby edges; and (3) It is difficult to obtain good performance on both edge position and edge detection. The tradeoff between edge position and edge detection is controlled by the size of the Gaussian filter. A small λ gives rise to more accurate edge position, but also more false edges. A large λ can reduce the false edges, but the edge position is shifted and some true edges are missing (or edge detection ability decreases). It is impossible to choose a λ that simultaneously suppresses noise and retains the details in the object boundaries. To

solve these problems, extensive research has already been done, but without useful results for our work.

Chen and Medioni have derived the mathematical formula for judging false zero crossing and correcting the bias of edge positions [Che 87]. They point out that a zero crossing corresponds to an edge, if and only if, $f' * f'' < 0$ and the gradient magnitude is larger than a threshold. It happens, however, that some valid edges may be missed when the λ is so large that f' will produce the wrong sign, or if an unsuitable threshold is used.

Raman's multiresolution scale space tracing algorithm [Ram 91] detects edges in different λs. These λs form a scale space. The algorithm first detects edges at a coarse scale (which gives few false edges), then follows their progress through the scale space, and tracing the contour through the scale space. Contours are refined starting with coarse values, which are then successively refined. The problems with this technique are that the coarse scales have already introduced inaccurate edge positions and that multicell edge detecting requires extended computer time and large storage capacity.

Lee's algorithm [Lee 91a] first detects edge points at small scale space, getting an intermediate edge image. Then the system checks each edge, deleting the ones whose length is below a threshold. For the rest of the edges, his technique calculates the edges' curvature $\mu(\chi)$, estimates their gradient variance $V(\chi)$ and computes a weight defined as $W(C) = \oint_C U(m(x))V(x)dx$. Finally, the algorithm deletes all edges with W(C) below a threshold. This algorithm can obtain rather good results with extensive computation and good threshold settings.

To eliminate some false zero crossings, an alternative zero crossing approach was developed by Lee [Lee 91b]. It is called the residual analysis edge detection. In this approach, the differentiation operation is replaced by residuals which are equal to the difference between the original image and its smoothed version. The zero crossing of the residuals yields edges provided that on either side the sign of the residual is constant for some area, A, and the gradient of the residual is significant [Gri 85]. By residual analysis,

the false zero crossings generated by triangular creases can be ignored since the gradient of the residual is very small. Lee proposed two criteria for further eliminating false zero crossings. The first criterion states that those zero crossings with which two associated regions, R^+ and R^-, are not both simply connected are considered as false ones. The second criterion computes the a quantity at zero crossing (x_0, y_0),

$$M_r(x_0, y_0) = \left[\int_R (x - x_0)[f(x, y) - d(x, y)]dxdy\right]^2 + \left[\int_R (y - y_0)[f(x, y) - d(x, y)]dxdy\right]^2 \quad (2\text{-}4)$$

and checks $M_r(x_0, y_0)$ against a threshold. If $M_r(x_0, y_0)$ is larger, the zero crossing is kept, otherwise it is removed. Although the residual edge detector can eliminate some false edges, it has not relieved the last two problems of LoG edge detectors mentioned above.

2.1.3. Statistical Edge Detection

The difference between statistical and non-statistical edge detectors lies in the criterion of labeling an edge point. The statistical edge detectors designate edge pixels based on results of statistical tests in the pixel's neighborhood, called the window.

One of such edge detector was published by Kundu [Kun 89]. In that work, he defined three types of regions: quasi-constant (QC), large linear varying (LLV) and quasi-two-value (QTV), and assumed the population of pixels inside each region has Gaussian distribution with mean, μ, and small standard deviation for QC or a large one for LLV. As the window of size n*n, centered at pixel(i, j) moves over the image in a raster scan fashion, three statistical testing steps are applied on each pixel. An edge candidate pixel must pass the three tests described in the following three steps.

- Step 1: (1) testing the dispersion of noise statistics

$$X_{p-1}^p - X_2^p \geq \gamma \quad \Rightarrow \quad \text{non-QC region;}$$

(2) thinning process

$$X_0 \le \frac{X^p_{p-1} + X^p_2}{2} \Rightarrow \text{having edges not wider than 2 pixels}$$

where p = n * n and X^p_i is the i^{th} element of the ordered pixel value set of the n * n window, $X = \{X^p_1, X^p_2, \ldots X^p_{p-1}, X^p_p\}$

- Step 2: (1) dividing the passed non-QC region with a increased size, R = (n+dn) * (n+dn) into two groups based on the 2^{th} order statistic

$$X_i \le \frac{X^R_{R-2} + X^R_3}{2} \Rightarrow X_i \text{ belongs to group L with mean } \mu_l$$

$$\text{otherwise} \Rightarrow X_i \text{ belongs to group H with mean } \mu_h$$

$$(i=1,2,\ldots P)$$

(2) testing

$$T = |\overline{x_h} - \overline{x_l}| + |\overline{y_h} - \overline{y_l}| \ge \beta \Rightarrow \text{non-QC region}$$

where (x_h, y_h) and (x_l, y_l) are the coordinates of μ_h and μ_l respectively.

- Step 3: Testing on the non-QC region passed step 2

$$|stat| = \frac{2*(B_l - R/2)}{0.5*\sqrt{R}} \le \eta \Rightarrow \text{pixel (i, j) is an edge pixel}$$

where $B_l = b_1 + b_2 + \ldots + b_R$. $b_i \in (0, 1)$ and is a Bernoulli variable with probability 1/2.

There are still many spurious edges and missing edges after the three tests detailed above, so the algorithm uses another non-statistical test on the window structures of 2D hypothesized contour segments. The test calculates a quantitative amount, called U-number, for every hypothesized contour segment, selects the largest U-number, U_{max}, and tests whether or not U_{max} is larger than a threshold ξ. If so, the central pixel is a part of a valid edge contour. Otherwise it is a spurious edge pixel. The edge detector works fairly well with properly threshold setting.

Another statistical edge detector was developed by Suk [Suk 84]. The outline of the algorithm is shown in Fig. 2-3. The two most important steps of the algorithm are

modality test and edge detection. The modality test is the heart of the algorithm. The modality test means (1) for every pixel in the testing window, several statistical tests, such as simple parametric test, test based on the gray level distribution, and test based on the homogeneity of spatial variance, are applied; (2) for spatial variance test, a number of different methods, such as ANOVA, shortcut method, Maximum F ratio and Cochran methods [Suk 84], are employed. Such redundancy tests increase the reliability and consistency of detection because the decision on the existence of a significant connected edge segment in the window is made by examining all of the test results. Therefore, even though some of the tests produce errorous results due to noise effects, the final decision based on the results of all tests has a much higher probability of being correct. During the modality test, a "no-decision" category is added to "acceptance" or "rejection" of the hypothesis since it is more reasonable to allow a "no decision" than to force a definite decision when in doubt. After the modality test, the final decision scheme on determining whether a window contains a connected edge segment is the majority vote approach to all of the test results. For each edge-containing window, the histogram thresholding and edge detection are used to find the edge segment position. In this edge detector, the window moving scheme is block by block rather than in a raster format, or pixel by pixel. Therefore, the size of the window is a critical parameter. Valid sizes are only those that are small enough so that the edge segment can cross the window and large enough to guarantee the validity of statistical tests. Of course, all thresholds in every test step also affect the performance of the detector.

2.2. Region Based Segmentation

Region based segmenters segment an image by grouping 'similar' pixels to form region patches. The basic principle is described as follows.

Let R represent the entire region. We may view segmentation as a process that partitions R into n subregions, R_1, R_2,....,R_n, such that

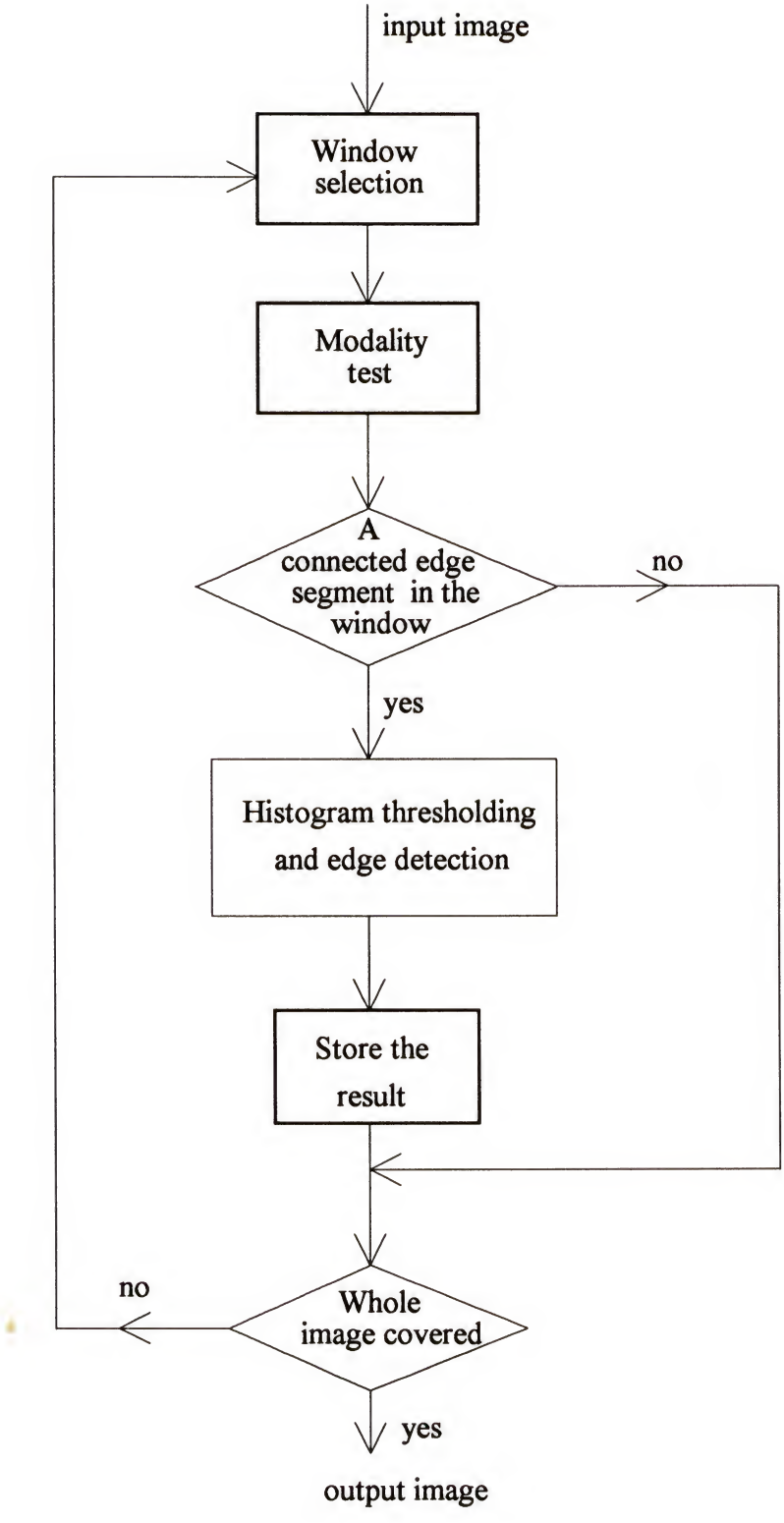

Fig. 2-3 Suk's Statistical Edge Detector

a) $\bigcup_{i=1}^{n} R_i = R$

b) Ri is a connected region, i=1,2,....n,

c) $R_i \cap R_j = \Phi$ for $\forall$ i and j, $i \neq j$

d) P(Ri) = true for i=1,2,...,n,

e) $P(R_i \cup R_j)$ = false for $i \neq j$.

Where P(Ri) is a logical predicate defined over the points in set Ri, and Φ is the null set.

Condition (a) indicates that the segmentation must be complete. Condition (b) requires that the points in a region must be connected. Condition (c) indicates that the regions must be disjoint. Condition (d) deals with the properties which must be satisfied by the pixels in a segment region. For example, P(Ri) can be some measure of uniformity. Condition (e) indicates that region Ri and region Rj are different. The variation of the region based segmentation lies in the different definitions of P(Ri) and the methods to measure $P(R_i)$. Four classical approaches are: histogram thresholding, region growing, region splitting and merging, and clustering approach [Gon 87].

2.2.1. Histogram Thresholding Methods

In the image histogram domain objects can be represented by the peaks in the image histogram if the image is noiseless. Therefore histogram thresholding techniques offer a fast and straightforward approach to extract objects from the background. One can pick out the objects by setting suitable thresholds, T_i, (see Fig. 2-4 (c)). The following introduces several histogram thresholding algorithms.

Global histogram thresholding techniques are based on histogram analysis of the entire image. They are suitable for images whose histograms have well-defined peaks. The thresholds are located at valleys between peaks. A popular method for finding the thresholds is optimal thresholding [Gon 87], in which the thresholds are set such that

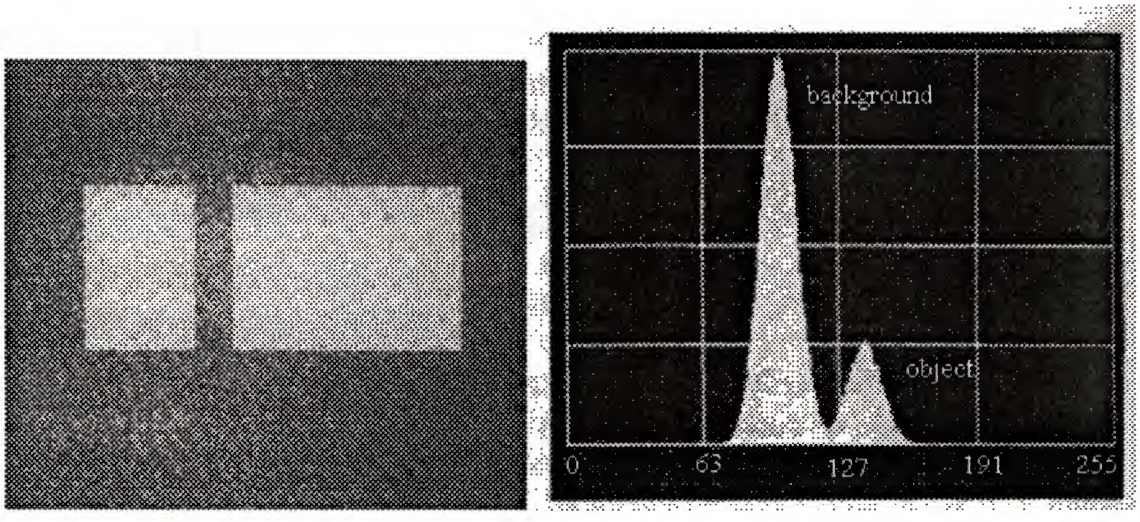

(a) (b)

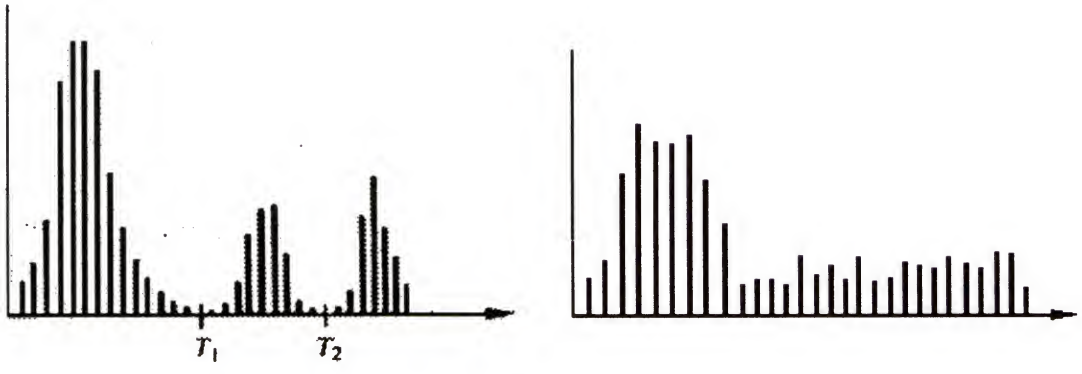

(c) (d)

Fig. 2-4 Image histogram
(a) Original image. (b) Histogram of (a).
(c) A histogram of well-defined peak characteristics.
(d) A histogram of pool-defined peak characteristics.

either the overall probability of error or the mean-square error between segmented image and the original image is minimum. This kind of optimal problem can be solved by traditional numerical methods, such as Newton's method. A more analytical method is (1) fitting the histogram by N-modal Gaussian density curve where N = the number of peaks in the histogram, or fitting the i^{th} peak by the a Gaussian distribution with mean μ_i and standard deviation, σ_i; (2) calculating the thresholds, T_i, between the i^{th} peak and $(i+1)^{th}$ peak, using the following formula

$$T_i = \frac{\mu_i + \mu_{i+1}}{2} + \frac{\sigma_i^2 \ln \frac{p_i}{p_{i+1}}}{\mu_i - \mu_{i+1}} \qquad (2\text{-}5)$$

where p_i is a priori probability of peak i. Thus the pixels with gray level between T_{i-1} and T_i are classified to the i^{th} segment, labeling as R_i (i=1,2, ... K, and K is the assumed number of segments). This method is suitable for the images having histograms with well separable peaks and approximate Gaussian distribution. (Note that Gaussian distribution histogram is assumed by many published papers, for example, in the papers cited earlier on the two statistical edge detectors). Many images, however, are quite different. This dissertation will describe a new algorithm for finding the optimal thresholds.

Another global thresholding algorithm was developed by Arnulfo and Gonzalez [Arn 87]. It segments a real image to a binary object-background image by iteratively updating the segmentation threshold based on the Taylor series expansion in a raster format. First, the algorithm uses Stockham's model to describe a visual gray level image, f(x, y) as the product of an illumination component, I(x, y), and a reflectance component, r(x, y). Second, in order to dynamically segment the image under varying lighting condition, the threshold is expressed as a recursive function of f. Third, under the assumption that changes in I(x, y) are smooth, for example linear or Gaussian illumination function, and that abrupt changes in f are due to r but with r values clustered in areas of constant reflectivity, the recursive function can be expanded as a Taylor series. Thus at

each pixel site, a corresponding threshold with an arbitrary initial value is iteratively modified, approaching a better and better value. At last, every pixel in the image is assigned to either object or background according the final threshold at corresponding sites.

The problems with such a global approach include the overlapping distributions that allow hidden objects and the loss of spatial information. Thus localized histogram thresholding approaches are used. The localized histogram algorithms divide a whole image into many small subimages and employ the histogram thresholding techniques over each localized histogram to label pixels to produce a segmentation. The size of the subimages varies depending on the different algorithm. For example, in Chow and Kaneko's algorithm [Cho 72], the window size is chosen such that the subwindow's histogram is bimodal so that the Gaussian curve fitting method can be used to find the optimal threshold. One of the problems with the localized histogram is that the artificial subimage boundaries are induced into the segmented image. To solve this problem, Beveridge developed an algorithm [Bev 89]. In his algorithm, the subimage size is 16x16 with 4-pixel overlap expansion in each direction, to correct situations in which a subimage boundary happens to divide an area in two, where a single region should be. The algorithm begins with first identifying all local maximals in the corresponding localized histogram as peaks and the points of minimum value between each adjacent pair of peaks as a valley, then applying three constraints to remove those peaks which have peak height $< \alpha$, peak-valley ratio $< \beta$, or peak distance $< \gamma$ (α, β, or γ is a threshold) where,

peak height = the magnitude of the histogram at the peak,

peak distance = the gray-level difference between two peaks,

peak-valley ratio = the peak height / the higher of the two neighboring valleys.

The valleys satisfying the three constraints correspond to those thresholds in the histogram which are used for thresholding the subimage into segments. To remove artificial boundaries between subimages, all pairs of regions adjacent at a subimage boundary are

compared using both a local and a global measure of similarity, called merge-score. The merge-score is defined as

$$\text{merge} - \text{score} = \frac{|\mu_a - \mu_b|}{\max(\sigma_a + \sigma_b, 1)} \tag{2-6}$$

where μ is the mean and σ is the standard deviation. For global measure, all pixels in the respective regions contribute to the computation of μ and σ. For local measure, only pixels within a fixed distance (usually 4 pixels) of the shared boundary are considered. Two regions are merged if and only if both the local and global merge-scores are below the specified thresholds.

2.2.2. Region Growing Method

Region growing is a computationally simple and conceptually sophisticated method for image segmentation. Region growing algorithms segment images by grouping pixels or subregions into large regions on the basis of some similarity criteria. The simplest of them is the pixel arrogation algorithm [Gon 87]. The algorithm starts with a set of 'seed' points and from these grows regions by appending to each seed point those neighboring pixels that have similar properties (e.g., gray level, texture, color). Two important problems are the selection of initial seeds that properly represent regions of interest, and the selection of suitable properties for including points in the various regions during the growing process. The resolutions of these two problems lead to many variations of the region growing approach.

Usually, seed selection needs a priori information on the nature of the problem. When a priori information is not available, one may proceed by computing at every pixel the same set of properties that will ultimately be used in assignment of pixels to regions during the growing process. If the result of this computation shows clusters of values, then the pixels whose properties place them near the centroid of these clusters can be selected as seeds.

The selection of similarity criteria is dependent not only on the problem under consideration, but also on the type of image data available. For example, the analysis of land-use satellite imagery is heavily dependent on the use of color. Often, a number of similarity measures are used simultaneously on a single image. Besides the similarity criterion, connectivity or adjacency information should be used in the region-growing process to prevent a meaningless result. One example of the use of such information is: (1) the absolute difference in gray level between the seed and a candidate pixel must not exceed 10% of the difference between the minimum and maximum gray levels in the entire image; and (2) any pixel added to the region must be 8-connected to at least one pixel previously included in the region.

The thresholds used in testing the similarities also affect the segmentation results. For example, the number of the segmented regions is at most equal to the number of seeds, depending on the threshold value. Even the priority of growing directions will affect the shape of regions.

2.2.3. Region Split and Merging Methods

Unlike region growing methods, region split and merging approaches segment images by splitting those regions whose P(Ri) = false and merging those whose $P(R_i \cup R_j)$ = true. One more practical example of split and merge algorithm has been implemented by initially subdividing an image, R, into a set of arbitrary, disjointed regions, then splitting a region if the variance of the region is larger than a threshold, or merging two adjacent regions if the contrast of two regions is smaller than a threshold, and finally labeling the pixels in R_i as the mean value of R_i.

A popular algorithm is called quadtree split and merging algorithm in which the geometric data structure is a quadtree (the quadtree is a tree in which each node has exactly four descendants) [Gon 87]. The algorithm is summarized as follows:

(1) The initial region R_0 = whole image.

(2) Split any region R_i into four disjointed quadrants where $P(R_i)$ = false.

(3) Merge any adjacent regions R_i and R_j for which $P(R_i \cup R_j)$ = true.

(4) Stop when no further merging or spliting is possible.

A simple illustration on the algorithm is shown in Fig 2-5. One problem of this algorithm is that the rectangular tessellation of the image domain often results in some false region boundaries. To remove the false boundaries, either the procedure of identifying and removing false boundaries is needed, or another data structure of a more geometric flavor is used. For example, in Schmitt and Chen's segmenter, a triangle structure is used in tessellating the image domain [Sch 91].

2.2.4. Clustering Approach

The cluster techniques may also be used in region based segmentation. In this case, the segmentation procedure can be considered as grouping the pixels with similar properties together by finding the optimal cluster center and assigning each pixel to the closest cluster center. In this kind of approach, the selection of similarity measure and how to find the optimal cluster centers lead to many algorithms, such as K-mean, Max-Min, etc. [Tou 77], algorithms. In fact, the histogram thresholding techniques can be seen as a kind of cluster technique in the histogram domain.

Usually, the region based algorithms are not robust to noise. In noisy cases, the segmentation results are uncompact, namely there are many small holes in the segmented images. Therefore, preprocessing (e.g. noise removing) or postprocessing (e.g., false region removing) is necessary.

2.3. Shape Based Segmentation--(Morphology Methods)

Since Serra and Sternberg introduced mathematical morphology to low-level image processing [Ser 82] [Ste 86], many useful image processing procedures using basic operators of mathematical morphology have been developed. Morphological image

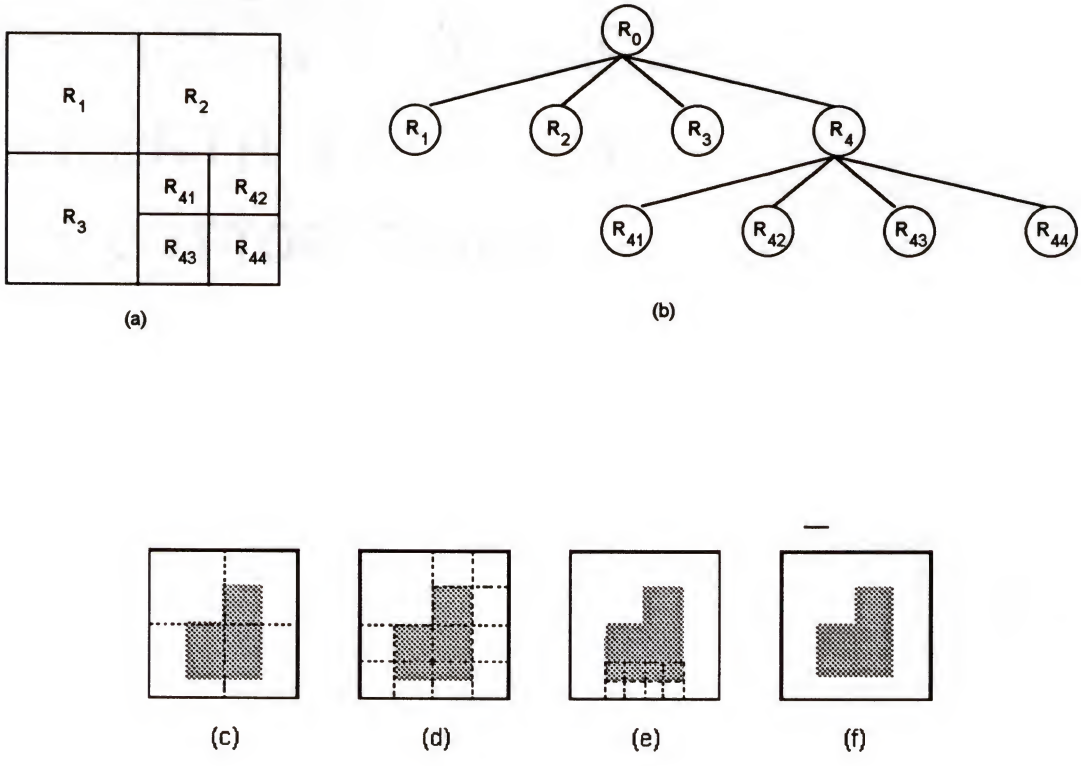

Fig 2-5 Split and Merge Algorithm

processing is a shape-oriented one. It tends to simplify image data by preserving the essential shape characteristics and eliminating irrelevancies. It treats the image as a set, and applies different set operations, such as dilation, erosion, opening and closing, and some basic image processing methods, like contrast enhancement, histogram equalization, etc., in low-level image processing. Several research achievements in this area are described below.

2.3.1 Morphological Segmenter

Klinger [Kli 88] and Thomas [Tho 91] have developed morphological segmenters for ultrasound images (Thomas' segmenter was an improvement on Klinger's work). The segmenters generate shape-oriented operators according to the a priori knowledge about the general size of image features for removing interfering data based on the image shape. The Thomas' segmenter consists of the following processing steps: (1)the gray scale opening with a disk-shaped structure element of 33 pixels in diameter, which morphologically filters the input image to obtain a slowly varying background image; (2) subtraction, which subtracts the background image from the original image; (3) contrast enhancement, which is used to produce a higher contrast image from the subtracted image since it is usually fairly dark; (4) thresholding on enhanced image, which produces a binary foreground-background image; (5) region labeling and object recognizing, out of which is selected the object of interests; (6) binary closing with a disk-shaped structure of 5 pixels, which is used to fill small holes and crevices on the object; and (7) binary opening with a disk-shaped structure of 9 pixels, whose purpose is to remove spurious extensions (size < 9 pixels) from the object. The performance of the segmenters is dependent of the accuracy of the shape and size of morphological structure elements which are determined by the prior knowledge of the application images.

2.3.2 Morphological Edge Detector

Noble used morphological operators for feature detection of noise free intensity images [Nob 88]. He detects edges/boundaries and junctions by using the difference operation of dilation and erosion, and the ridges and corners by the difference of the image surface opening and closing. The element used in the morphological operators is a 3 x 3 disk structure. The boundary points generated by the algorithm include stripe regions (smooth surface patches), edges (singular curves, i.e., steps, ridges, valleys and thin bars) and junctions (singularity points). The algorithm is sensitive to noise.

2.3.3 The Implementation of Morphological Operators

In the Salembier's multiresolution decomposition and adaptive filtering [Sal 91], rank order filters (ROF) are used to implements the gray scale morphological dilation, erosion, opening and closing with a box-shaped structure element. According to his notation, if x_i represents the input signal, M a mask containing N points, j an index belonging to M and r the normalized filter rank ($0 \le r \le 1$), the ROF output at location i, y_i, denoted as $R_{r,M}[x_i]$, is calculated by (1) taking all the points x_{i-j} belonging to the mask centered on i, (2) sorting their values in ascending order, and (3) taking the n^{th} value (n = r*(N-1)+1) of the ordered list, that is

$$y_i = R_{r,M}[x_i] = \underset{n= r*(N-1)+1}{\text{Rank}} (x_{i-j},\ j \in M) \qquad (2\text{-}7)$$

Thus the morphological operators on x_i are expressed as follows:

dilation: $\text{Dil}[x_i]=R_{1,M}[x_i]$ (2-8a)

erosion: $\text{Ero}[x_i]=R_{0,M}[x_i]$ (2-8b)

opening: $\text{Open}[x_i]=R_{1,M}[R_{0,M}[x_i]]$ (2-8c)

closing: $\text{Close}[x_i]=R_{0,M}[R_{1,M}[x_i]]$. (2-8d)

Salembier's work provides a simpler way of implementing morphological operators of structure elements.

CHAPTER 3
ADVANCED IMAGE SEGMENTATION

Many basic segmentation approaches have been reviewed in Chapter 2. In this chapter, more advanced image segmentation approaches are described. These methods are adaptive, optimizing, or integrating image segmentation algorithms.

3.1 Adaptive Segmentation

One of the keys to effective image segmentation is the selection of the appropriate control parameters in the segmentation algorithms for each image. However, this is very difficult in most cases, but one may try adaptive adjustment of parameters based on test images.

3.1.1. Adaptive Scheme Based on Genetic Algorithm

This adaptive scheme is based on the genetic algorithm, in which the selection of control parameters is viewed as a search through the hyperspace of all possible parameter combinations. The algorithm determines the parameter set which maximizes the segmentation quality criteria. The genetic adaptive approaches do not require complex segmentation quality surface descriptions, domain specific knowledge, or measure of goal distance, and are also independent of the particular image segmentation technique which is used since they use simple recombination of existing high quality parameter sets and a method of measuring current segmentation quality. Usually, genetic adaptive systems are more complicated in implementation.

An example using this kind of adaptive scheme can be found in Bhanu, Ming and Lee's paper [Bha 91]. They built an Adaptive Image Segmentation System shown in

Fig. 3-1. The system works as follows. (1) Image analysis unit analyzes the image characteristics (first order statistics and histogram properties; a total of 48 total image properties from R, G, B, and Y components) and passes them together with the external variables to the genetic learning unit. (2) The genetic learning unit selects a possible parameter set by comparing the current image properties with those of images processed previously (which are stored in the global population). The parameter sets form the seed population for the genetic process. This population is maintained and updated by the genetic learning unit. (3) Each of the parameter sets is sent to the image segmentation unit where images are segmented. (4) The segmentation results are evaluated using several segmentation quality measures. The evaluated results are combined and normalized in a weighted sum that represents the overall segmentation quality. (5) The evaluated results are fed back into the genetic unit as a "reward" to the associated parameter set and are used to adjust those parameters. If none of the members in the seed population is acceptable, the genetic learning unit begins recombining the parameter sets using crossover and mutation genetic operators. This adaptive adjusting cycle repeats until acceptable segmentation quality results have been achieved.

3.1.2. Knowledge Directed Adaptive Scheme

Another adaptive scheme is a knowledge directed one. This kind of scheme is especially suitable to specific applications since prior knowledge about the images can be obtained. Duncan's algorithm of Knowledge Directed Left Ventricular Boundary Detection in Equilibrium Radionuclide Angiocardiography [Dun 87], Michael and Nelson's Model-Based System for Automatic Segmentation of Bones from Digital Hand Radiographs [Mic 89], Raya's Rule-Based System for Low-level Segmentation of 3-D Magnetic Resonance Brain Images [Ray 90], and Morris' Rule-Based System for Dimensional Analysis of Glass Containers [Mor 89] all belong to this genre. All of these

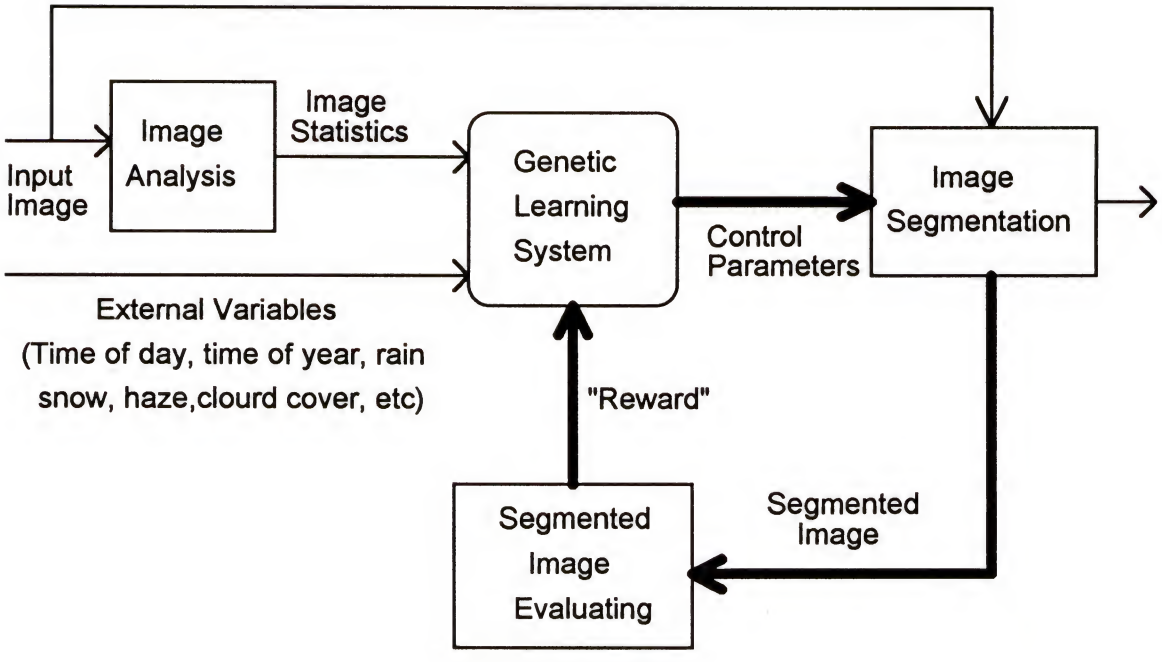

Fig. 3-1 An Adaptive Image Segmentation System

algorithms are context dependent, that is the segmentation performance depends on prior knowledge of correct segmentation.

For context independent knowledge directed adaptive segmentation, it is necessary to have either well-defined goals or a set of optimization criteria for evaluating performance. In the system with well-defined goals, performance parameters can be found that measure the distance from the goal at any stage of the process. These parameters provide a feedback by which the system can modify its strategy for segmentation. However, the goals can usually be defined precisely only in high-level image processing (e.g., shape, color distribution, size, etc.), at least not at low-level image processing (e.g., noise removing, edge detection, segmentation, etc.). To establish the connectivity between high-level goal and low-level processing, Kohl et al have developed a system. They devise an intermediate-level which translates high-level goals into appropriate low-level process specifications including the selection of algorithms, parameter setting, etc. In this way, high-level interpretation processes gain the capability of refining segmentation data according to predefined goals and/or current hypotheses regarding the content of the image, and thereby improve the quality of the overall system. Without well-defined goals, one must define a set of measurement parameters for evaluating performance. Thus knowledge rules can direct the modification of segmentation parameter settings based on the performance measurements. An example of this method has been used in a rule based image segmentation system [Lev 85].

3.1.3. Analytical Adaptive Scheme

A more analytical adaptive scheme is to define the control parameters as the function of pixel values. Thus the parameters are automatically adjusted during image processing according to the changes of images. For example, in Hancock's edge detector [Han 91], he adaptively estimates the hypothesis thresholds by adopting Bayesian framework to model images. In this way, the hypothesis thresholds used in Canny's edge

detector can be related to the parameters of the image model which are varied with image statistics. This kind of adaptive scheme is easy to implement. This dissertation adopts this kind of adaptive scheme.

3.2 Segmentation by Cost Function Optimization

In recent years, many researchers have focused their research on algorithms that segment images by optimizing some cost functions (called objective functions in some papers). The cost functions measure the image characteristics, such as noise, discontinuities, connectivities, smoothness, etc. In this kind of segmentation techniques, it is critical to properly define the cost function and the process of obtaining the optimal solution of the cost function.

3.2.1. Cost/Objective Function Minimization Approaches to Edge Detection

One of the methods of cost function minimization edge detection defines cost function as measurement of edge detection quality. The basic idea used in the cost function minimization edge detection is:

1) an edge detecting algorithm is used to obtain an initial edge configuration;
2) a cost function is introduced that measures edge quality, such as continuity, smoothness, thinness, location, etc. to form a total cost function C, which is the weighted linear combination of all edge cost functions;
3) C is minimized using a suitable optimization technique.

The final edge configuration is one with minimum C.

Among such edge detection algorithms, the algorithm due to Tan et al [Tan 92] works very well on images which are not very noisy. The algorithm consists of two stages, dissimilarity enhancement and cost function minimization. The dissimilarity enhancement detects edge candidates by calculating the degree of region dissimilarity, d(i, j) that exists at each pixel site (i, j) and assigning pixels as edge pixels, s, if d(i, j) is large ($0 \le d(i, j) \le 1$).

The algorithm defines the sum of a linear combination of five weighted cost factors on all pixels as the cost function, or

$$C(s) = \sum_{i,j} \sum_{k=1}^{5} C_k(s(i,j)) \qquad (3\text{-}1)$$

The problems in this kind of edge detection algorithms are: (1)the final results of this algorithm strongly depend on the initial edge configuration; (2) it is difficult to define an effective cost function and edge strategy; and (3) reaching a global optimum is difficult.

Another kind of approach for cost function minimization edge detection defines the likelihood on edge hypothesis or the likelihood ratio, the edge hypothesis to non-edge hypothesis, as the objective function. This kind of approach maximizes the function at each pixel site to detect edges. Many edge detectors based on Bayesian decision rule use this approach [Fua 90] [Jai 90] [Tuc 91]. The difficulty of this kind of approach is to select a proper model and define suitable statistics for testing the edge hypothesis and/or non-edge hypothesis. For example, in Jain and Nadabar's algorithm [Jai 90], they first use the Markov random field (MRF) to model the edge detection problem. Then they define a 3*6 pixel neighborhood for calculating the edge statistic of the central pixel for vertical edge and 6*3 pixel neighborhood for horizontal edge. The edge statistic, Es, is set to be equal to the absolute difference of average intensity value between 9 left side pixels and 9 right side pixels (or 9 up side pixels and 9 down side pixels for the horizontal case). The likelihood distribution of non-edge hypothesis is assumed as a t-distribution. The likelihood distribution of edge hypothesis is set to be a distribution which is linear within the [0, σ(Es)] interval and constant in (σ(Es), 255] where σ(Es) is the standard deviation of Es. The likelihood ratio of the edge hypothesis to non-edge hypothesis is maximized by the Highest Confidence First algorithm.

A more widely used cost function minimization method is edge detection based on the cost function derived from discretization of the functional obtained from regularization principles or stochastic estimate techniques used in Markov random field (MRF). Its cost

function is now some energy function, membrane energy function for the regularization model and Gibb's energy function for the MRF model (in fact, these two energy functions are of the same form if the Gaussian MRF model--the most popular model--is used). The variations lie in the difference of the definition of each term in the function and the approaches to solve the optimization problem. The theory and implementations on this kind of edge detection are widely available in the literature [Tor 86] [Hua 87] [Sim 88] [Dai 89] [Li 90]. The advantage of this method is that the control parameters in the process can be made adaptable. (The dissertation will describe the method in detail in Chapters 5 and 6)

3.2.2. Region Based Segmentation with Cost Function Optimization

MRF model region based segmentation is a cost function minimization method for region based segmentation. The cost function is a Gibb's energy function of Gaussian MRF, denoted as E. It is defined as:

$$E = \left(\sum_{m,n} \frac{(f_n - d_m)^2}{2 * \sigma^2}\right) + \sum_{c \in C} V_c(f_n) \tag{3-2}$$

and

$$V_c(f_n) = \begin{cases} -R & \text{if all } f_n \text{ in } C \text{ are equal} \\ R & \text{otherwise} \end{cases} \tag{3-3}$$

where d represents input image data set with M different values, f is the output image data set with N different values (N<<M), σ is the standard deviation of the noise, C is a clique associated with a neighborhood system and R is a constant. Segmentation consists of assigning each input image pixel with value d_m to a suitable output value f_n which minimizes the cost function, E.

The first term of E measures the error caused by assigning d_m to f_n when d_m is not equal to f_n. The second term, called clique potential function, measures the extra cost

when introducing a discontinuity. From Eqs. 3-2 and 3-3, we can see that the MRF based approach is in fact a clustering method with spatial constraints since it is the same as the K-mean cluster algorithm if R=0. By adding the $V_c(f)$ term to the K-mean cluster algorithm one can handle the noise cases. If pixels in a neighborhood are noisy, the second term plays a major role in minimizing E, that is, it assigns f_n to a d_m, which tends to smooth the neighborhood.

Murray [Mur 87], Derin [Der 87], Wright [Wri 89] and Chou [Cho 89] have used the principle described above in their segmentation algorithms with differences in the clique structure and value, the optimization approach, and additional constraints. The most widely used optimization approach used in this optimization process is simulated annealing.

Here, the parameter R controls the final segmented results. The smaller the value of R, the smaller the regions. If R is too small, it will cause incompact segmented regions. If R is too large, it will cause oversmoothing between regions and therefore cause region deformations. Another controlling parameter is the number of desired clusters (objects), K. If K is larger than the actual object number, false segments will be generated. If K is less than the object number, some objects cannot be recognized.

Another kind of region segmentation with cost function optimization defines the criterion which estimates segmentation quality as the cost function. Monga [Mon 87] has developed such an algorithm, called the optimal region growing segmentation algorithm. He defines a criterion function which is a monotonic and symmetrical function of M classical criteria, such as spatial variance, intensity contrast, mean-square-error, etc. The algorithm first initially segments images into a very oversegmented intermediate result, then merges the regions according to the optimal value of the criterion function. Since the M criteria are decomposed in a hierarchical manner, the optimization procedure is completed by finding the local optimum for each criterion hierarchically rather than by finding the global optimum for all M criteria. Thus the optimization is simplified, and the

region merging is also hierarchically carried out. The segmentation results of the algorithm will depend on the selection of the criteria and the arrangement of the hierarchy.

3.3 Integrating Region and Edge-Based Segmentation

Since different segmentation schemes have their own distinct advantages and disadvantages, and the results from different schemes are usually not consistent, many researchers integrate both region and edge information in the segmentation procedure to retain superiorities and overcome shortcomings. We can classify these approaches as hybrid segmentation approaches. There are two schemes for integration of region and edge segmentation. One is the interactive scheme, another is the result-modification scheme.

3.3.1 Hybrid Segmentation with Interactive Scheme

The interactive scheme segments images by either utilizing the information obtained from edge detection as additional criterion to guide the region based segmentation procedure in forming regions or as constraints to prevent forming false regions, or employ information from region analysis in edge detection.

One example of interactive segmentation algorithm is developed by Yu and Juha [Yu 91]. The algorithm combines region growing with derivative edge detection. In the algorithm, the uniformity used as the similarity measurement of the region growing is gray level uniformity, and the edge pixels are labeled by a Canny detector. The algorithm iteratively follows the following steps:

- Calculate the average gray level of pixel $f_{i,j}$ on a window centered at $f_{i,j}$ with arbitrary shape. This step is for reducing the influence of noise.
- If the gray level uniformity of $f_{i,j}$ is satisfied and $f_{i,j}$ is not an edge pixel in the edge model image, the pixel is grown. If $f_{i,j}$ is an edge pixel, a small neighborhood is

tested. The region growing procedure stops if at least one edge pixel is found among the tested neighbors, otherwise region growing continues.

. If gray level uniformity of $f_{i,j}$ is not satisfied and the pixel is also an edge pixel, the region growing stops. Otherwise the neighborhood is searched for edge pixels. The growing procedure stops at the nearest edge pixel which is located, if any are found. Otherwise the growth stops at the reference pixel.

The algorithm can generate more accurate region boundaries but is not robust to noise because both region growing and derivative edge detection suffer from noise.

Wright has also integrated edge information in his MRF region based segmenter [Wri 89]. He introduced a hidden edge variable, $l_{r,s}$, into the original cost function (Eq. 3-2). $l_{r,s}$ indicates if there exists an edge between pixels, r and s. If so $l_{r,s} \neq 0$, else $l_{r,s} = 0$. He replaced item $V_c(f_n)$ (Eq. 3-3) by $V_2(f_n)$ which is defined as:

$$V_2(f_n) = \begin{cases} V_c(f_n) & \text{if } l_{r,s}=0 \\ 0 & \text{otherwise} \end{cases} \qquad (3\text{-}4)$$

In this way, the algorithm does not introduce an extra cost function for edge points, and therefore allows the existence of discontinuities (edges).

In the modular feedback image segmentation system of Anderson et al [And 87], two-way interactivity is used. It is assumed that the number of regions is known approximately and it is used to estimate the corresponding parameters of an edge detection process. Then the edge detection result is used to initialize and assist a region growing process where a local similarity threshold T (which is used to judge whether two points belong to the same region) is gradually increased until the expected number of regions is found.

3.3.2 Integrated Segmentation Using Result Modification Scheme

Segmentation using result modification scheme follows three steps: (1) generating initial edge based segmentation results, (2) generating region based segmentation results,

(3) generating final segmentation by mapping the results from (1) and (2). The simplest mapping strategy is logical AND or OR operation. However, it usually cannot yield good results. Research on mapping strategy resulted in many algorithms [Yok 89] [Pav 90] [Had 90].

Pavlidis and Liow 's mapping strategy [Pav 90] employed two cost functions: one for false boundary elimination, denoted as F(e), another for boundary position modification, denoted as F_m. Both functions use the region boundary from region based segmentation as the reference, and integrate the contrast information which is a variation of the image gradient along the boundary. The algorithm generates edge information by first order derivatives and regions by a quadtree split-merge algorithm. F(e) is defined as:

$$F(e) = \frac{|\text{ sum of contrasts along boundary e }|}{\text{length of boundary e}} + \beta \frac{\text{number of direction change along boundary e}}{\text{length of boundary e}} \qquad (3\text{-}5)$$

The boundaries with "small" F(e) are eliminated. The first term can be interpreted as the strength of the boundary seen as an edge segment. The second term penalizes for long straight lines which most often correspond to artificial boundaries generated by the quadtree split-merge algorithm. To avoid introducing unacceptable topologies, two constraints, region constraint and boundary constraint, are set. F_m is defined as:

$$F_m(i,j) = \frac{1}{L}\sum_{i,j}\{|\nabla I(i,j)| - \alpha * \kappa(i,j) - \gamma * |\varphi'(i,j)|\} \qquad (3\text{-}6)$$

The boundary point is modified to the optimal (i, j) which maximizes $F_m(i, j)$. $\nabla I(i, j)$ is the image gradient, which corresponds to fidelity to data since it is maximum when the boundary runs along the points of maximum contrast or gradient magnitude. $\kappa(i, j)$ is the curvature, which favors "smoothness" and avoids sharp turns in a contour. $\varphi'(i, j)$ corresponds to the changes in direction of gradient along the contour, which should be small since large $\varphi'(i, j)$ means noise points. The algorithm generates accurate region

boundaries for not very noisy images but is more complicated and involves many parameter settings.

All the advances described above can be combined. By such a combination, one can make a segmentation algorithm with adaptive, optimum, and integrated property, and therefore, make maximal use of various advantages in different advanced segmentation algorithms to the greatest extent. This dissertation develops such an advanced combination segmentation approach.

CHAPTER 4
MAIN PROBLEMS ASSOCIATED WITH EXISTING ALGORITHMS

By examining various segmentation algorithms, we can summarize the main problems associated with them.

1) The first problem is the threshold or parameter setting. All of the algorithms involve a threshold/parameter setting which affects the segmentation qualities to a great extent. However, setting a suitable threshold/parameter, for a practical application, is not a trivial problem, especially with noisy images. Thresholding itself is an ill-posed problem and the skin lesion pictures come from various sources. Therefore there is no guarantee to find the right threshold for the set of all input images and for all areas of the images needed in a practical melanoma identification system. Fig. 4-1 shows the threshold setting effects in Sobel edge detectors. A small threshold will give rise to many false edges like the result shown in Fig. 4-1(c) and a large threshold will cause missing of true edges which can be seen in Fig. 4-1(d). Fig. 4-2 shows the parameter setting effect in a MRF region based segmenter. A small parameter, R, gives incompact segmented results (see Fig. 4-2(c)). A large R causes oversmoothness between regions and therefore causes deformations of the regions (see Fig. 4-2(d)).

2) The second problem is noise effects. Any noise may introduce dissimilarities into the images. Therefore, schemes using differentiation operations (for example the edge detectors) will enhance the noise as well as sharpen edges, and the schemes based on image dissimilarities (such as region based segmentation algorithms) will give rise to false results.

3) The third problem is noise suppression effects. To handle noisy cases, filters with lowpass property (such as median filters and Gaussian filters) are used to remove noise before image segmentation. However, these filters also blur images which will cause shift of edge positions and remove true edges as well as suppress noise. Figs. 4-3 and Fig. 4-4 show the effects of the filter size. Fig. 4-3 is the results of a Sobel edge detector combined with a median filter, and Fig. 4-4 shows the results of a LoG edge detector in which a Gaussian filter is used. From the figures we can see that the larger the filter size is, the stronger the ability of noise removal but the more the missing of true edges and the less accurate the edge positions.

4) The fourth problem is the inconsistency problem. Usually, edge based segmentation results and region based segmentation results can not be matched very well. There are three kinds of inconsistencies between edge based and region based segmentation. (1) A region boundary is not an edge segment, and there are no edges nearby. (2) A region boundary corresponds to an edge but it does not coincide with the edge. (3) There exist edges with no boundaries near them. Fig. 4-5 shows the inconsistencies.

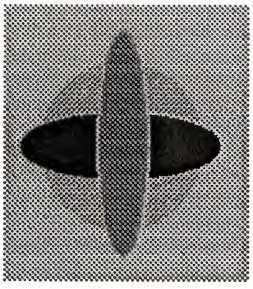

(a) Original image

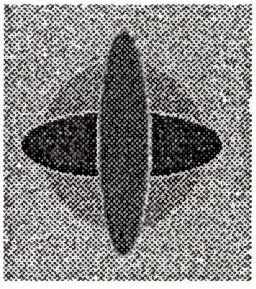

(b) Noisy image

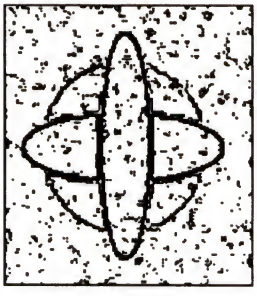

(c) Edges from Sobel
(W=3, T=20)

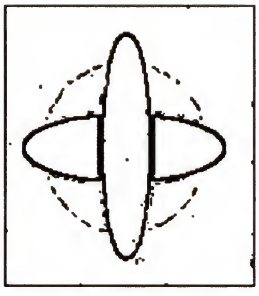

(d) Edges from Sobel
(W=3, T= 50)

Fig. 4-1 The Effects of Threshold, T, in a First Order Derivative Edge Detector
(Sobel edge detector with a median filter)

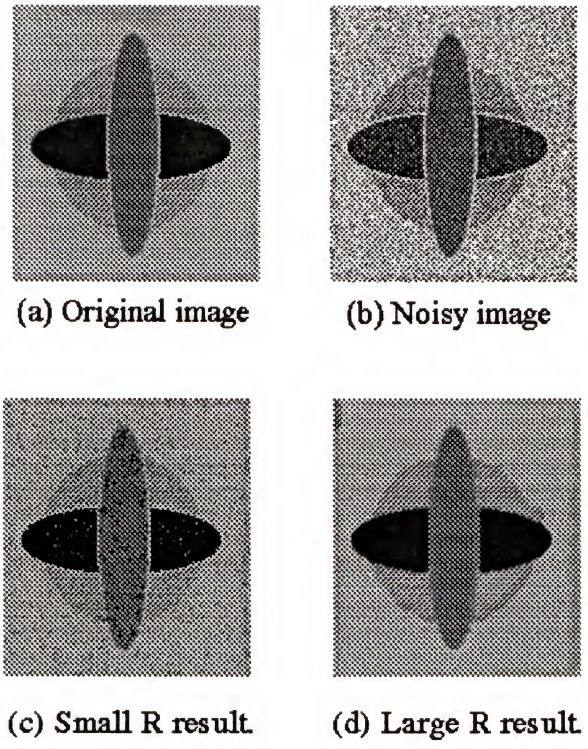

Fig. 4-2 Parameter, R, Effects in MRF Region Based Segmentation (4-level).

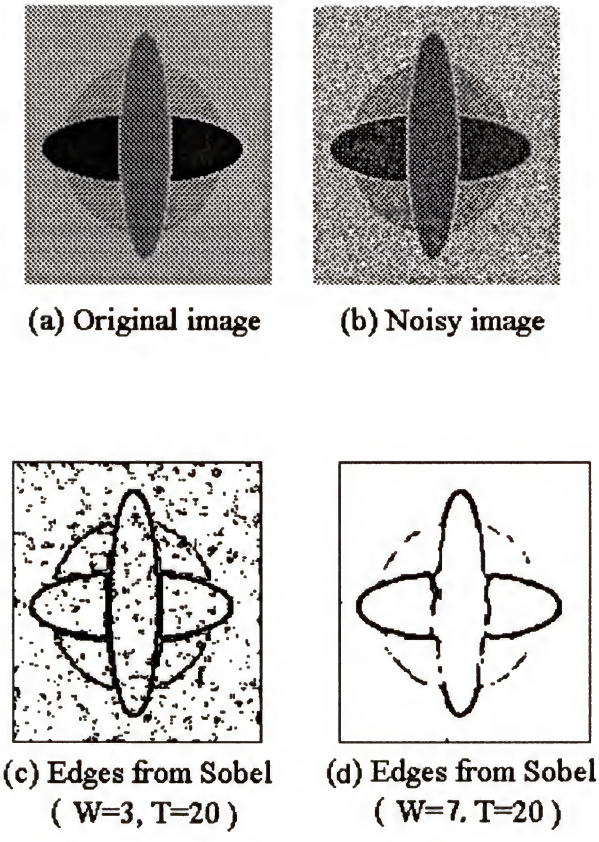

Fig. 4-3 The Effects of Filter Size, W, in a First Order Derivative Edge Detector (Sobel edge detector with a median filter)

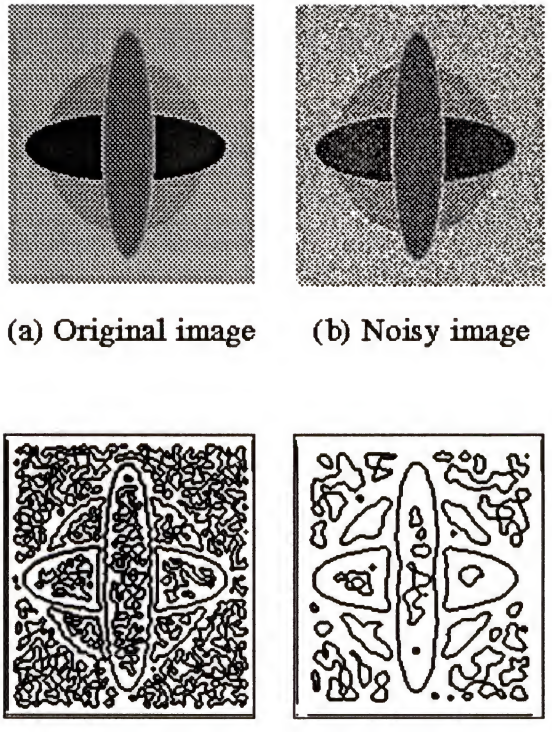

(a) Original image (b) Noisy image

(c) LoG (λ= 4) (d) LoG (λ= 12)

Fig. 4-4 The Filter Size, λ, Effects of LoG Edge Detector

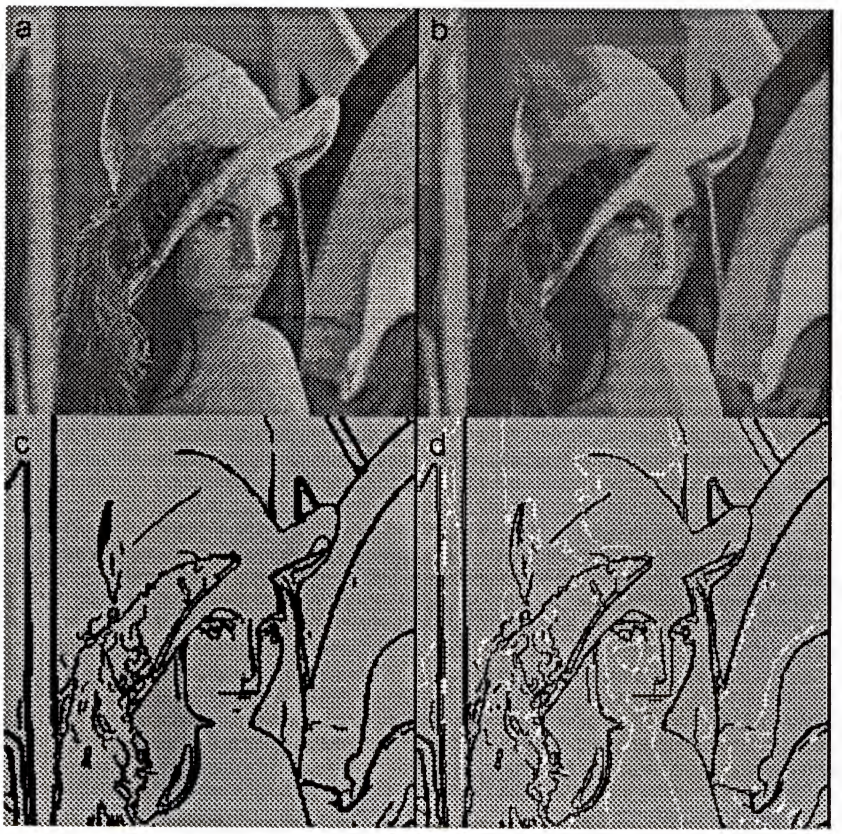

Fig. 4-5 Inconsistency Problem between Edge Based and Region Based Segmentation
(a) Original image (256-level).
(b) Segmentation result from region based approach.
(c) Edge result from edge based approach.
(d) Mapping image of edges and region boundaries
white lines --- region boundaries not matched with edges
black lines --- region boundaries matched with edges.

PART I

LITERATURE REVIEW

Introduction

To solve the problem described in Part I, a hybrid segmentation approach was developed. It has three stages: (1)PEDBOR stage; (2)LVDSO quantization stage; and (3) a mapping stage.

In Stage I, a new algorithm, called PEDBOR, is used to remove noise and detect edges simultaneously. PEDBOR is the abbreviation of Pixel-Feature-Controlling Edge Detection Based On Regularization. It is an edge detection method based on the regularization model, but has several critical improvements compared with other regularization processing techniques. The improvements are: (1) simple optimization method, (2) a specialized threshold function, (3) classification of pixels based on both magnitude and orientation of the image gradient, (4) the adaptive pixel-feature-controlling regularization procedure. These empower the PEDBOR algorithm to operate without setting parameters, and result in a well-posed and well-conditioned process, that is, robust to noise. By using PEDBOR in Stage I, both noise removed images and edge images with high quality can be obtained. They provide good references for Stage II and Stage III.

In Stage II, a quantization method using an iterative largest-variance-direction-split-optimization (LVDSO) in the histogram domain of the color space is applied to the noise removed image. Here an oversegmenting parameter is used to quantize the noise removed images into initially segmented images. Oversegmenting means producing more segmented regions than there are objects in the original image. Such a parameter setting has two advantages: (1) avoiding the difficulty of setting an exact parameter, and (2) resolving the third problem of inconsistencies mentioned in Chapter 4, namely edges with no boundaries near them. Of course, this incurs an additional computational cost due to

the many false regions in the segmented result. These false regions will be eliminated in Stage III.

Stage III is a mapping procedure. It uses the edge image from Stage I as the reference of true regions, and uses the segmented images from Stage II as the reference of true edges to remove false edges and false regions. The final segmentation images show uniformity, compactness, dissimilarity, and accurate and continuous boundaries.

CHAPTER 5
REGULARIZATION BASICS

In machine vision as well as in most numerical problems, data is noisy. Noise in the phototransduction process is ultimately unavoidable. It is well known that differentiation for edge detection is very sensitive to noise (including noise introduced by digitization). Even a small amount of noise may disrupt the differentiation operation needed for edge detection. Thus edge detection is an ill-posed problem. Well-posedness and numerical stability of the differentiation step require the regularization of image intensity by a regularizing filter operation preceeding differentiation. The regularization provides a general framework to transfer ill-posed problems in the early vision analysis (e.g., edge detection, surface reconstruction, etc.) into well-posed problems by restricting the class of admissible solutions using constraints such as smoothness.

Regularization of the ill-posed problem of reconstructing f from the original data d, such that $Af = d$ can be described as selecting suitable norms $\| \bullet \|$ (usually quadratic) and a stabilizing functional $\| Qf \|$. There are three main methods of standard regularization [Tor 86]:

1) Among the possible f that satisfy $\| Qf \| \leq C_1$, find f that minimizes

$$\| Af - d \| \tag{5-1}$$

2) Among the possible f that satisfy $\| Af-d \| \leq C_2$, find f that minimizes

$$\| Qf \| \tag{5-2}$$

3) Find f that minimizes

$$\| Af - d \|^2 + \lambda \| Qf \|^2 \tag{5-3}$$

where λ is a regularization parameter, and C_1 and C_2 are constants.

The first method consists of finding the function f that satisfies the constraint $\|Qf\| \leq C_1$, and best approximates the original data. The second method computes the function f that is sufficiently close to the data d and is the most "regular", or the most "smoothing". In the third method, the regularization parameter, λ, controls the compromise between the degree of regularization of the solution, that is the smoothness of the f, and its closeness to the original data. If the regularization is viewed as a filter, then λ controls the scale of the filter. In order to keep edges as well as remove noise in an image, the third method is used. The simplest forms for Q are $Q = d/dx$ or $Q = d^2/dx^2$ [Sch 64] [Rei 67]. The choice of the form corresponds to a priori constraint of smoothness on the intensity function to handle discontinuities in the observation or in the reconstructed attribute. In this case, Eq. 5-3 can be written as

$$\int [f(x) - d(x)]^2 dx + \lambda \int [f'(x)]^2 dx \tag{5-4}$$

for $Q = d/dx$.

In the edge detection based on the regularization, edges are viewed as discontinuities with certain height. Thus the edge detection problem can be modeled as an optimization problem that minimizes the membrane energy function

$$E(f,d) = \iint_{\Omega} (f-d)^2 dx dy + \lambda \iint_{\Omega} (f_x^2 + f_y^2) dx dy \tag{5-5}$$

where $f_x = \partial f / \partial x$ and $f_y = \partial f / \partial y$. The function is a variation of Eq. 5-4 in two dimensions. It fits a weak membrane (a weak membrane is a membrane that satisfies weak continuity constraints) to noisy data. The edges are detected by marking the points where discontinuities in the membrane height occur. This regularization model can remove noise or smooth images, and keep discontinuities or detect edges in the image. The trade-off between smoothness and edge detection is controlled by the parameter λ.

To see the effect of λ, we can view the regularization operation as a regularizing filter. If the edges are labeled by detecting the zero crossing of f-d, then it has been proven

that all discontinuities (including edges and noise) with height, S, satisfying equation 5-6 can be kept in f, and others are smoothed [Lee 88].

$$\frac{\lambda * 2v}{\sqrt{2\pi}} \leq S \tag{5-6}$$

where v (> 0) measures the slope away from the discontinuities. From this equation, we can see that the larger the λ, the stronger the smoothing ability and the weaker the ability of keeping discontinuities because the processed image data becomes more regular and retains less fidelity of f to d. Note that keeping discontinuities in the original data d is equivalent to choosing f = d.

To simplify the problem, divide λ into two parts, or let $\lambda = L / \beta$. In the discrete case, by using the difference method and letting $\lambda = L / \beta$, Eq. 5-5 can be written as:

$$E(f,d) = \frac{1}{\beta}\{\sum_{i,j}\beta\ (f_{i,j} - d_{i,j})^2 + \sum_{i,j} L^h_{i,j}(f_{i,j+1} - f_{i,j})^2 + \sum_{i,j} L^v_{i,j}(f_{i+1,j} - f_{i,j})^2\} \tag{5-7}$$

In Eq. 5-7 L is divided into two components, or $L = (L^h, L^v) = \{(L^h_{i,j}, L^v_{i,j})\}$ to control the spatial smoothness and discontinuities of the output image f in both x and y directions. The smoothness varies directly with the magnitude of L. β controls the fidelity of f to d. The first term on the right side of Eq. 5-7 measures the closeness of output data f to the input data d. The second and third terms take into account the price paid whenever a discontinuity is introduced, and thus preventing the creation of discontinuities everywhere.

For such an optimization problem, a suitable optimization method should be used. In standard regularization [Tik 77], L is chosen such that the membrane energy function is a convex function and therefore a standard calculus optimization method is used in optimizing E(f, d). In this way the computation is simplified. However, its problem is the global assumption of smoothness, or setting $L_{i,j}$, by disregarding the discontinuities in the scene of the physical characteristics of edges. This result is ill suited to image deblurring because the rapid growth of E(f, d) as $(f_{i,j+1} - f_{i,j})$ increases inhibits the recovery of large

intensity gradients (thus enforces a strong smoothness), and slow growth of E(f, d) as $(f_{i,j+1} - f_{i,j}) \rightarrow 0$ promotes excessive smoothing. Small intensity differences (or high order analogs) incur a relatively small "penalty". Thus finally the transitions become gradual changes and the solution will be oversmoothed.

To bypass this problem, nonstandard regularization models [Ter 86][Li 90a] introduce a piecewise function called "line process." In these models, L is set to be the line process function, and a new cost factor measuring the line process itself is added into Eq. 5-7. Two popular line process functions are the Boolean function and the sigmoid function defined as follows. The Boolean line process function is

$$L^{h}_{i,j} = \begin{cases} 1 & \text{if } |dx| = |f_{i,j} - f_{i,j-1}| < T \\ 0 & \text{otherwise} \end{cases} \tag{5-8a}$$

$$L^{v}_{i,j} = \begin{cases} 1 & \text{if } |dy| = |f_{i,j} - f_{i-1,j}| < T \\ 0 & \text{otherwise} \end{cases} \tag{5-8b}$$

The sigmoid line process function is

$$L^{v} = 1 - 1/(1 + \exp(-\frac{(f_{i+1,j} - f_{i,j})^2 - T}{A})) \tag{5-9a}$$

$$L^{h}_{i,j} = 1 - 1/(1 + \exp(-\frac{(f_{i,j+1} - f_{i,j})^2 - T}{A})) \tag{5-9b}$$

Graphs of the line process functions are shown in Fig 5-1 and Fig. 5-2. Their basic idea is that when the directional gradient magnitude of the pixel, |dx|, is larger than a threshold T, the $L_{i,j}$ is set to be "Off", otherwise to be "On". The "Off" state means $L_{i,j} = 0$ for Boolean line process function, or $L_{i,j}$ = small value for sigmoid function. The "On" state corresponds $L_{i,j} = 1$ for Boolean line process function, or $L_{i,j}$ = large value for sigmoid function. When the discontinuities have large intensity gradient magnitudes, $L_{i,j}$ is small and the total penalty is still small. Thus the discontinuities with high steps larger than T are

kept and therefore the oversmoothing is relieved. The values of $L_{i,j}$ vary inversely with discontinuity height. The value $L_{i,j} = 1$ leads to the strongest smoothness, and $L_{i,j} = 0$ prevents any smoothing operations. In this way, the line process function controls the smoothness and discontinuities of the solution. The main problems associated with such line process function settings are:

(1) The cost function is not convex, therefore other optimization methods, such as simulated annealing, direct, or relaxation method, are needed to solve the optimization problem. However, the simulated annealing method is computationally expensive, and the other two methods converge only when the penalty term is large, which also generates an oversmoothed solution.

(2) The line process function setting regards the discontinuities only in the scene of discontinuity magnitude, which will cause the following problems:

. All discontinuities which have gradient magnitudes larger than a threshold, T, will be kept no matter whether they are noise or not, and all pixels with gradient magnitudes less than T will be smoothed no matter whether they are true edges or not.

. Setting T is a difficult problem for practical applications.

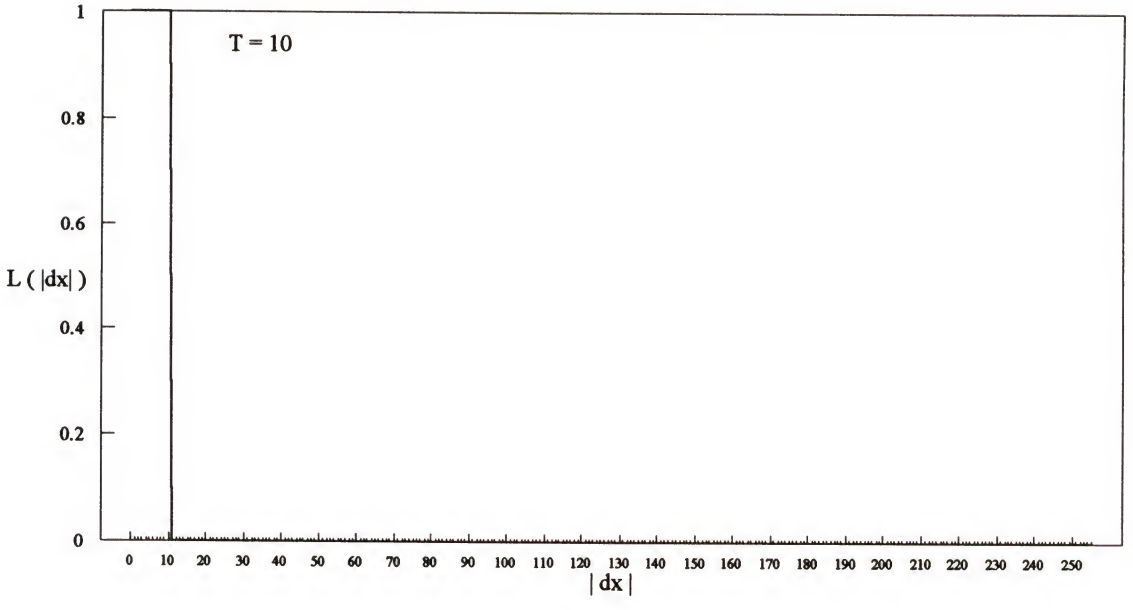

Fig. 5-1 Boolean Line Process Function

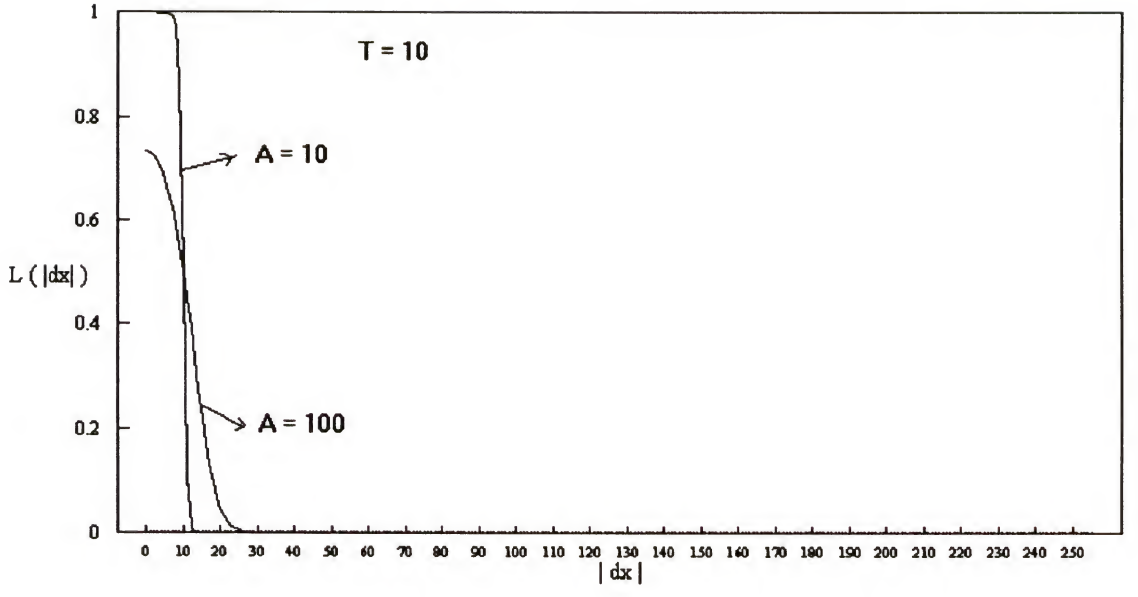

Fig. 5-2 Sigmoid Line Process Function

CHAPTER 6
PEDBOR ALGORITHM

A new algorithm has been developed to solve the problems in traditional regularization procedures. The new algorithm is called PEDBOR, an abbreviation of Pixel-Feature-Controlling Edge Detection Based On Regularization. It uses the same regularization model defined by Eq. 5-5 with a line process function, but has several critical improvements compared with other regularization processing techniques. These improvements are:

(1) Use of a non-interacting line process function in the optimization. This not only makes optimization simple, but also allows employing additional knowledge about the physical nature of edges to control the regularization procedure.

(2) Both magnitude and orientation information of an image gradient are used in classifying image pixels as edge pixels (E-pixels), homogeneous region pixels (HR-pixels), and noise pixels (N-pixels). This information is used to set line process functions.

(3) For the different types of pixels, different line process functions are set based on the desired line process function properties. This prevents the oversmoothing of edges and undersuppression of noise. The other parameter that controls the fidelity of processed images to the original images is also set according to the pixel type. Therefore, the whole regularization course is adaptivelly controlled by pixel features.

(4) In the computation of the line process function and pixel classification, a data driven threshold function is used for all images. This makes threshold setting adaptable and avoids the difficulty of setting a threshold.

PEDBOR detects edges during iterative regularization by finding the discontinuities $L = \{ L_{i,j} \}$ $((i, j) \in pixel_{edge})$ which separate regions with homogeneous properties. Each iteration consists of two main phases: a classification phase and a noise removal phase. In Phase I, pixels are grouped into three categories: edge pixels (E-pixels), homogeneous region pixels (HR-pixels) and noise pixels (N-pixels). The classification criterion uses information about the magnitude of the gradient and the orientation distribution of the gradient in the neighborhood of each pixel. The threshold used in classification is a preset function of image intensity. It has low enough values so that almost all true edges can be detected for most images, as well as a number of extraneous ones. Later these extra edges are pruned by examining their gradient orientations. In Phase II, a regularization process is applied to the pixels to remove noise. During regularization, information obtained from the classification phase is used to activate line processes and to set fidelity-controlling parameters.

6.1. Optimal Update Rule for Minimizing the Cost Function E (f, d)

As mentioned above when line process is introduced into the cost function E(f,d), the standard calculus optimization methods are not suitable to use since the function is not convex. However, if we use the line process function in a non-interactive way, we can still utilize the standard calculus method. Non-interactive way involves two aspects: (1) terms do not interact with each other, (i.e., there is no term for "organizing" the boundaries added to the E(f, d)); and (2) they do not interact with the E(f,d) (i.e., find the minimum of E(f, d) by iteratively finding individual minE(f,d) for each *given* β, $L^h_{i,j}$ and $L^v_{i,j}$). Under this assumption, the optimal update rule for minimizing the function E (f, d) can be obtained by the following analysis.

The membrane energy function E is the functional of f, given d. Now introduce a new variable t into f, or $f = \{ f(x, y, t) \}$. This new variable may be thought of as 'time' indicating the evolution of the Energy function as the data is refined, hence as a function

of 'time'. Thus the E is a function of the parameter t, given f and d. To find the minimum E, we require that the energy E should not increase along the trajectory f (x, y, t) as the system evolves with time, or $dE/dt \leq 0$. A simple dynamic system with characteristic $dE/dt \leq 0$ is determined by the differential equation

$$\frac{\partial f(x,y,t)}{\partial t} = -\rho \frac{\partial E}{\partial f_{i,j}} \tag{6-1}$$

where $\rho > 0$ is a normalization quantity. Thus, a dynamic updating rule for the continuous minimization problem can be obtained by setting the first derivative of the cost function, E(f,d) with respect to $f_{i,j}$ to zero for given β, $L^h_{i,j}$ and $L^v_{i,j}$, or

$$\begin{aligned}\frac{\partial E(f,L)}{\partial f_{i,j}} = \frac{\partial}{\partial f_{i,j}}\{&\beta (f_{1,1}-d_{1,1})^2+....+\beta (f_{i,j}-d_{i,j})^2+....\\ &+L^h_{1,0}(f_{1,1}-f_{1,0})^2+L^v_{0,1}(f_{1,1}-f_{0,1})^2\\ &+L^h_{i,j-1}(f_{i,j}-f_{i,j-1})^2+L^h_{i,j}(f_{i,j+1}-f_{i,j})^2+....\\ &+L^h_{i-1,j}(f_{i,j}-f_{i-1,j})^2+L^v_{i,j}(f_{i+1,j}-f_{i,j})^2+.....\}\\ =0\end{aligned}$$

or

$$\begin{aligned}&\beta(f_{i,j}-d_{i,j})^2+[L^h_{i,j-1}(f_{i,j}-f_{i,j-1})-L^h_{i,j}(f_{i,j+1}-f_{i,j})]\\ &\quad+[L^v_{i-1,j}(f_{i,j}-f_{i-1,j})-L^v_{i,j}(f_{i+1,j}-f_{i,j})]=0\end{aligned}$$

By rearranging this equation, the optimal update rule for minimizing the function E (f, L) is as follows:

$$f^{t+1}_{i,j} = (L^h_{i,j}f^t_{i,j+1}+L^h_{i,j-1}f^t_{i,j-1}+L^v_{i,j}f^t_{i+1,j}+L^v_{i-1,j}f^t_{i-1,j}+\beta_{i,j}d_{i,j})/\Lambda \tag{6-2a}$$

and

$$\Lambda = (L^h_{i,j}+L^h_{i,j-1}+L^v_{i,j}+L^v_{i-1,j}+\beta_{i,j}) \tag{6-2b}$$

From the last formula we can see that $f^t_{i,j}$ in the $(t+1)^{th}$ iteration is in fact equal to the weighted average of its four neighbors plus the effect of input data, $d_{i,j}$. The weights

are just equal to the values of $L_{i,j}$. Fig. 6-1 shows the relationship of Eq. 6-2a. The larger the $L_{i,j}$, the stronger the smoothness. If $L^{h}_{i,j} = 0$, no smoothness will be allowed, and at the same time a discontinuity/edge is signaled at site (i, j). Now we can determine L and β based on the knowledge of the physical properties of different data types without affecting the generalization of the problem. That is, the regularization procedure can be adaptivelly controlled by additional knowledge about the physical nature of the edges to get better results.

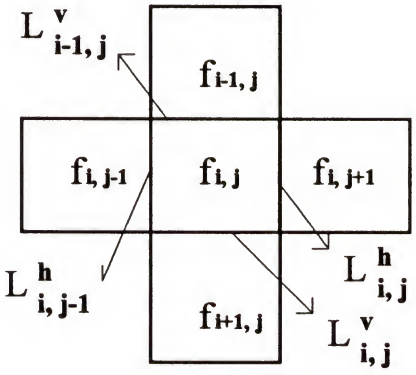

Fig. 6-1 The 4-connectivity Neighborhood Used in the Update Rule.

6.2. JND Threshold Function

An additional improvement is the JND threshold function. JND means "just noticeable difference". It is well known that the human eye possesses different capabilities for luminance discrimination under different background conditions. The visual threshold is lower in the medium gray region and much higher in the very bright and dark regions. One research result [Wan 91] shows that the JND of luminance depends on the background luminance intensity, and puts forth a JND threshold function defined by the following formula:

$$T(i,j)=\begin{cases} 2*(-0.85\, I_{i,j}+40) & \text{for } 0\le I_{i,j}\le 40 \\ 12 & \text{for } 40\le I_{i,j}\le 100 \\ 2*(0.09\, I_{i,j}-3) & \text{for } 100\le I_{i,j}\le 255. \end{cases}$$

The numeric values in the above expression depend on monitor settings and vary depending on the hardware employed, but they may be adapted to a standardized setup. In this dissertation a monitor setting was used that allowed the maximum intensity just at the maximum light-level of the display CRT. By examining many standard gray level and color images, a modified JND threshold function was developed. It is more suitable to PEDBOR algorithm:

$$T(i,j)=\begin{cases} -0.5\, I_{i,j}+38 & \text{for } 0\le I_{i,j}\le 64 \\ 6 & \text{for } 64\le I_{i,j}\le 160 \\ 0.05\, I_{i,j}-2 & \text{for } 160\le I_{i,j}\le 255 \end{cases} \qquad (6\text{-}3)$$

where $I_{i,j}$ is the representative intensity value of a pixel at site (i, j). For noiseless images, $I_{i,j}$ is equal to $f_{i,j}$. For noisy images, $I_{i,j}$ is the average intensity of pixels in (i, j)'s neighborhood, or

$$I_{i,j}=\frac{1}{9}\sum_{k=-1}^{1}\sum_{l=-1}^{1} f_{i+k,j+l}. \qquad (6\text{-}4)$$

The difference between original function and modified function can be seen easily from Fig. 6-2. Such a threshold function is data driven. Since the modified function has low values, it can be used for most pictures without missing of true edges. Of course, it also gives rise to many false edges. To eliminate the false edges, the pixel-feature-controlling regularization is needed.

6.3. Classifying Pixels

To suppress noise and preserve true edges, identifying them is the key point in the algorithm. In the previous nonstandard regularization approach, pixels are just classified as edge pixels and non-edge pixels by using only magnitude information of the image

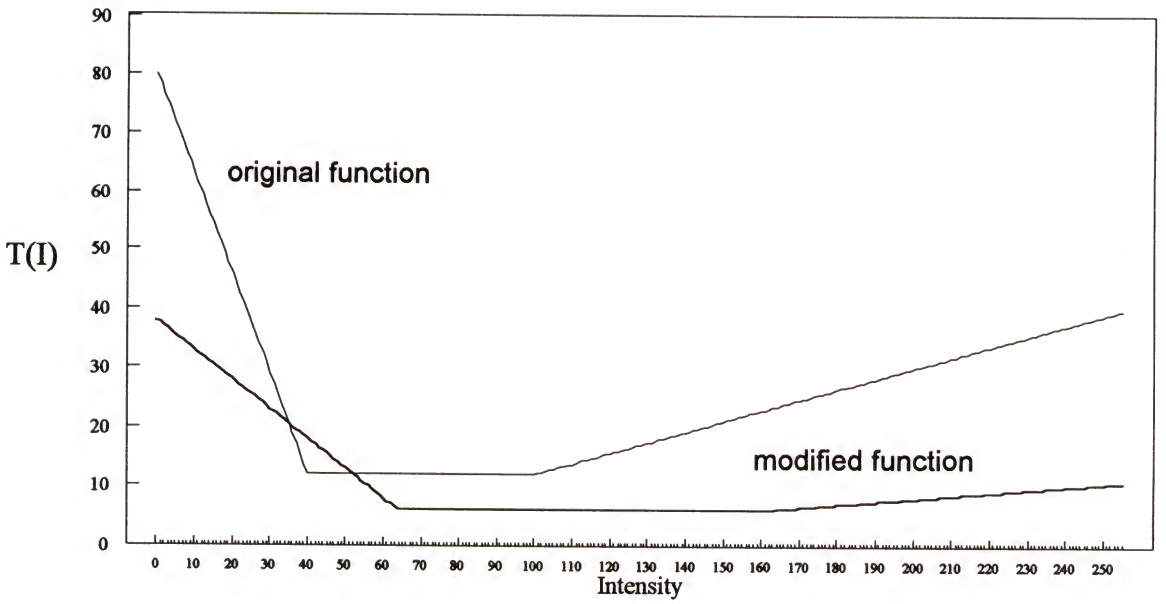

Fig. 6-2 JND Threshold Function

gradient. Unfortunately, magnitude information of the image gradient is not enough to identify the true edge pixels and noise pixels since noise pixels also have a large gradient magnitude. Hence, PEDBOR utilizes both magnitude and orientation information of the image gradient and edge structure information to classify image pixels.

Gradient information needed in classifying pixels can be calculated in the following manner: the gradients of pixel (i, j) in horizontal direction and in vertical direction are

$$dx(i,j) = (f_{i,j+1} - f_{i,j-1})/2 \tag{6-5a}$$

$$dy(i,j) = (f_{i+1,j} - f_{i-1,j})/2 \tag{6-5b}$$

respectively; the gradient magnitude and orientation of pixel (i, j) are

$$|\, dx\,(i,j)\,|,\ |\, dy\,(i,j)\,| \tag{6-6a}$$

$$GO(i,j) = QUA[\tan^{-1}(dx(i,j)/dy(i,j)] \tag{6-6b}$$

respectively. In the above, QUA[.] means quantizing the continue "arctan" operation value into one of the equally divided orientation zone values. For example, an 8--orientation zone has 8 different values: 0, 45, 90, 135, 180, 225, 270, 315 and 360 degrees (see Fig. 6-3).

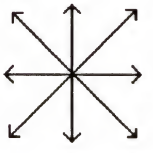

Fig. 6-3 8-orientation Zone of GO

For an n*n pixel region, we can identify it as a constant intensity, a noisy, or an edge-containing one by analyzing the distribution of GO(i, j) ((i, j) the n * n neighborhood). Regions with a unique orientation are constant intensity ones. Regions with two or a few more strong orientations may contain several line fragments in different directions, such as a curve, a corner or line crossing. Regions with equal orientation scores

in many directions are noisy regions. Fig. 6-4 shows the GO distributions of different regions.

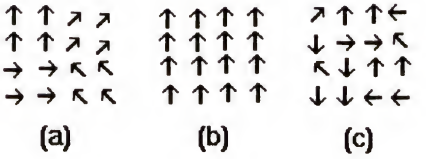

Fig. 6-4 GO Distributions of Different Regions.
(a) An edge-containing region.
(b) A constant intensity region.
(c) A noisy region.

Besides using gradient information of images, we also use the physical structure information of edges. Considering that edges are the boundary of different regions, they must have certain structures. In other words, some edge structures are forbidden. In our application, the edge structures shown in Fig. 6-5 and their rotations in any direction are forbidden. Edges with length less than 3 pixels are also forbidden.

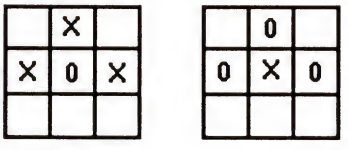

Fig. 6-5 Forbidden Edge Structures
x--edge pixel. 0--non-edge pixel. blank--edge or non-edge pixel.

Based on the analysis above, we can obtain the following classification rule:

. pixel (i, j) is an E-pixel if $|dx(i, j)| \geq T(I_{i,j})$ or $|dy(i, j)| \geq T(I_{i,j})$, GO(i, j)'s ($(i, j) \in$ n*n neighborhood) have less than 4 directions (for small noise image less than 5) and (i, j) is not a forbidden edge pixel;

. pixel (i, j) is an HR-pixel if $|dx(i, j)| < T(I_{i,j})$ and $|dy(i, j)| < T(I_{i,j})$;

. pixel (i, j) is a noise pixel (N-pixel) if it is neither an E-pixel nor an HR-pixel.

6.4. Setting the Line Process Function

We have seen the problems caused by standard regularization and nonstandard regularization with Boolean and sigmoid line process functions. These line process function settings do not consider the characteristics of different pixels. That is, they do not satisfy the properties of a desired line process function. A desired line process function should have the following properties:

. For noise pixels, the larger the noise, the larger the values of the line process functions and therefore the stronger the smoothness;

. For those intensity regions which are more sensitive to noise, the function should have high values (note that regions with high ability of luminance discrimination are also more sensitive to noise);

. For true edge pixels, the function value should be zero to inhibit any smoothness.

Besides, the selection of the line process function must guarantee the stability of the iteration process.

Based on these properties, a set of line process functions is established in PEDBOR according to the pixel types. For noise pixels, the line process function is defined as:

$$L^{h}_{i,j} = \begin{cases} \dfrac{1}{(1+\exp(-|dx|/T(I_{i,j})))} & \text{if } |dx| \geq T(I_{i,j}) \\ 1-\dfrac{1}{(1+\exp(T(I_{i,j})-|dx|))} & \text{otherwise} \end{cases} \qquad (6\text{-}7a)$$

$$L^{v}_{i,j} = \begin{cases} \dfrac{1}{(1+\exp(-|dy|/T(I_{i,j})))} & \text{if } |dy| \geq T(I_{i,j}) \\ 1-\dfrac{1}{(1+\exp(T(I_{i,j})-|dy|))} & \text{otherwise} \end{cases} \qquad (6\text{-}7b)$$

For edge pixels, the line process function is set as:

$$L_{i,j}^{h} = \begin{cases} 0 & \text{if } |dx| > T(I_{i,j}) \\ 1 - \dfrac{1}{(1+\exp(T(I_{i,j}) - |dx|))} & \text{otherwise} \end{cases} \tag{6-8a}$$

$$L_{i,j}^{v} = \begin{cases} 0 & \text{if } |dy| > T(I_{i,j}) \\ 1 - \dfrac{1}{(1+\exp(T(I_{i,j}) - |dy|))} & \text{otherwise} \end{cases} \tag{6-8b}$$

For homogeneous region pixels, the line process function has the following form:

$$L_{i,j}^{h} = 1 - \frac{1}{(1+\exp(T(I_{i,j}) - |dx|))} \tag{6-9a}$$

$$L_{i,j}^{v} = 1 - \frac{1}{(1+\exp(T(I_{i,j}) - |dy|))} \tag{6-9b}$$

The corresponding curves of these line processes are shown in Fig. 6-6. In the figure, (a) and (b) correspond to the line process function for noise pixels, (c) to one for edge pixels, and (d) to one for homogeneous pixels. The curve in Fig. 6-6 (a) is with respect to the magnitude of the pixel gradient. We can see that the larger the magnitude, that is the stronger the noise, the larger the function value and therefore the stronger the smoothness. Fig. 6-6 (b) is with respect to the intensity level. From this curve, we can see that the region which is most sensitive to noise, or intensity levels between 64 and 160, has the highest function values. The other two line process functions satisfy the desired properties also.

As mentioned before, the regularization parameter, $\lambda = L / \beta$, automatically controls the scale of the filter if the regularization is viewed as a filter. Thus, such a setting for line process functions is equivalent to form a scale space adaptivelly adjusted by pixel

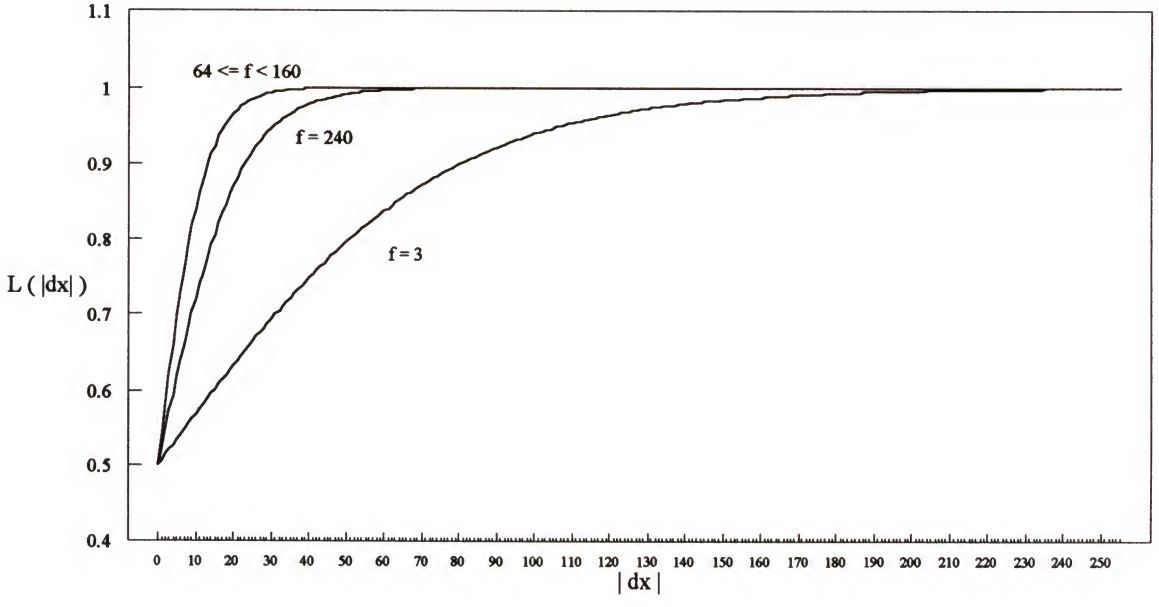

(a) Line Process Function for Noisy Pixels with Respect to the Magnitude of the Pixel Gradient.

Fig. 6-6 Line Process Functions

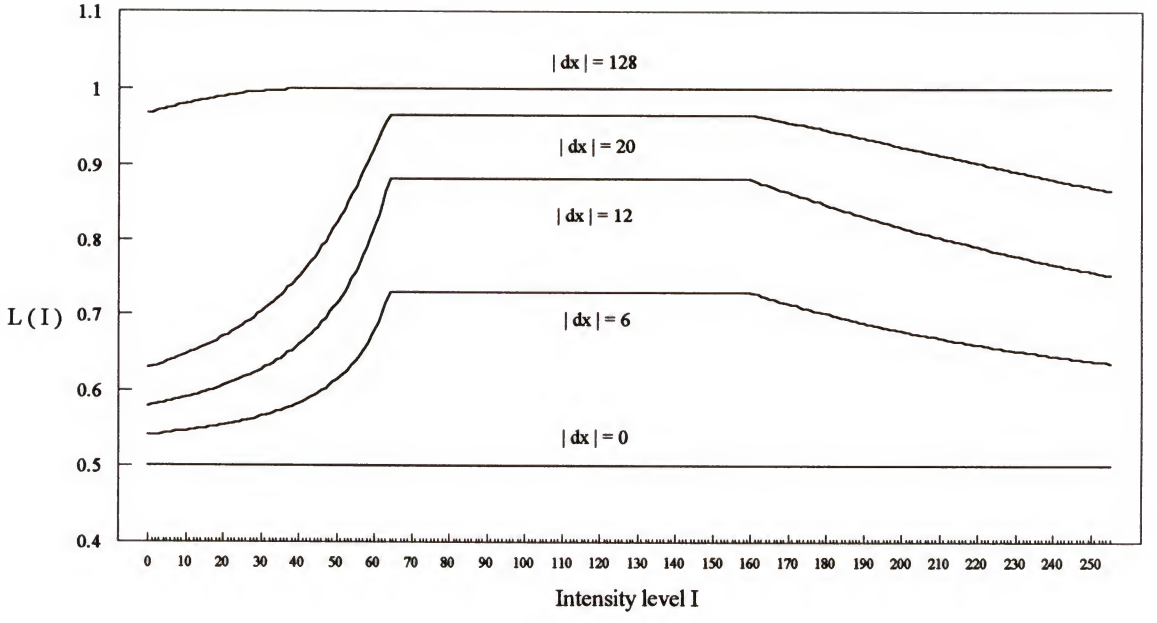

(b) Line Process Function for Noisy Pixels with Respect to the Intensity Level.

Fig. 6-6 Continued

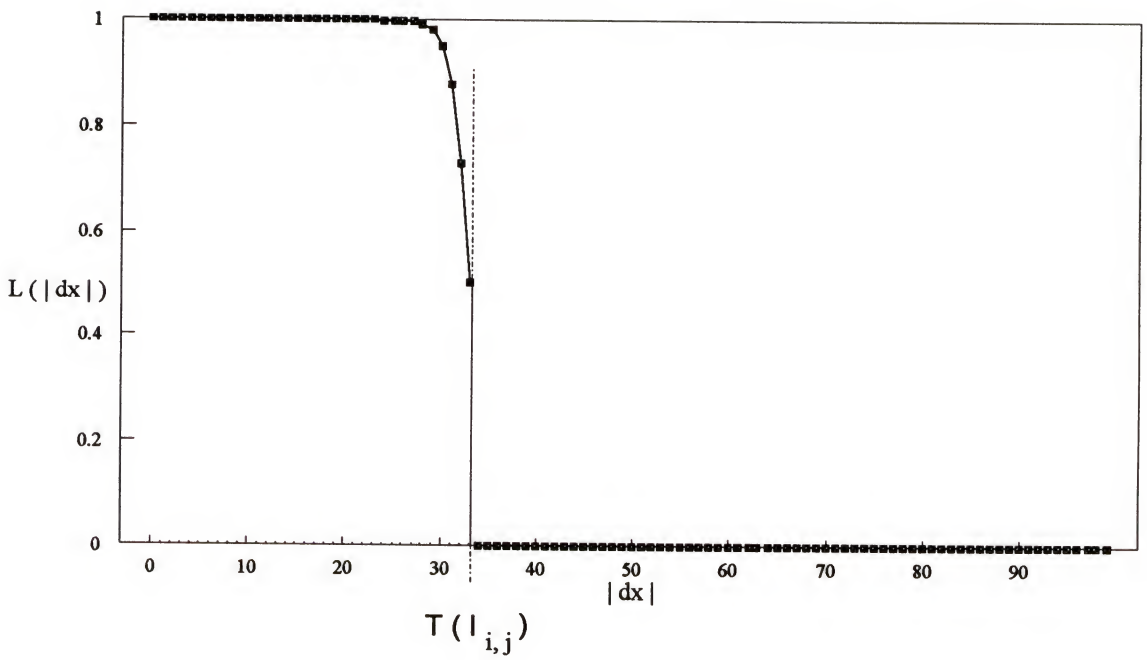

(c) Line Process Function for Edge Pixels.

Fig. 6-6 Continued

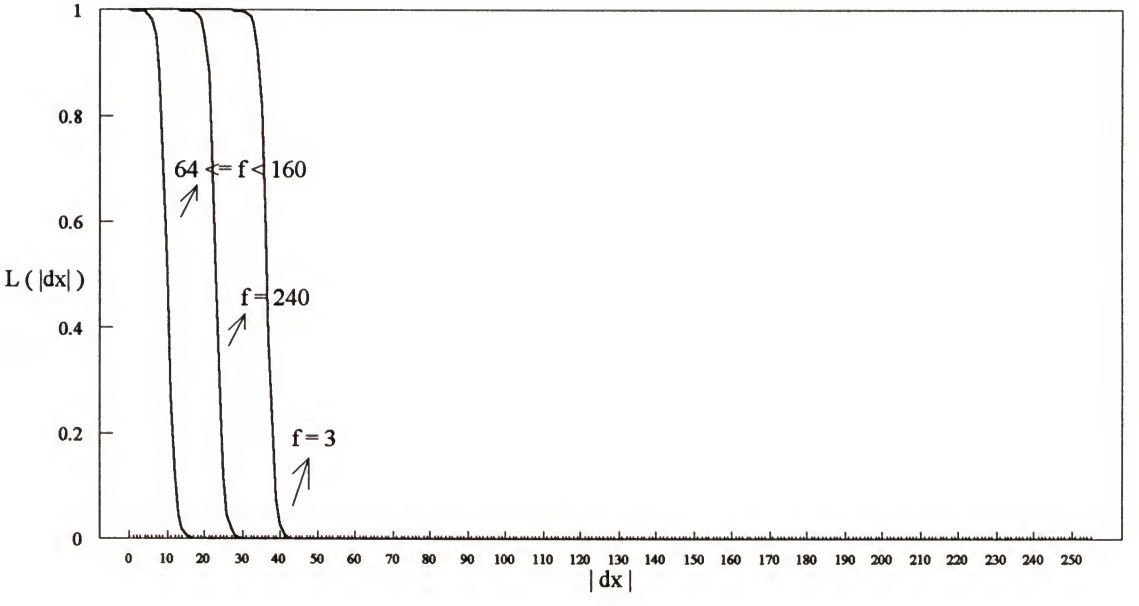

(d)Line Process Function for Noisy Pixels

Fig. 6-6 Continued

characteristics. Is it a useful scale space? The analysis in section 6-6 will answer this question.

6.5. Implementation of PEDBOR

The PEDBOR can be implemented by iteratively following the steps below.

Step 1. Initialize $f = d$.

Step 2. Calculate $T(I_{i,j})$ for each pixel using Eqs 6-3 and 6-4.

Step 3. Classify each pixel using Eqs. 6-5 and 6-6, and the classification rule.

Step 4. Calculate line process values using Eqs. 6-7 to 6-9 and set the parameter $\beta_{i,j}$ as follows:

$$\beta_{i,j} = \begin{cases} 0.01 & \text{for HR-pixel and E-pixel} \\ 0.001 & \text{for N-pixels.} \end{cases}$$

Step 5. Calculate new $f_{i,j}$ using Eq. 6-2.

Step 6. Repeat step 2 to step 5 until $|N^{t+1}_{E-pixel} - N^{t}_{E-pixel}| < \varepsilon$ ($N^{t}_{E-pixel}$ is the number of E-pixels in the t th iteration) or iteration times are larger than a predetermined number.

Step 7. Scan in line process domain and label a pixel at site (i, j) as an edge pixel if $|dx(i, j)| > T(f_{i,j})$ or $|dy(i,j)| > T(f_{i,j})$.

6.6. Analysis of PEDBOR

In this section we present properties of PEDBOR, such as stability, smoothing and edge keeping ability, and iterative behavior. For simplicity, the 1-D signal case is used, and the dependencies on the input data are ignored, that is let $\beta = 0$.

6.6.1. Stability of PEDBOR

The stability problem concerns the unbounded growth or the controlled decay or boundness of the exact solution of the finite-difference equations. The essential criterion defining stability is that the numerical process should limit the amplification of all effects due to initial conditions.

The iterative process of PEDBOR represented by Eq. (6-2) can be written in matrix form as follows:

$$\underline{f}_{t+1}=A_t \underline{f}_t +\underline{d} \tag{6-10a}$$

where A, called iteration matrix, is an N*N matrix of known elements. It is defined by

$$A_t=\begin{bmatrix} \cdots & \cdots & \cdots & \cdots & \cdots & \cdots & \cdots \\ \cdots & 0 & \dfrac{L_{x-2}}{L_{x-2}+L_{x-1}} & \dfrac{L_{x-1}}{L_{x-2}+L_{x-1}} & 0 & \cdots & \cdots \\ \cdots & \cdots & 0 & \dfrac{L_{x-1}}{L_{x-1}+L_x} & \dfrac{L_x}{L_{x-1}+L_x} & 0 & \cdots \\ \cdots & \cdots & \cdots & \cdots & \cdots & \cdots & \cdots \end{bmatrix} \tag{6-10b}$$

N is the number of data points. In order for the process to be stable, for some norm, A_t must satisfy

$$\|A_t\| \le 1 \qquad \text{for } \forall\, t \tag{6-11}$$

so that a general property of the definition of a norm follows that:

$$\|A_{n-1}A_{n-2} \cdots A_1A_0\| \le \|A_{n-1}\|\,\|A_{n-2}\| \cdots \|A_1\|\,\|A_0\| \le 1 \tag{6-12}$$

for n iterations.

The infinity norm of a matrix is simply the maximum sum of the moduli of the elements of the matrix. Since the values of the line process function, L_x, are always positive, the infinity norm of our iteration matrix is unity because

$$\|A_t\|_\infty = \frac{L_{x-1}}{L_{x-1}+L_x}+\frac{L_x}{L_{x-1}+L_x}=1 \tag{6-13}$$

In addition, the largest moduli of the eigenvalues of the square matrix cannot exceed its infinity norm, i.e.,

$$\rho(A) \leq \|A_t\|_\infty \tag{6-14}$$

which means that the 2-norm of A_t is also bounded by unity. Therefore, the adaptive iteration process is stable, since $\|A_t\| \leq 1$ is always guaranteed during the iterative process.

6.6.2. The Ability of Smoothing and Edge Keeping.

The smoothness of the image and the detection of edges in the results of PEDBOR are controlled by line process functions. In order to observe the effects of our line process functions or the abilities of edge smoothness and edge keeping of PEDBOR, we evaluate the term $\frac{d}{dt}(|\frac{df}{dx}|)$ which represents the change of gradient or contrast $|\frac{df}{dx}|$ along the iteration measure dimension (t). If $\frac{d}{dt}(|\frac{df}{dx}|) > 0$, the gradient magnitude will increase as the iteration progresses, achieving a discontinuity sharpening effect. If $\frac{d}{dt}(|\frac{df}{dx}|) = 0$, the discontinuity step is kept. If $\frac{d}{dt}(|\frac{df}{dx}|) < 0$, then gradient magnitude will be smaller and smaller as iterations progress and the discontinuities will be smoothed eventually. Therefore, the following relation should be satisfied:

$$\frac{d}{dt}(|\frac{df}{dx}|)\begin{cases} < 0 & \text{for noise or homogeneous pixels} \\ \geq 0 & \text{for edge pixels} \end{cases} \tag{6-15}$$

By exchanging the order of the differentiation, Eq. (6-15) can be rewritten as:

$$\frac{d}{dt}(|\frac{df}{dx}|) = \begin{cases} \frac{d}{dt}(\frac{df}{dx}) = \frac{d}{dx}(\frac{df}{dt}) & \text{if } \frac{df}{dx} > 0 \\ -\frac{d}{dt}(\frac{df}{dx}) = -\frac{d}{dx}(\frac{df}{dt}) & \text{if } \frac{df}{dx} < 0 \end{cases} \tag{6-16}$$

We can get the solution of Eq. (6-16) by first finding df/dt. We find df/dt by the following analysis.

Recalling Eq. (6-2), PEDBOR can be viewed as an iterative weighted averaging process. In 1-D case, Eq. (6-2) can be reformulated as:

$$f^{t+1}(x) = C^t(x) * f^t(x-1) + C^t(x+1) * f^t(x+1) \tag{6-17a}$$

with

$$C^t(x) + C^t(x+1) = 1 \quad \text{and} \quad 0 \le C^t(x), C^t(x+1) \le 1$$

to guarantee the stability of the iterative process. In the equation,

$$C^t(x) = \frac{L^t(x)}{L^t(x)+L^t(x+1)}, \quad C^t(x+1) = \frac{L^t(x+1)}{L^t(x)+L^t(x+1)} \tag{6-17b}$$

Rewrite Eq. (6-17a) as follows:

$$\begin{aligned} f^{t+1}(x) - f^t(x) &= C^t(x) * f^t(x-1) + C^t(x+1) * f^t(x+1) - f^t(x) \\ &= C^t(x+1) * [f^t(x+1) - f^t(x)] - C^t(x) * [f^t(x+1) - f^t(x)] \\ &= \frac{L^t(x+1) * [f^t(x+1) - f^t(x)] - L^t(x) * [f^t(x+1) - f^t(x)]}{L^t(x+1)+L^t(x)} \end{aligned}$$

that is

$$\frac{\partial f}{\partial t} = \frac{1}{L^t(x+1)+L^t(x)} \nabla(L \nabla f) \tag{6-18}$$

where $\nabla = \frac{\partial}{\partial x}$ corresponding to the differentiation in the spatial domain. Here $L^t(x+x) + L^t(x) > 0$. Eq. (6-18) can be represented as:

$$\frac{df(x,t)}{dt} = \frac{1}{L(x+1,t)+L(x,t)} \{\frac{d}{dx}[L(x,t)\frac{df(x,t)}{dx}]\} \tag{6-19}$$

Note that we will denote df(x)/dx as $f_x(x)$ in the following.

Plugging Eq. (6-19) into Eq.(6-16), we can get:

$$\frac{d}{dt}(\frac{df}{dx}) = \frac{d}{dx}(\frac{df}{dt}) = \frac{d}{dx}\{\frac{1}{L(x+1,t)+L(x,t)}\frac{d}{dx}[L(x,t)f_x(x,t)]\}$$
$$= \frac{L_{xx}(x,t)f_x(x,t)+2L_x(x,t)f_{xx}(x,t)+L(x,t)f_{xxx}(x,t)}{L(x+1,t)+L(x,t)}$$
$$+ [L_x(x,t)f_x(x,t)+L(x,t)f_{xx}(x,t)]* \frac{d}{dx}[\frac{1}{L(x+1,t)+L(x,t)}] \quad (6\text{-}20)$$

Usually, we model a discontinuity in a real image as a step function blurred by the lowpass property of equipment. Fig 6-7 shows the profiles of such discontinuities. For profile (a), at the location of the discontinuity, $f_x > 0$ and $f_{xxx} << 0$. For figure (b), $f_x < 0$, and $f_{xxx} >> 0$. At the point of inflection, $f_{xx} = 0$ since the inflection point corresponds to the point with maximum slope. Under the settings of the line process function of PEDBOR, $L_x = 0$ because $f_{xx} = 0$.

The following relations could be obtained by using Eq. (6-20) and corresponding line process functions. If the discontinuity is caused by noise, which has L(x, t) of Eq. (6-7),

$$\frac{d}{dt}(|\frac{df}{dx}|) = -\frac{L(x,t)|f_{xxx}(x,t)|}{L(x+1,t)+L(x,t)}[1+\frac{L(x,t)|f_x(x,t)|}{T}\exp(-\frac{|f_x(x,t)|}{T})] < 0 \quad (6\text{-}21)$$

where T is the threshold. If the discontinuity corresponds to a homogeneous pixel, for which L(x,t) is represented by Eq. (6-9),

$$\frac{d}{dt}(|\frac{df}{dx}|) = -\frac{L(x,t)|f_{xxx}(x,t)|}{L(x+1,t)+L(x,t)}(1-\frac{|f_x|}{1+\exp(T-|f_x|)}) \quad (6\text{-}22)$$

If the discontinuity corresponds to an edge pixel, then

$$\frac{d}{dt}(|\frac{df}{dx}|) = \begin{cases} \frac{L(x,t)|f_{xxx}(x,t)|}{L(x+1,t)+L(x,t)}(\frac{T}{2}-1) & \text{for } |f_x(x,t)| = T \\ 0 & \text{for } |f_x(x,t)| > T \end{cases} \quad (6\text{-}23)$$

Note that in PEDBOR, $T_{min} = 6$.

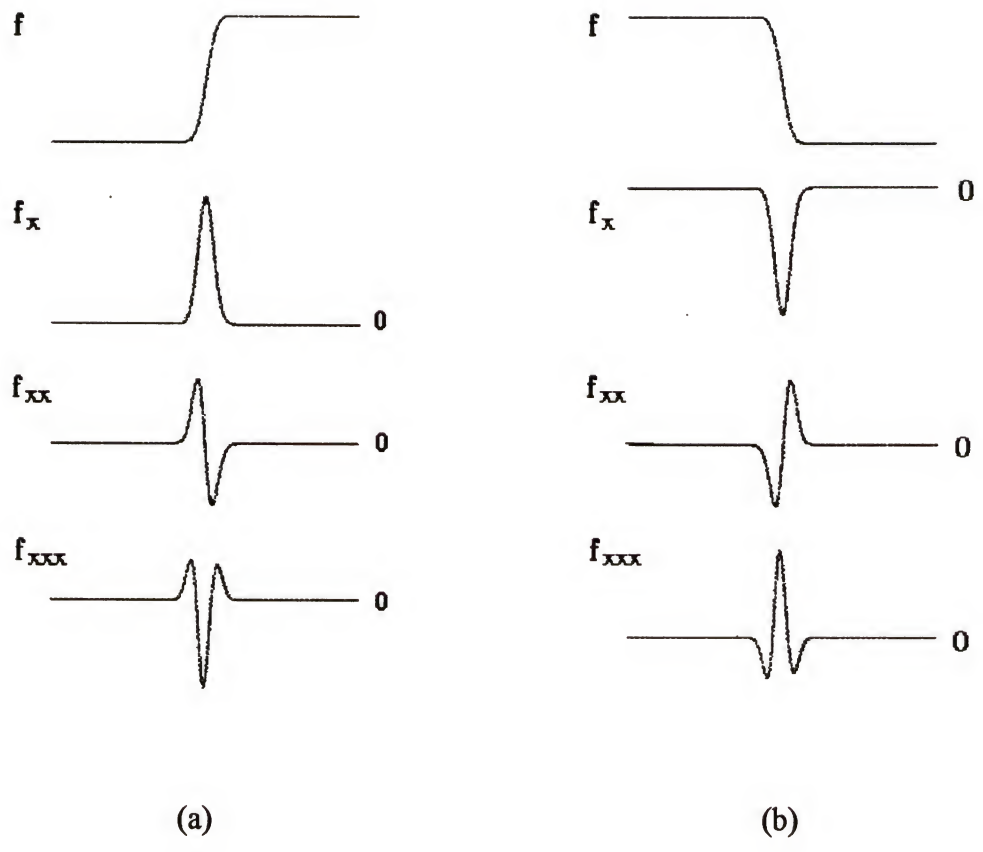

Fig. 6-7 Profiles of a Discontinuity.

From Eq. (6-21), (6-22) and (6-23), we can obtain the following conclusions. (1) For noise pixels, $\frac{d}{dt}(|\frac{df}{dx}|) < 0$ and also the larger the noise the larger the L(x,t), and therefore the larger the magnitude of $\frac{d}{dt}(|\frac{df}{dx}|)$, which causes a stronger and quicker smoothness. (2) For homogeneous pixel, whether $\frac{d}{dt}(|\frac{df}{dx}|) > 0$ or not will depend on the factor $1 - \frac{|f_x|}{1+\exp(T-|f_x|)}$. Fig 6-8 shows the curve of the factor. From it we can see that $\frac{d}{dt}(|\frac{df}{dx}|) < 0$ when $|f_x| < T$. (3) All edges with $|f_x| = T$ are sharpened because $\frac{d}{dt}(|\frac{df}{dx}|) > 0$, and other edges with $|f_x| > T$ are kept since $\frac{d}{dt}(|\frac{df}{dx}|) = 0$. These results agree with the properties of the desired line process functions described in the beginning of section 6.4.

Note that the sigmoid line process function used by some previous regularization algorithms has the $\frac{d}{dt}(|\frac{df}{dx}|)$ defined as:

$$\frac{d}{dt}(|\frac{df}{dx}|) = C * L(x,t) f_{xxx}(x,t)[1 - \frac{2 * f_x^2(x,t)}{1+\exp(T-f_x^2(x,t))}] \qquad (6\text{-}24)$$

where C is a constant.

The curve of the sigmoid line process function is shown in Fig. 6-9. It is evident that the $\frac{d}{dt}(|\frac{df}{dx}|)$ is not larger than zero for those discontinuities with the $|f_x|$'s which are not large enough to make $L(x,t) \cong 0$ even though the discontinuities correspond to true edges. On the other hand, when the discontinuities are very large so that the $L(x,t) \cong 0$, forbidding smoothness, they will be kept even though they are caused by noise. For Boolean line process function,

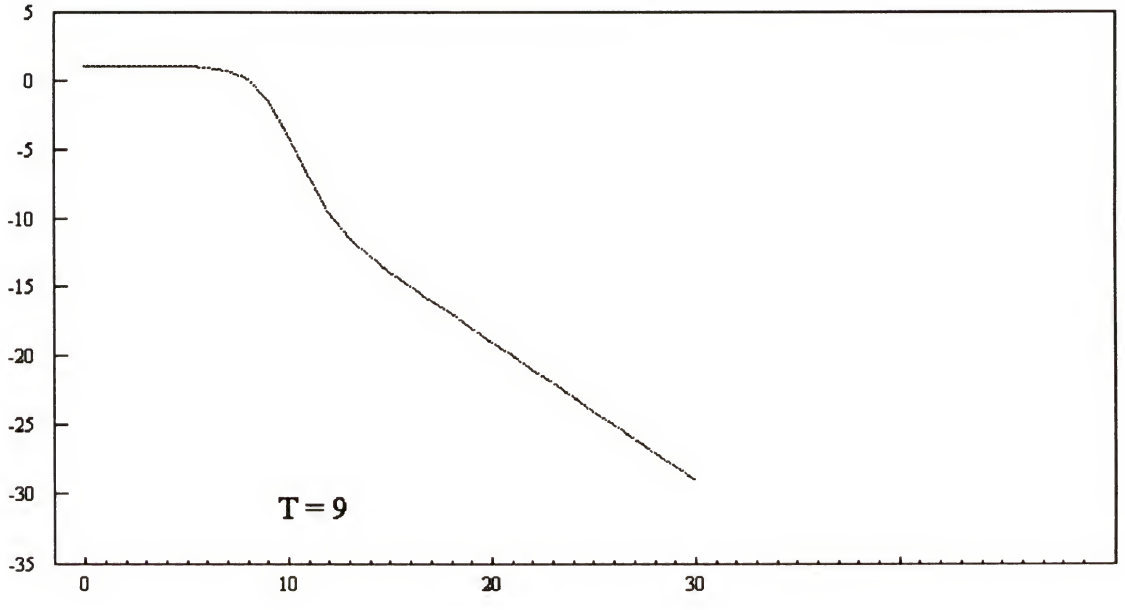

Fig. 6-8 The Curve of $1 - \dfrac{|f_x|}{1+\exp(T-|f_x|)}$

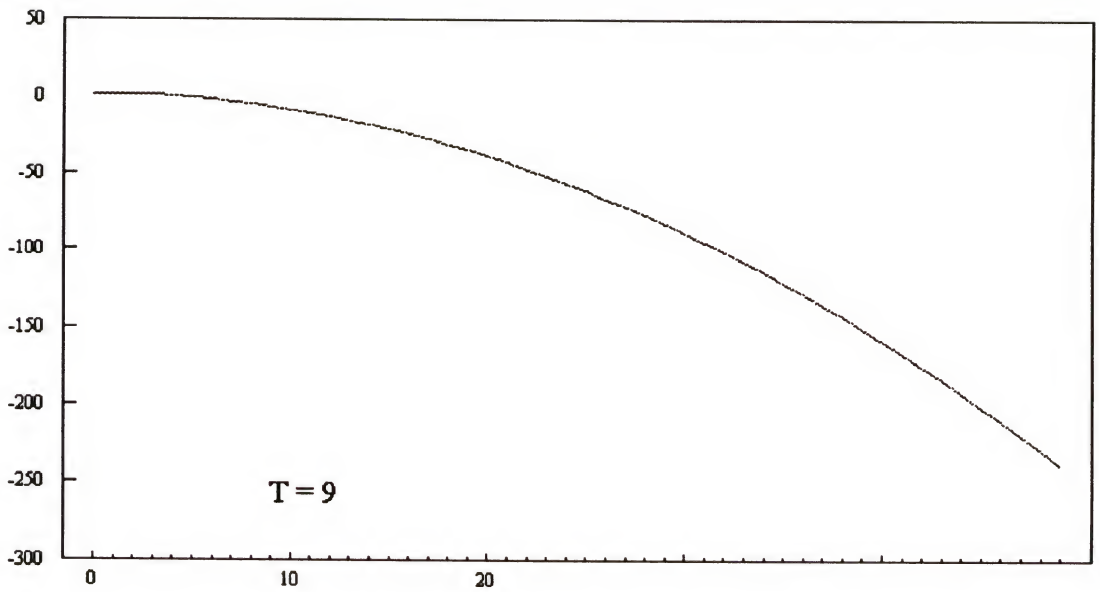

Fig. 6-9 The Curve of $1 - \dfrac{2 * f_x^2(x,t)}{1 + \exp(T - f_x^2(x,t))}$

$$\frac{d}{dt}(\left|\frac{df}{dx}\right|)=\begin{cases} -|f_{xxx}(x,t)| & \text{if } |f_x(x,t)| \geq T \\ 0 & \text{otherwise} \end{cases} \quad (6\text{-}25)$$

which will keep all discontinuities with $|f_x(x)| \geq T$, and smooth other ones.

6.6.3. Iterative Behavior

Theoretically, the termination criterion of the implementation of PEDBOR should be the convergence, that is, no pixel value changes in the final output will occur in a new iteration. In this case, the resulting image consists of piecewise constant regions. However, this needs extremely large number of iterations. It is important to realize that there are two different operations affecting the images as the iteration proceeds: one is the detecting of edges that will survive, the other is the smoothing of regions, i.e., noise removal. For edge detection, 50 iterations have been found to be enough for the types of images that are subject of this work. For noise removal, more iterations lead to better results. A comprise iteration number is 100.

PEDBOR will generate two output images. One is an edge image consisting of edge segments which are thick and not continuous but have accurate positions and fewer missing and false elements. The other is a noise removed image consisting of regions with small spatial variation. Instead of using a great many iterations to get the constant region image and using thinning algorithms and connecting algorithms to get thin and continuous edges, our hybrid segmentation approach generates constant regions in Stage II (quantizing noise removed images to regions,) and forms thin and continuous boundaries in Stage III (mapping the edge image with the region image result from the second stage of this hybrid approach.)

6.7 Practical Considerations in the Implementation of the PEDBOR

6.7.1. Use of a Lookup Table for Speed Up

In PEDBOR, to calculate the gradient orientation of a pixel, the arctan operation is applied on each pixel in each iteration. The calculation of the arctan is very time consuming. For example, on an IBM PS2-80/386, each arctan calculation needs 205 μs. Thus an image of 512*512 pixels will take 90 minutes for just the arctan calculations in the 100 iterations. A lookup table can be used to speed up this calculation. Recall Eq. (6-6b) for computation of gradient orientation; we can see that for a 256-level image, the lookup table has 512 * 512 = 262,144 entries (512 for x-direction and 512 for y-direction). Thus 263 kb extra storage is needed for a software implementation. When the algorithm is implemented under Windows environment, the lookup table can be preloaded into an addressed memory and all entries are directly accessible. In this case, the time of searching for the entries becomes neglibile and the time for arctan calculations is reduced to the time of loading the lookup table. Under memory limited environments, although the lookup table can be stored in several separated data segments, the lookup table is usually not preloaded into memory but on the hard disk with a file-open status. In this case, various fast search strategies can be used for entry search. To reduce the storage and speed up the search operation, the lookup table with 262144 entries can be modified to one with fewer entries by combining triples with the same orientation values. After eliminating the redundancy in both x-direction and y-direction, the number of entries can be reduced to 1529, and the storage size can be reduced from 263 kb to 30 kb. Table 6-1 in Appendix A gives the modified lookup table.

6.7.2. Implement PEDBOR Block by Block

When image processing algorithms are implemented on the PC and under non-Windows environment, an image must be divided into blocks and processed block by

block because of the limitation of memory size (usually, each data segment cannot exceed 64 kb, and total data segment is limited to 640 kb, dependent on the memory model being used). In this case, block effects, such as artificial edges between blocks, the missing of those edges located at four block boundaries, intensity non-consistency of adjacent blocks, etc., may occur in the output images. To prevent these block effects, block overlap is necessary. The overlap size must be suitable since block sizes not large enough to overlap can't eliminate block effects and too large an overlap size increases the redundancy of operations. Usually, a minimum overlap size is adopted. For the PEDBOR algorithm, the minimum overlap size is 3 on each side (see Fig. 6-10), 1 for gradient operation, 1 for edge structure mapping, and 1 for regularization operation. For efficiency, the block size should be as large as possible, dependent on the memory size.

6.7.3. A Consideration for Parallel Implementation of the Algorithm.

The algorithm can be implemented in parallel in task based or block based parallel scheme. The former assigns different processors to different tasks, such as edge information calculation, edge structure mapping, and regularization. The latter assigns different processors for each subimage block. During parallel implementation, synchronizing must be set in each iteration cycle for the block based scheme as well as for the task based scheme. In many algorithms, no synchronization is necessary during iterations. The operations are applied on every block in the whole iteration without interactive information propagation between adjacent blocks. By setting synchronization in each iteration, blocks are merged after each iteration and redivided for each new iteration, and therefore the modified information of each block in the last iteration will be propagated by the overlap pixels. In this way, intensity inconsistency between adjacent blocks can be prevented.

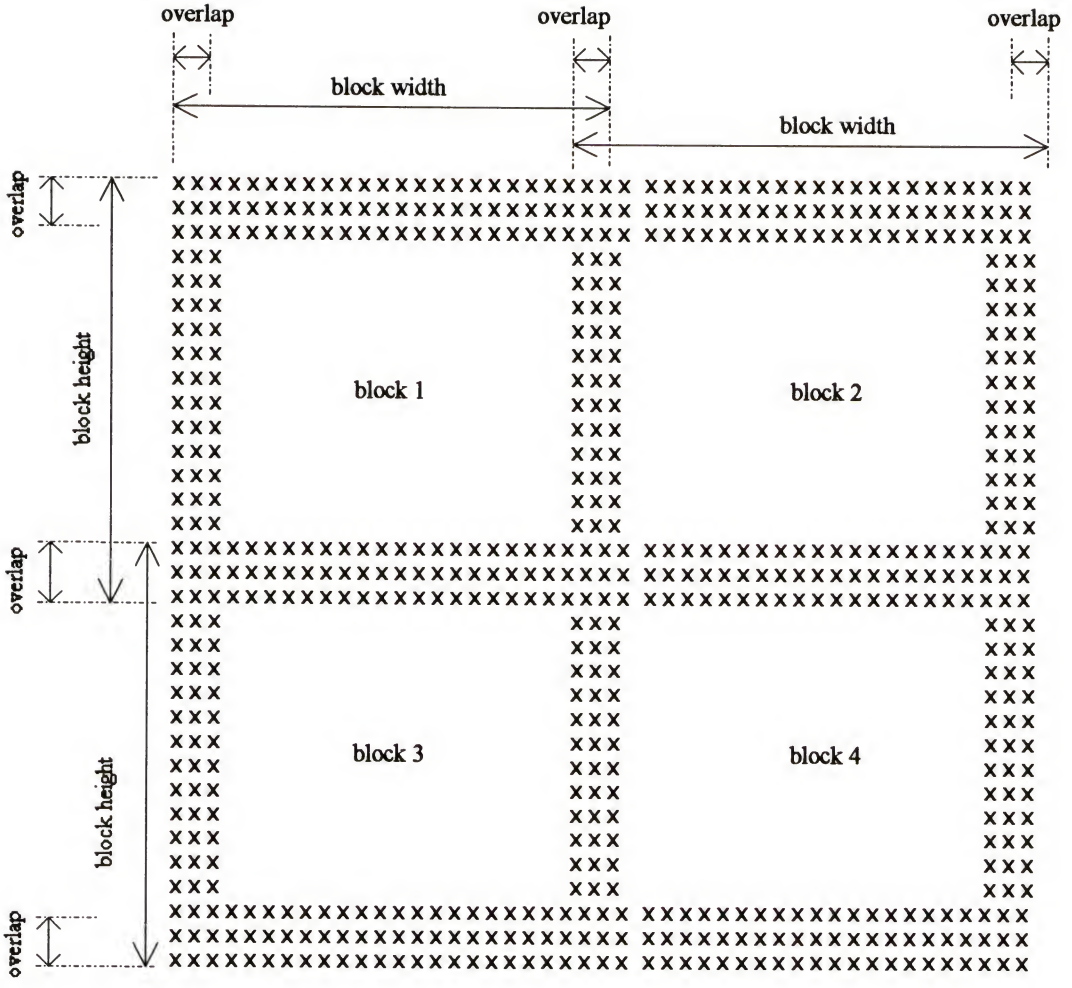

Fig. 6-10 Block Dividing Strategy

CHAPTER 7
LVDSO QUANTIZATION

PEDBOR can generate both edge images and noise removed images with high quality. However, the noise removed images are still intensity images with 256 levels rather than well-segmented images. Thus it is necessary to use region based segmentation algorithms to segment the images into object regions. In our hybrid segmentation approach, an iterative largest-variance-direction-split-optimization algorithm (LVDSO) is used to quantize noise removed images into initially segmented images. The reasons for employing the quantization technique are that:

1) In region segmentation, assigning input image data with a large number of different values to output data with a small number of different values is equivalent to requantizing the input data.
2) The procedure has only one parameter that needs to be set. The parameter is the number of clusters, K, in an image.
3) The processing can be carried out in the histogram domain rather than in the spatial domain. This allows faster processing since the histogram has at most 3 * 256 different entries for a 24 bit/per pixel color image.

LVDSO belongs to global histogram thresholding segmentation techniques. But here the optimum thresholds are found by minimizing the average sum-of-squared-errors which are called quantization errors and equal to the difference between the segmented image and the input image. Such a problem can be modelled as follows.

Consider the input data with N distinct values denoted by a set $\{X_n\}$ (n =1, 2, ..., N). The objective of the quantization is to find K (K<<N) representative levels $\{R_k\}$ (k

=1, 2, ..., K), called centers of cluster Ω_k, such that the average sum-of-squared-errors defined by

$$E = \sum_{n=1}^{N} \|X_n - R_k\|^2 * P(X_n) \tag{7-1}$$

is minimum, where P (X_n) is the probability of X_n occurring. If the cluster center is chosen as the statistical mean of the corresponding cluster, that is,

$$R_k = U_k = \sum_{X_n \in \Omega_k} X_n * P(X_n) \tag{7-2}$$

then the Eq. (7-1) becomes

$$E = \sum_{X_n \in \Omega_k} \|X_n - U_k\|^2 * P(X_n) = \sum_{k=1}^{K} \sigma_k^2 \tag{7-3}$$

In this equation σ_k^2 is the variance of cluster Ω_k. That means we can assign the input pixel with level X_n to a cluster Ω_k which minimizes the sum of the variance of each cluster.

This is another optimization problem. Instead of using regular optimization methods, such as standard calculus, simulated annealing, direct, or relaxation methods, we find the solution of the optimization problem by using the iterative largest-variance-direction-split-optimization procedure. The procedure is described below.

For a full color image with 256 different levels for each primary color, quantizing must be carried out in 3-bands of Red, Green and Blue, which is a 3-dimensional quantization problem. Assume that

Input data set: $X_r(I), X_g(I), X_b(I)$ $(I = 0,1,2,...,255)$

Output data set: $U_r(k_r), U_g(k_g), U_b(k_b)$, $(k_r + k_g + k_r = K)$

The computational procedure follows the steps presented below.

Step 1. Initialize k=1 and calculate the histograms of each band:

$H_r = \{ h_r(I) \}$, $H_g = \{ h_g(I) \}$, $H_b = \{ h_b(I) \}$ (I=0, 1, 2, ... , 255)

$$h_z(I) = \sum_{y=I} y \quad y \in (0, 255),\ z = r, g, b \tag{7-4}$$

and the probabilities:

$$p(X_z(I)) = \frac{h_z(I)}{L},\quad z = r, g, b. \tag{7-5}$$

where L is the number of pixels in an image.

Step 2. Calculate the variances and means of each band of data using Eq. (7-2) and (7-3).

Step 3. Partition one band with largest variance into two regions. The partition point T_{opt} is located at the point that minimizes E(T) defined by

$$\begin{aligned} E(T) = & \sum_{X(I) \in \Omega_{k1}} \|X(I) - U_{k1}(T)\|^2 * P(X(I)) \\ & + \sum_{X(I) \in \Omega_{k2}} \|X(I) - U_{k2}(T)\|^2 * P(X(I)) \end{aligned} \tag{7-6}$$

Step 4. Calculate the variances and means of $\Omega_{k1}(T_{opt})$ and $\Omega_{k2}(T_{opt})$ and set k = k+1.

Step 5. Check if k = K, if so stop the iteration, otherwise go to Step 3.

Step 6. Assign input data into the closest T_{opt}

In the procedure, the parameter, K, is predetermined. Our hybrid segmentation approach quantizes the image with an oversegmenting parameter, or a larger K than the expected number of regions in the image, to avoid picking an accurate K and to ensure that all true object edges are preserved in the segmentation. We calculate K by the following formula:

$$K = N_{peak}(R) + N_{peak}(G) + N_{peak}(B) - N_{overlap} + 1 \tag{7-7}$$

where $N_{peak}(R)$, $N_{peak}(G)$ and $N_{peak}(B)$ are the number of peaks in the R, G and B histograms respectively, and $N_{overlap}$ is the number of the same peak positions in the R,

G and B histograms. Fig. 7-1 gives an example of calculating K. Note that the number of actual clusters in the segmented image is equal to $k_r * k_g * k_r$ rather than K.

By using the LVDSO, an oversegmented image can be obtained. We call the oversegmented image the initially segmented image. In the initially segmented image, there are still some false regions due to the oversegmentation and the inconsistency of the histogram thresholding segmentation scheme itself. These false regions will be eliminated in Stage III.

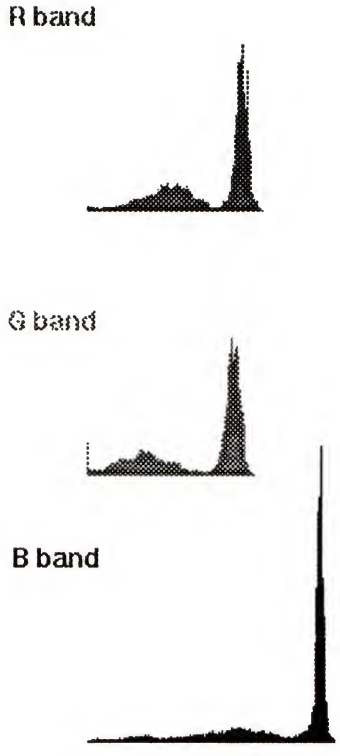

N_{peak} (R) =2, N_{peak} (G) =2, N_{peak} (B) =1, $N_{overlap}$ =1.

K = 2 +2 +1 - 1 +1 =5

Fig. 7-1 The Example of the Calculation of K

CHAPTER 8
MAPPING EDGE IMAGES WITH INITIAL SEGMENTATION

As mentioned above, the results of the edge based segmentation and region based segmentation are not consistent. There are three kinds of inconsistencies between edge based and region based segmentations. (1) A region boundary is not an edge segment, and there are no edges nearby. (2) A region boundary corresponds to an edge but it does not coincide with the edge. (3) There exist edges with no boundaries near them. See Fig. 4-5. The main reasons causing the inconsistencies are the inconsistency existing between the different segmentation schemes themselves as well as noise effects and unsuitable parameter settings. Many edge detectors adopt the area operation scheme, while many region based segmenters use the point operation scheme. For example, derivative edge detectors detect region boundaries by detecting the magnitude of the difference between two adjacent points, while region based segmenters form region boundaries by assigning each pixel to a class based on the similarity distance between the pixel and the center of that class. Usually, it is difficult to say which segmentation result, edge based one or region based one, is better. A more reasonable way is adopting an integration scheme, which combines the information of both edge based and region based schemes, to get a more consistent result. On the other hand, noise and unsuitable parameter setting also cause some false edges and false regions. An example is the third type of inconsistency mentioned above, error caused by an oversegmentation parameter, or larger than necessary K set in Stage II of our developed approach. However, decreasing such a parameter setting increases the first type of inconsistency.

In order to get a high quality segmentation result, our hybrid segmentation approach uses a mapping procedure. It utilizes the edges in the edge image as the

boundary reference of the true regions and the boundaries of initially segmented images as the true edge reference to remove false edges and false regions. The mapping procedure includes two phases.

- Map the edge image with the boundaries of the region image to form true region boundaries.
- Merge those regions between which no true boundaries exist.

The basic idea of the mapping procedure is described as follows.

Consider the boundary between an arbitrary pair of adjacent regions R1 and R2. Assume that there are N_b points along the boundary. These N_b points are called boundary candidates. For each candidate, verify whether there is a corresponding edge point in the edge image; if so mark it as a matched point. Let Ne be the number of matched points. If the ratio Ne/N_b is larger than some value (in our approach, the value is between 0.6 and 0.7), it is likely that the boundary is a true boundary. As a result, the final region boundaries consist of all true boundaries. If no boundary exists between two regions, the regions are merged.

In Stage II, a histogram quantization algorithm is used to obtain initially segmented images. Thus region patches are labeled by their cluster centers in the histogram domain. This means that two patches with different spatial location but similar properties may have the same labels since the spatial information cannot be contained in the image histogram. Therefore it is necessary to relabel region patches by combining spatial information to give each patch a unique label before performing the mapping procedure. The relabeling course is completed by a grouping procedure. The grouping procedure employs 8-connectivity as spatial measurement, alternatively growing and tracking back to group pixels with the same cluster center labels and 8-connectivity together.

After the relabeled image is obtained, the mapping procedure is applied to it. The mapping procedure consists of the following steps.

Step 1. From top to bottom and left to right, for the i^{th} region, R_i, calculate those mapping ratios which exist between R_i and its adjacent regions.

Step 2. Check all these mapping ratios. If there are any regions with the mapping ratio smaller than the predetermined value (say 0.7), then pick out one of them which has the minimum mapping ratio, and implement Step 3. Otherwise go to Step 4.

Step 3. Between R_i and the selected region, merge the smaller region into the larger one, then go to Step 1.

Step 4. Check whether or not the mapping procedure has been applied to all regions. If so, terminate the procedure. Otherwise go to Step 1.

Fig. 8-1 shows an example of the merge strategy (assume the mapping ratio threshold is set to 0.7). Fig. 8-1 (a) is the initial region labels. In this region configuration, the mapping ratios between region E and A, region D and C, and region B and C are all less than 0.7 (see Fig. 8-1 (b)). Since the mapping procedure is applied to each region in the fashion of top-to-bottom and left-to-right, region A is first merged into region E, and region C is then merged into region D. After these mergings, the region labels become as shown in Fig. 8-1 (c). The corresponding mapping ratio graph is shown in Fig. 8-1 (d). At this time, only the mapping ratio between region D and B is less than 0.7. Therefore region B is merged into region D. The final region labels and corresponding mapping ratio graph are shown in Fig. 8-1 (e) and (f) respectively.

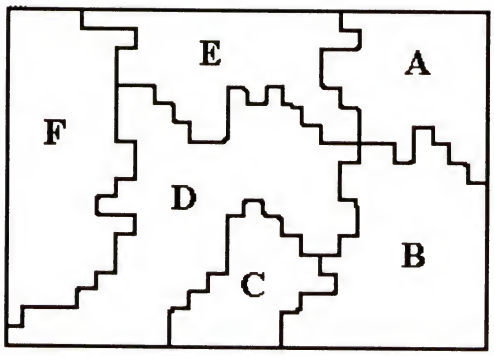

(a) Initial region labels

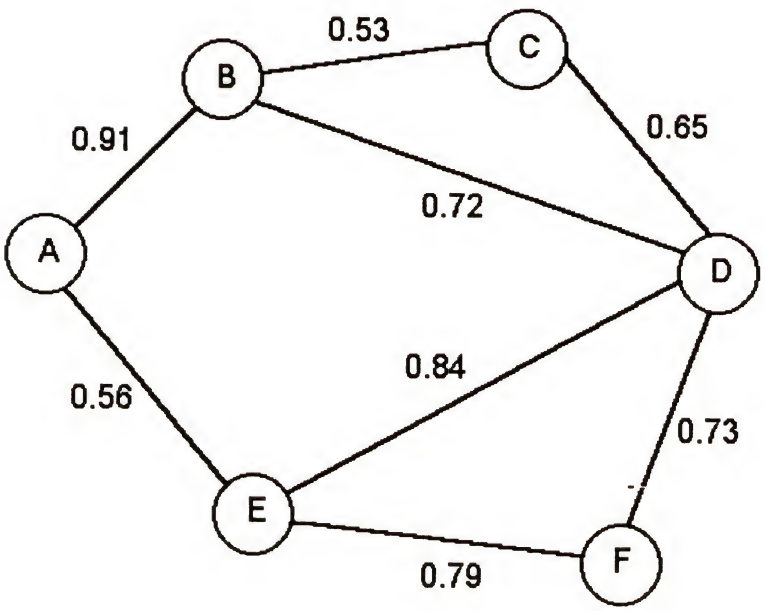

(b) Mapping ratio graph of (a)

Fig. 8-1 Merging Strategy Used in the Mapping Procedure

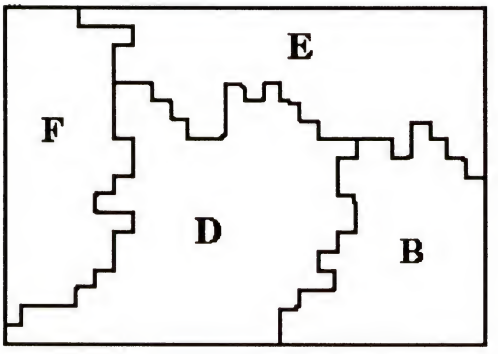

(c) Region labels after merging region E and A, and region D and C

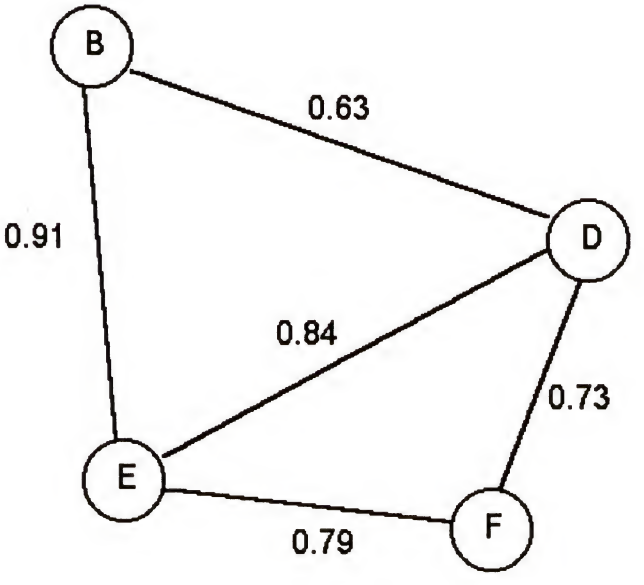

(d) Mapping ratio graph of (c)

Fig. 8-1 Continued

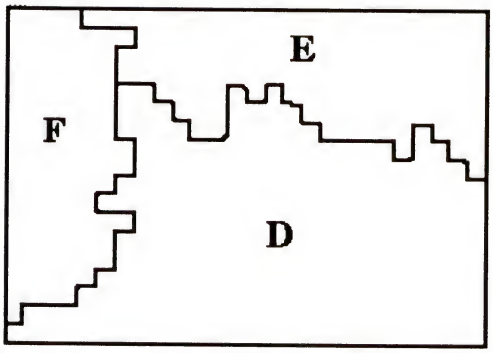

(e) Final region labels

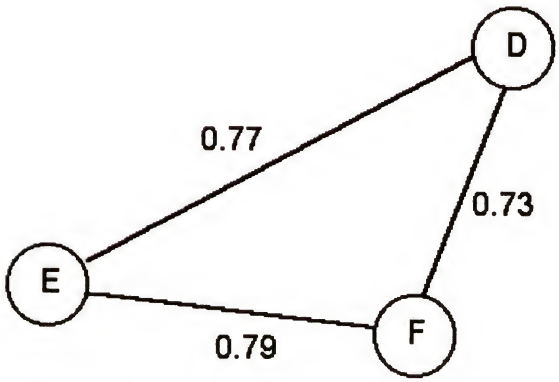

(f) Mapping ratio graph of (e)

Fig. 8-1 Continued

CHAPTER 9
EXPERIMENTAL RESULTS

In this chapter, many expriement results are presented. Since the PEDBOR algorithm is the key of the developed approach, the chapter first evaluates PEDBOR in section 1 by comparing it with several other tranditional algorithms to show the quality of performance of PEDBOR. All these algorithms have been tested on both synthetic images and real images, including melanoma photographs. Quantitative evaluation is made on three synthetic images with different signal-to-noise ratios. The visual evaluation was done on both synthetic images and real images. Section 2 shows the visual evaluation results of applying the hybrid segmentation approach to images of malignant melanoma.

9.1 Evaluation of PEDBOR

9.1.1 Quantitative Evaluation of PEDBOR Algorithm

To evaluate the PEDBOR algorithm, quantitative evaluation was made on three synthetic images with different signal-to-noise ratios, SNR = 1, 3, 5 and 7 dB. The first image is a 4-level image with background intensity 200, and object intensities of 150, 100, and 50 (Fig. 9-1(a)). The second image contains two bars with 3- and 4-pixel widths (Fig. 9-2(a)). The third image is a checkerboard (Fig. 9-3(a)). Both bar image and checkerboard image have background intensity 150 and foreground intensity 100. Gaussian noises with standard deviation of 10, 16, 25 and 39 are added to the images to obtain noisy images with SNR values of 7, 5, 3 and 1. Figs. 9-1 to 9-3 show the three images and corresponding noisy images.

In the quantitative evaluation, the SNR for edge detection is defined as:

$$\mathrm{SNR} = 10\log\frac{h}{\sigma} \tag{9-1}$$

where h is the edge height and σ is standard deviation of the noise. In all three images, h's are all equal to 50.

Three quantities: P_f, P_m and S_m, are used as performance measures. P_f and P_m evaluate edge detection results. P_f is called the false alarm probability, which is equal to the conditional error probability of assigning an edge pixel given a non-edge pixel. P_m is called the missed detection probability, which is equal to the conditional error probability of assigning a non-edge pixel given a true edge pixel. S_m is the measurement evaluating noise removed image. S_m is the average variance of the image, which measures the smoothness of non-edge regions of an image. The smaller the P_f, P_m and S_m, the better the results. Note that the false alarm pixels are not only really false object edges but include thickened edges and false object edges as well. Similarly, missing detection pixels are not just real missing object edges but include thinned edges and missing object edges. So two other measures, false object edges and missing object edges, are used to indicate if there are false object edges introduced and if any object edges are missing.

For comparison, two other algorithms are applied to the same images. First is the Sobel edge detector of threshold T with a median filter of filter size W, denoted as MedSob. Second is the nonstandard regularization algorithm with sigmoid line process function of parameter T1 followed by a Sobel edge detector of threshold T2, denoted as SIGMR. The results from both Sobel edge detectors and regularization approaches are the best ones of the experimental results with different parameters. The "best" means fewest false and missing objects.

Tables 9-1 to 9-3 give the quantitative evaluation results. In the tables, some detectors have two results, (1) and (2), under the same SNR, where, (1)'s correspond to

the results of minimum missing object edge cases and (2)'s to the results of minimum false object edge cases.

9.1.2 Visual Evaluation

The visual evaluation was done on both synthetic images and real images. Figs. 9-4 to 9-9 show the results of three synthetic images. Fig. 9-10 shows the evaluation of the checkerboard image surface, from which we can more directly compare the ability of noise removal and edge keeping of the algorithms.

The real image is a standard gray level image, "Lena". Corresponding noisy images of "Lena" are generated by adding Gaussian white noise with standard deviation of 20 and 30. Fig. 9-11 shows the original "Lena" image and its noisy counterparts. Four algorithms: PEDBOR, MedSob, SIGMR and LoG, are used on these images. The parameters for both MedSob and SIGMR have the same meanings as above. The LoG edge detector has the controlling parameter λ. Figs. 9-12 and 9-13 show a set of corresponding results.

From the experiments, we can see that PEDBOR has the best performance. It is much more robust to noise than other algorithms. It gives rise to fewest false edges and missing edges and gives more accurate edge positions in edge images. Also its smoothed images have the least blurring on edges and the most smoothing in homogenous areas. PEDBOR is a well-conditioned as well as a well-posed algorithm, that is, its solution is robust against noise. By using the PEDBOR, a high quality noise removed image and an edge image can be obtained. They provide a good references for Stage II and Stage III.

9.2 Application to the Computer Diagnostic System of Malignant Melanoma

Figs. 9-14 to 9-15 show several experimental results of our hybrid segmentation approach for images of malignant melanoma. In the figures, (a)s are original images, (b)s and (c)s are noise removed images and edge images generated by PEDBOR, (d)s are

quantization results of (a)s, (e)s are quantization results of (b)s, or initially segmented images, and (f)s are final segmented images. Comparing several segmented results from different stages shown in pictures (d)s, (e)s and (f)s respectively, we can see that the segmentation of the original image is not uniform and compact, and the boundaries are not continuous because of the effects of noise and the roughness of the skin lesions. By using PEDBOR, noise in the images are reduced greatly. However, there are still many false regions in the initial segmentation results shown in the (e) pictures due to the improper quantization parameter and the inconsistency of the algorithm itself. After the mapping stage, the final segmented images have the best results. That is, they have the fewest false regions, their regions are uniform, compact and show dissimilarity, and the region boundaries are continuous and thin.

Table 1. Quantitative Evaluation Results of 4-level Image

SNR	detector type	Pm	Pf	Sm	false objects	missing objects
7 db	PEDBOR	0.02114	0.00443	2.6153	No	No
	MedSob (W=3, T=30)	0.01126	0.01405	13.8342	No	No
	SIGMR (T1=40, T2=10)	0.03738	0.03078	8.9567	No	No
5 db	PEDBOR	0.04711	0.00988	5.4109	No	No
	MedSob (W=7, T=20)	0.22632	0.02474	12.671	No	No
	SIGMR (T1=50, T2=10)	0.09012	0.04375	15.842	Some	No
3 db	PEDBOR	0.08039	0.02489	20.102	No	No
	MedSob (1) (W=5, T=20)	0.19406	0.06500	38.983	Some	No
	MedSob (2) (W=7, T=20)	0.22376	0.04205	30.605	No	some
	SIGMR (T1=50, T2=15)	0.24270	0.05228	38.207	Many	No
1 db	PEDBOR	0.11009	0.03572	29.907	Fewer	No
	MedSob(1) (W=7, T=20)	0.22427	0.08113	70.819	Many	No
	MedSob (2) (W=7, T=30)	0.48643	0.03493	70.819	Some	Many
	SIGMR (T1=50, T2=15)	0.15361	0.23077	317.156	Many	Some

Table 2. Quantitative Evaluation Results of Bar Image

SNR	detector type	Pm	Pf	Sm	false objects	missing objects
7 db	PEDBOR	0.00605	0.00043	2.2954	No	No
	MedSob (W=3, T=30)	0.01010	0.00026	13.112	No	No
	SIGMR (T1=40, T2=10)	0.38911	0.00026	5.9277	No	Some
5 db	PEDBOR	0.01815	0.00284	5.7683	No	No
	MedSob (W=3, T=30)	0.05645	0.00302	35.662	No	No
	SIGMR (T1=50,T2=10)	0.48185	0.00379	8.2973	Few	Many
3 db	PEDBOR	0.05040	0.00646	13.472	Few	Few
	MedSob (1) (W=3, T=30)	0.17339	0.05731	92.436	Many	Some
	MedSob (2) (W=5, T=30)	0.67742	0.00310	34.819	Few	Many
	SIGMR (T1=50, T2=10)	0.46169	0.53430	39.491	Some	Many
1 db	PEDBOR	0.20161	0.02404	31.470	Few	Few
	MedSob (1) (W=5, T=20)	0.42943	0.17511	90.672	Many	Some
	MedSob (2) (W=7, T=20)	0.89718	0.03817	48.292	Some	Many
	SIGMR (T1=50,T2=10)	0.36694	0.28421	367.493	Many	Many

Table 3 Quantitative Evaluation Results of Checkerboard Image

SNR (db)	detector type	Pm	Pf	Sm	false objects	missing objects
7	PEDBOR	0.00332	0.00027	2.27263	No	No
	MedSob (W=3, T=20)	0.00664	0.00027	13.0030	No	No
	SIGMR (T1=30, T2=15)	0.02434	0.00518	8.71332	Few	Few
5	PEDBOR	0.01217	0.00586	5.22317	No	No
	MedSob (W=3, T=30)	0.02987	0.02165	14.5882	No	No
	SIGMR (T1=50,T2=15)	0.24336	0.00198	23.4948	Few	Many
3	PEDBOR	0.02655	0.01438	11.2249	No	No
	MedSob (1) (W=5, T=20)	0.12058	0.06107	37.1881	Some	Few
	MedSob (2) (W=5, T=30)	0.43363	0.00967	37.1881	No	Many
	SIGMR (T1=50, T2=12)	0.27544	0.04430	50.3117	Some	Many
1	PEDBOR	0.10398	0.03564	32.2599	Few	No
	MedSob (1) (W=5, T=20)	0.22235	0.20876	91.1897	Many	Some
	MedSob (2) (W=7, T=20)	0.89718	0.03817	63.7568	Some	Many
	SIGMR (T1=50, T2=15)	0.27765	0.31591	355.038	Many	Many

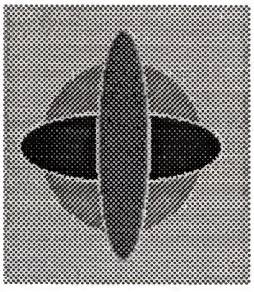

(a)

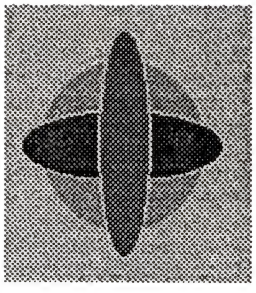

(b)

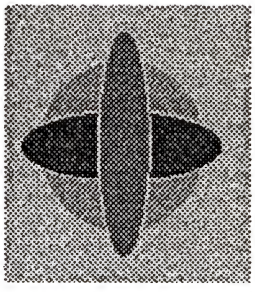

(c)

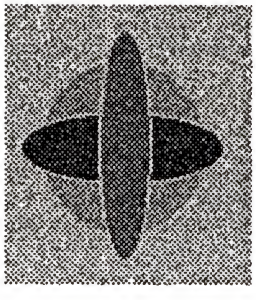

(d)

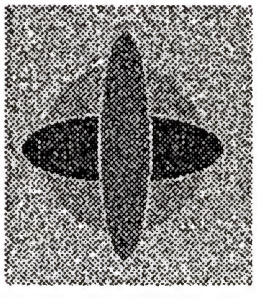

(e)

Fig. 9-1 4-level Images
(a) Original image. (b) 7 dB noisy image.
(c) 5 dB noisy image. (d) 3 dB noisy image. (e) 1 dB noisy image.

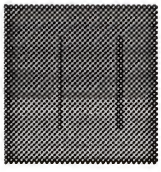

(a)

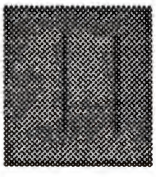

(b)

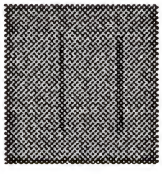

(c)

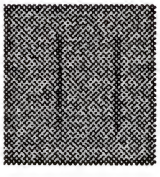

(d)

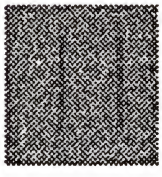

(e)

Fig. 9-2 Bar Images
(a) Original image. (b) 7 dB noisy image.
(c) 5 dB noisy image. (d) 3 dB noisy image. (e) 1 dB noisy image.

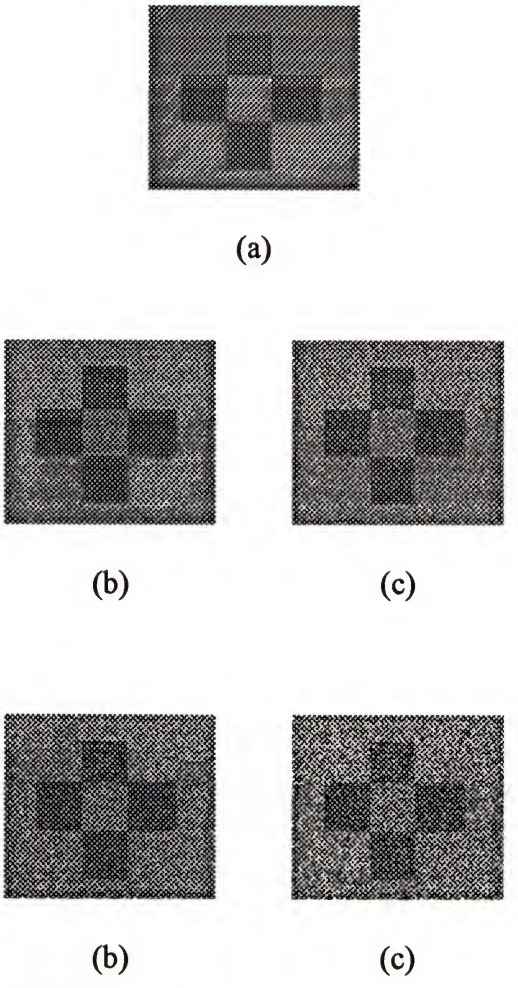

Fig. 9-3 Checkerboard Images
(a) Original image. (b) 7 dB noisy image.
(c) 5 dB noisy image. (d) 3 dB noisy image. (e) 1 dB noisy image.

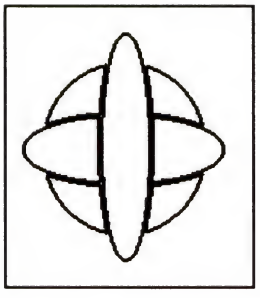

(a) Original Edges.

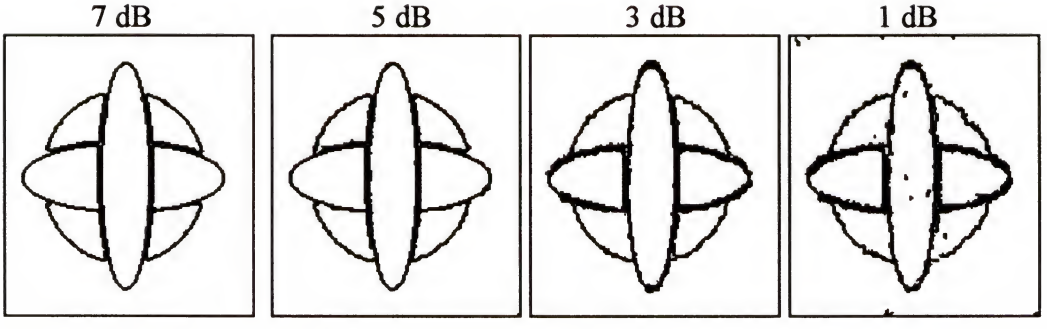

(b) PEDBOR Results.

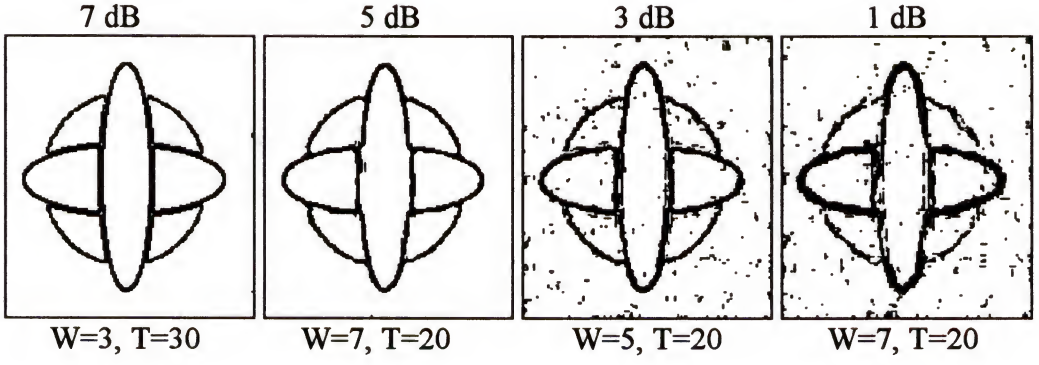

(c) The Results of the MedSob (1).

Fig. 9-4 Edge Detection Results for the 4-level Images

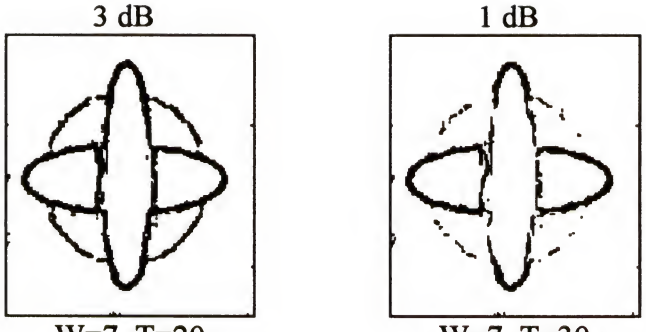

(d) The Results of the MedSob (2).

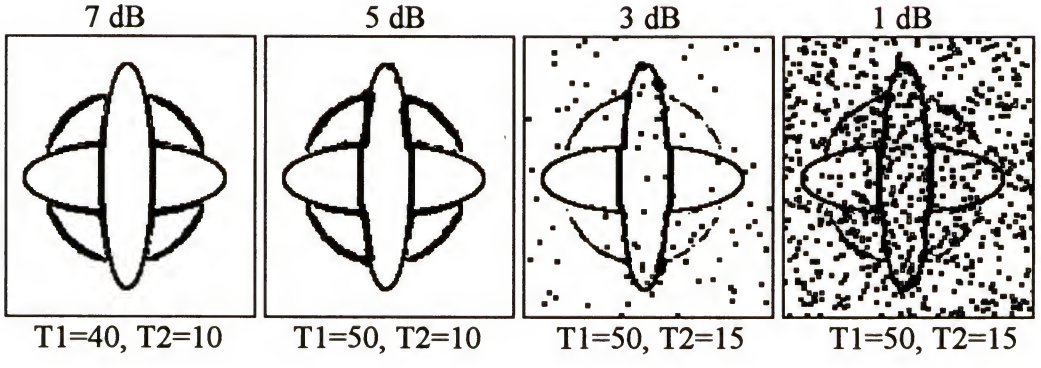

(e) The Results of SIGMR.

Fig. 9-4 Continued

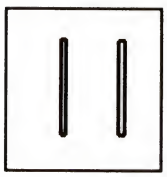

(a) Original Edges.

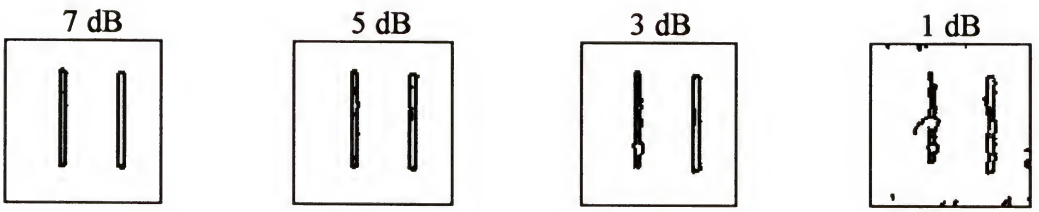

(b) The Results of the PEDBOR.

(c) The Results of the MedSob (1).

Fig. 9-5 Edge Detection Results for Bar Images

(d) The Results of the MedSob (2).

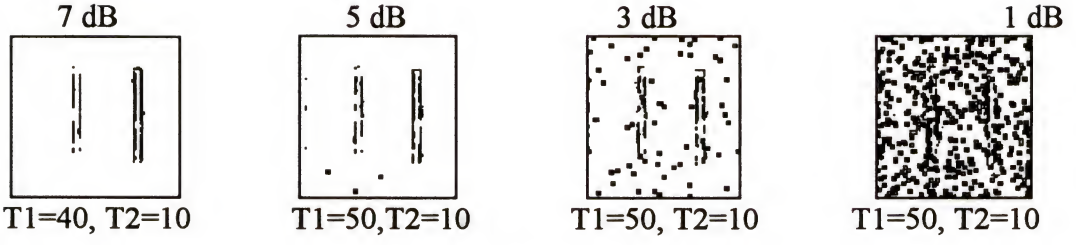

(e) The Results of SIGMR.

Fig. 9-5 Continued

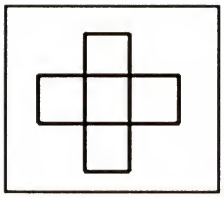

(a) Original Edges.

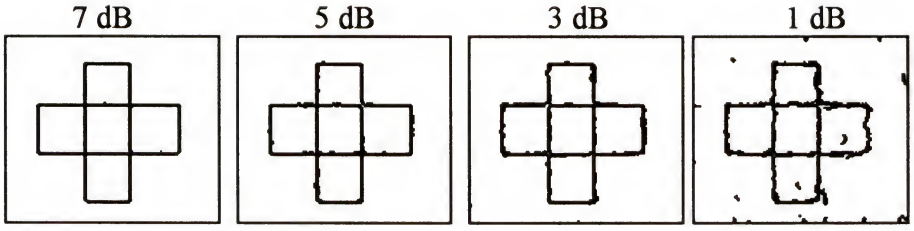

(b) The Results of the PEDBOR.

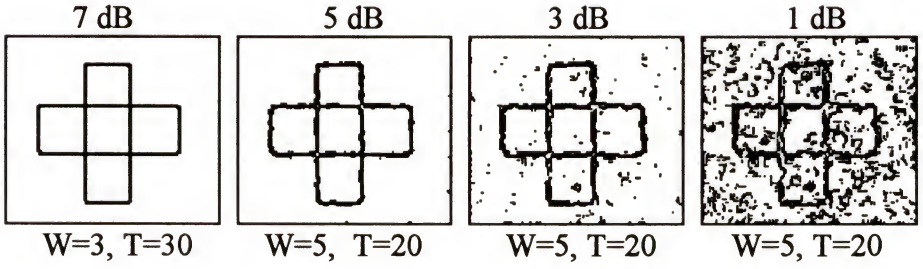

(c) The Results of the MedSob (1).

Fig. 9-6 Edge Detection Results for Checkerboard Images

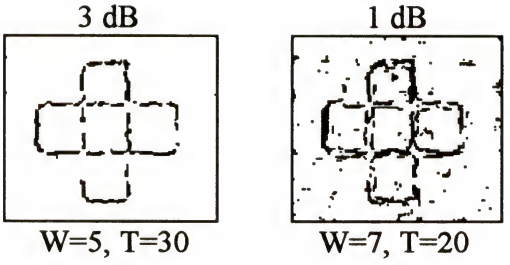

(d) The Results of the MedSob (2).

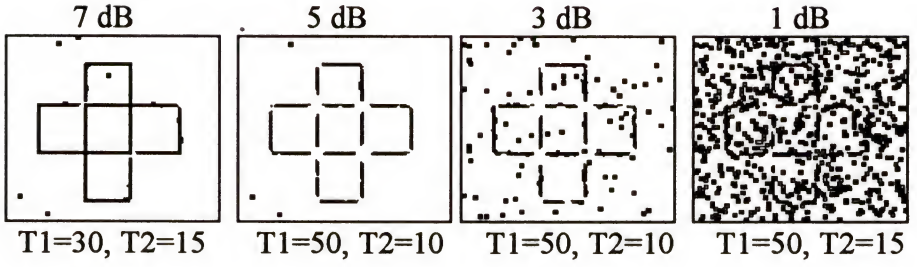

(e) The Results of SIGMR.

Fig. 9-6 Continued

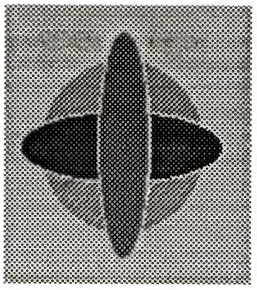

(a) Original Image

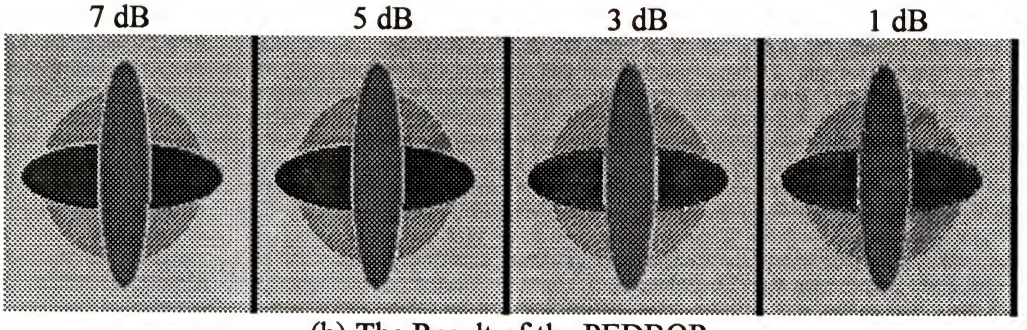

(b) The Result of the PEDBOR

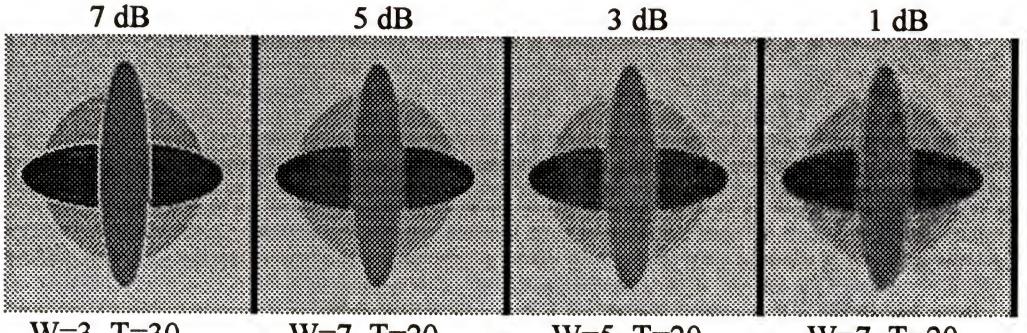

(c) The Result of the MedSob

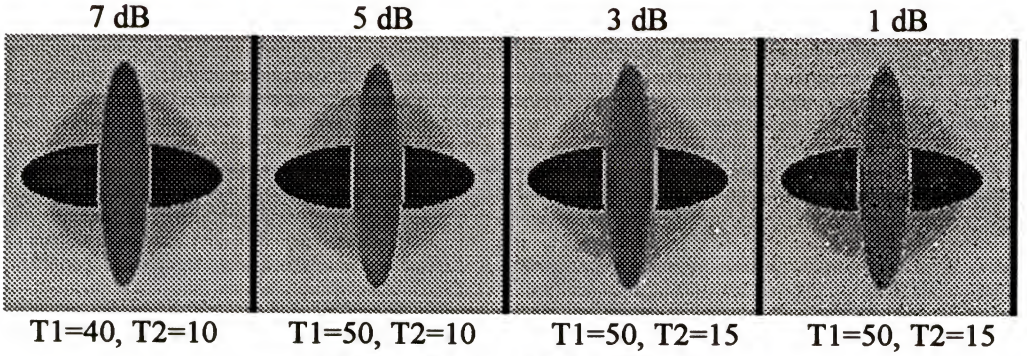

(d) The Results of the SIGMR.

Fig. 9-7 Noise Removed Images for 4-level Images.

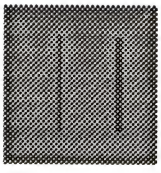

(a) Original Image

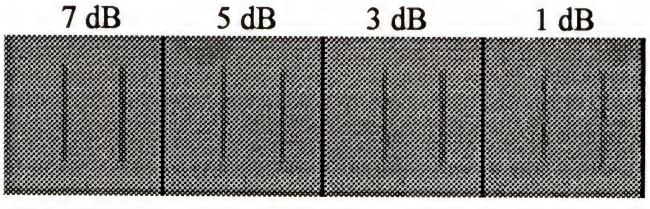

(b) The Results of the PEDBOR.

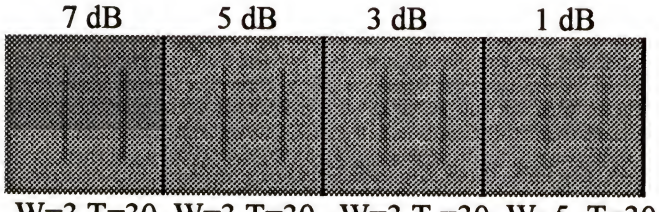

(c) The Results of the MedSob.

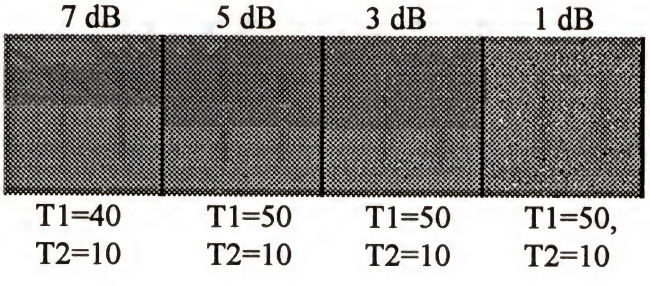

(d) The Results of SIGMR.

Fig. 9-8 Noise Removed Images for Bar Images.

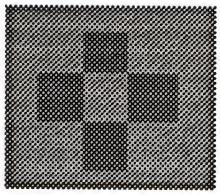

(a) Original Image

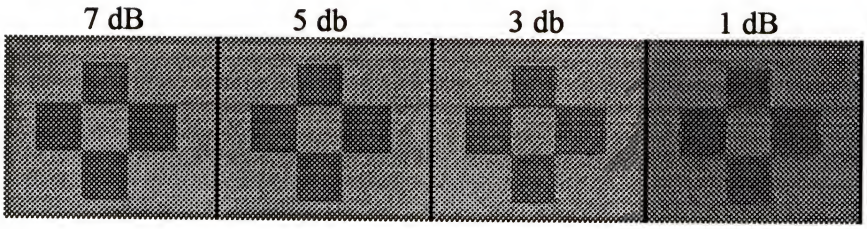

(b) The Results of the PEDBOR.

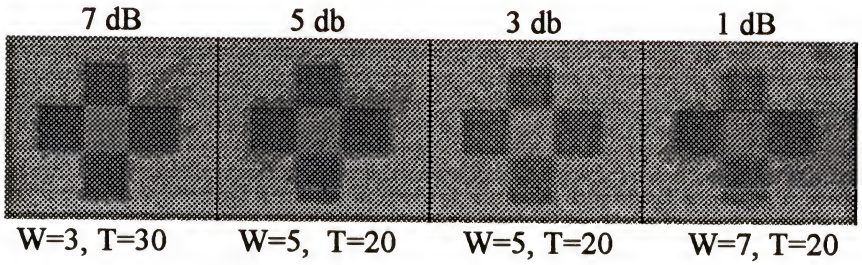

(c) The Results of the MedSob.

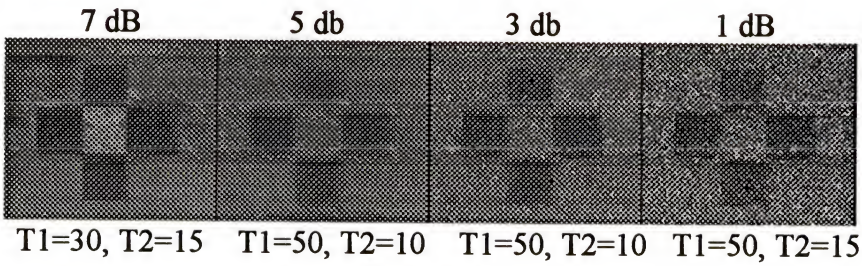

(d) The Results of the SIGMR.

Fig. 9-9 Noise Removed Images for Checkerboard Images.

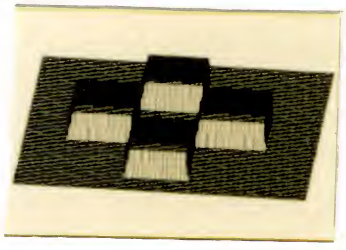

(a)

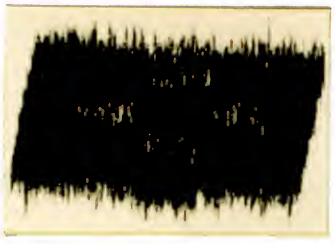

(b)

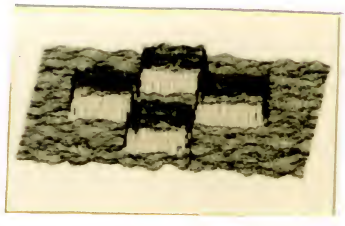

(c)

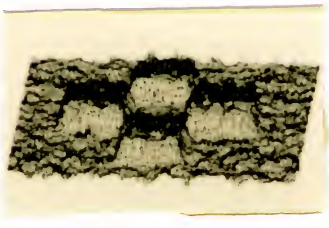

(d)

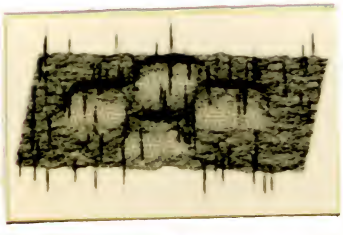

(e)

Fig. 9-10 Evaluation of Image Surface
(a) Original image surface. (b) Noise image surface (SNR=3db).
(c) PEDBOR surface. (d) SIGMR surface. (e) MedSob surface.

(a) Original Image

(b) Noisy Image ($\sigma = 20$).

(c) Noisy Image ($\sigma = 30$).

Fig. 9-11 Lena Image and Corresponding Noisy Images.

(a) Original Edges.

(b) PEDBOR Result for $\sigma = 20$.

(c) PEDBOR Result for $\sigma = 30$.

Fig. 9-12 Edge Detection Results for Lena Images.

W=3, T=20

W=5, T=20

W=7, T=20

(d) MedSob Results for $\sigma = 20$.

Fig. 9-12 Continued

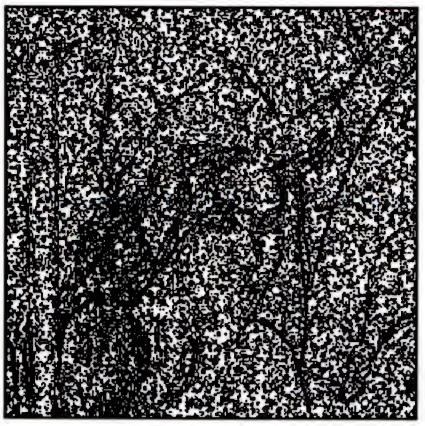

W=3, T=30

W=5, T=30

W=7, T=20

(e) MedSob Results for $\sigma = 30$.

Fig. 9-12 Continued

T1 =30, T2= 10

T1 =50, T2= 10

T1=255, T2=6

(f) SIGMR Results for $\sigma = 20$.

Fig. 9-12 Continued

T1=30, T2=10 T1=50, T2=10

(g) SIGMR Results for $\sigma = 30$.

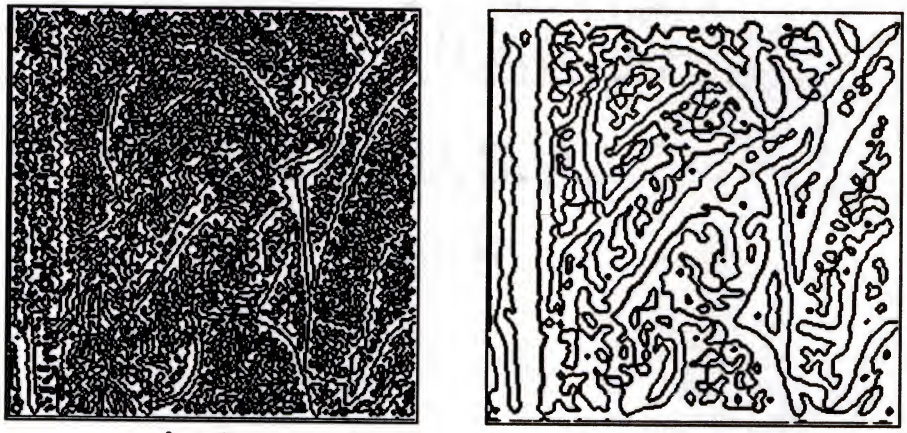

$\lambda = 2$ $\lambda = 9$

(h) LoG Results for $\sigma = 20$.

Fig. 9-12 Continued

(a) Original Image

(b) Noisy Image ($\sigma = 20$)

(c) PEDBOR Result.

Fig. 9-13 Noise Removed Results for Lena's Noisy Image with $\sigma = 20$.

W = 3

W = 5

W = 7

(d) The Results of MedSob with the Median Filters of Size W.

Fig. 9-13 Continued

T1 = 20

T1 = 50

(e) The Results of SIGMR with variation of the Regularization Parameter T1.

Fig. 9-13 Continued

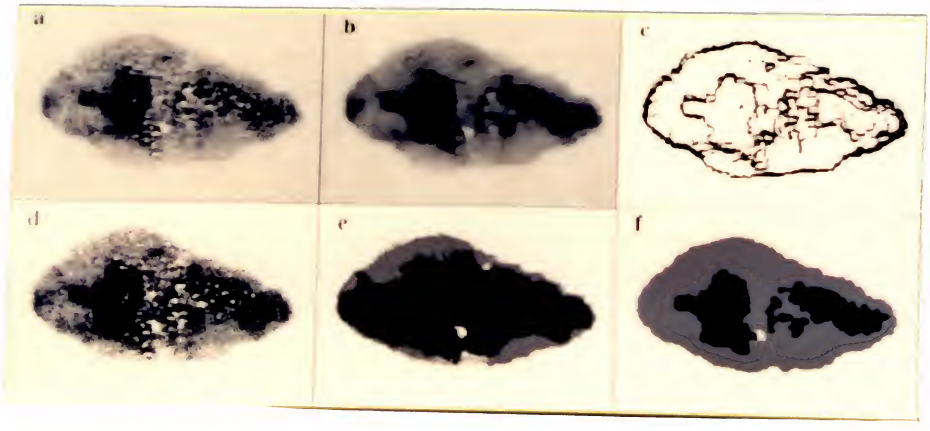

Fig. 9-14 Experimental Results for Malignant Melanoma Image 1.

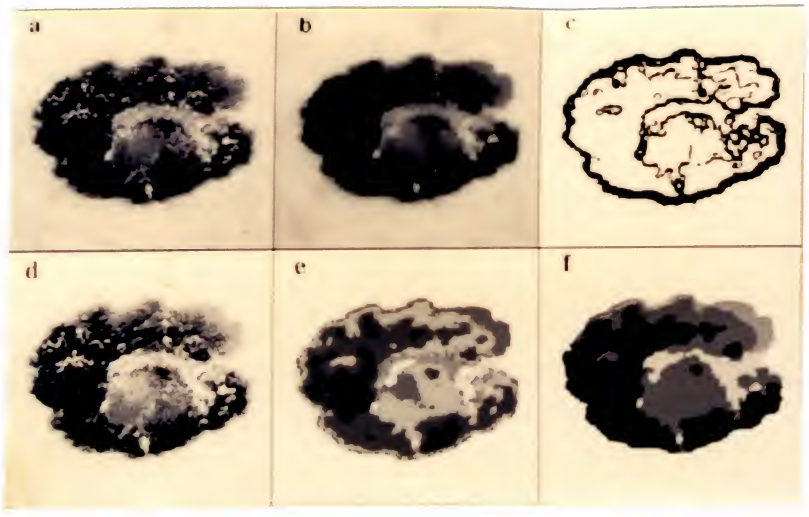

Fig. 9-15 Experimental Results for Malignant Melanoma Image 2.

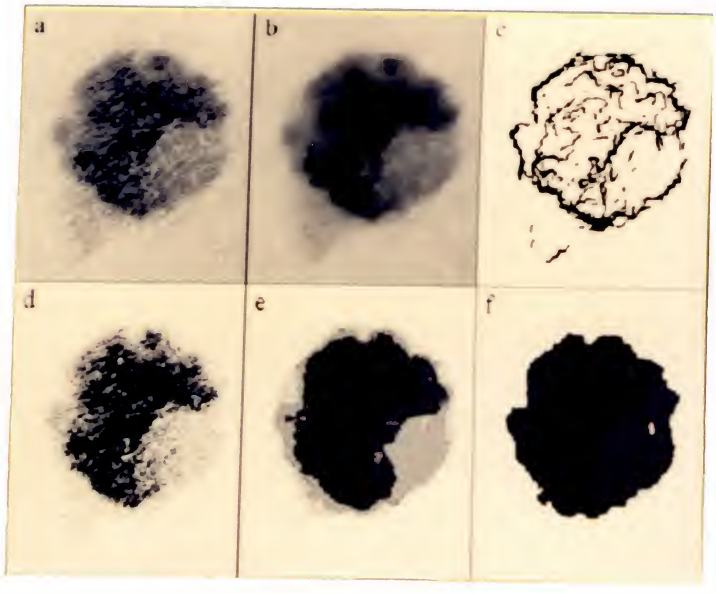

Fig. 9-16 Experimental Results for Malignant Melanoma Image 3.

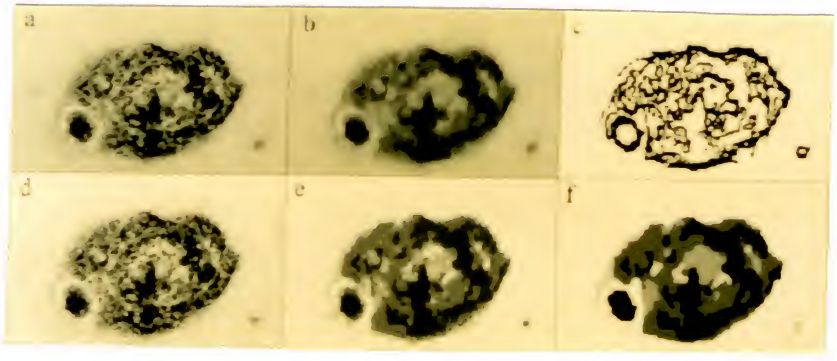

Fig. 9-17 Experimental Results for Malignant Melanoma Image 4.

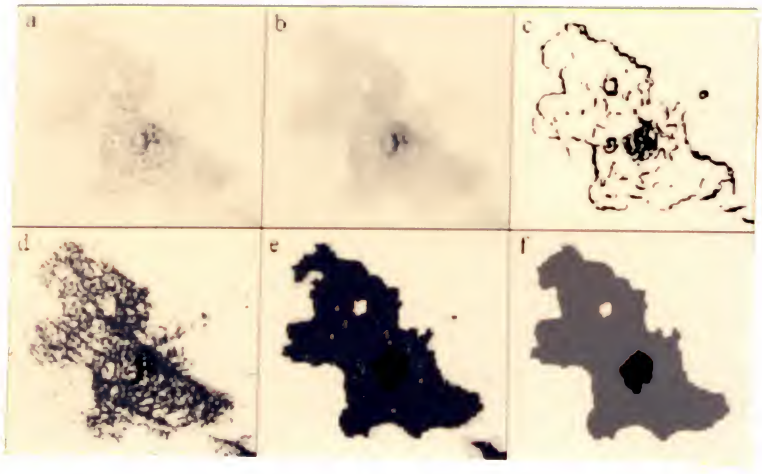

Fig. 9-18 Experimental Results for Malignant Melanoma Image 5.

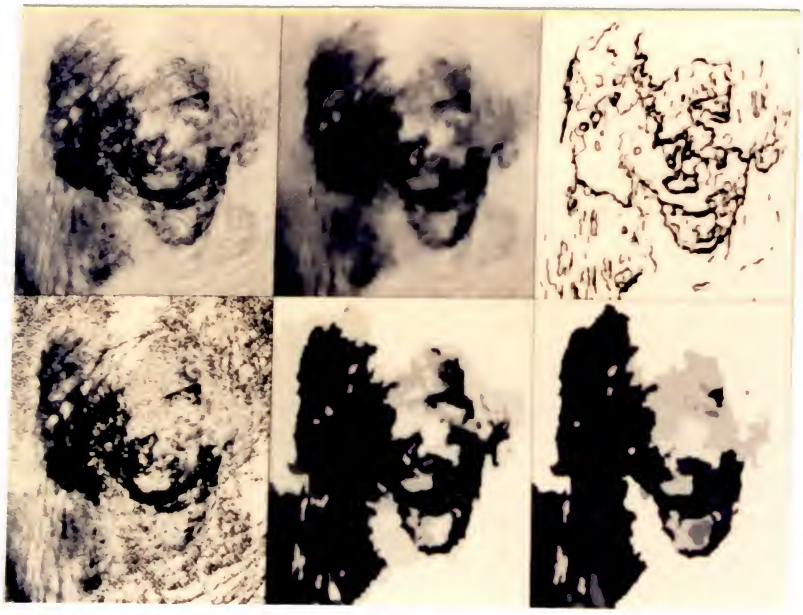

Fig. 9-18 Experimental Results for Malignant Melanoma Image 6.

CHAPTER 10
SUMMARY AND CONCLUSIONS

10.1 Summary

The objective of this study is to develop a new segmentation approach for a computer diagnostic system of malignant melanoma and to show that the developed approach outperforms traditional approaches.

The developed approach is an adaptive, optimal and integrating one. It has three stages: 1) PEDBOR; 2) LVDSO quantization; 3) mapping. In Stage I, a new algorithm, PEDBOR, is used to remove noise and detect edges simultaneously. It is based on the regularization model, but has critical improvements. With the improvements, the whole regularization procedure is adaptively controlled by pixel features, which makes the algorithm robust to noise. In Stage II, an iterative LVDSO quantization is applied to quantize noise removed images into initially segmented images. Stage III is a mapping procedure. It uses edge images and initially segmented images as references to remove false edges and false regions. The experimental results show that the approach can generate uniform, compact and dissimilar segmentation results. The segmentation results are also consistent with dermatologists' observation results.

10.2 Significance of This Research

A new and promising hybrid segmentation approach for a computer diagnostic system of malignant melanoma is proposed in this study. For a practical computer image analysis systems, such as the computer diagnostic system of malignant melanoma described here, there are many kinds of image sources, which require that the algorithm must be robust to various kinds of noise and that image processing parameters change

over a wide range. Also such systems will be used by many who lack image processing knowledge, which makes choosing processing parameters difficult for them. Therefore, the segmentation algorithm for the system must be robust to noise and be universally suitable to the class of application images without the difficulty for user input of processing parameters. The developed hybrid segmentation approach satisfies these requirements.

The developed approach is superior to traditional approaches in several aspects.

(1) The approach avoids the difficulty with setting a threshold in edge detection and setting clustering parameters in quantization. The results of our approach are minimally dependent on the threshold/parameter setting.

(2) PEDBOR uses a pixel-feature-controlling regularization process to avoid oversmoothing of edges and undersuppression of noise. This makes the approach much more robust to various sources of noise than other traditional approaches.

(3) Combining edge based segmentation results with region based segmentation results makes segmentation results more consistent.

By using this approach, the segmented results better define the image features. This provides a consistent model for high level analysis, such as texture, color, shape, size, etc., and for classification of a malignant melanoma lesion.

10.2 Recommendations for Future Research

Since the proposed approach is new, many follow-up studies are possible. Specifically, the studies in speeding up the algorithms are of high interest in the future. Several aspects in the speed up of the algorithms can be considered. First, reduce the computation redundancy in implementing the algorithms. Second, consider the strategy of the parallel implementation of the algorithms. Third, implement the algorithms in hardware. How the algorithms can be efficiently implemented in parallel and in hardware remains to be investigated.

APPENDIX A
Modified Lookup Table

Index	Ymax	Ymin	Xmax	Xmin	OG	Index	Ymax	Ymin	Xmax	Xmin	OG
1	-255	-254	-255	-104	160	35	-173	-172	-255	-70	160
2	-253	-252	-255	-103	160	36	-171	-169	-255	-69	160
3	-251	-249	-255	-102	160	37	-168	-167	-255	-68	160
4	-248	-247	-255	-101	160	38	-166	-165	-255	-67	160
5	-246	-244	-255	-100	160	39	-164	-162	-255	-66	160
6	-243	-242	-255	-99	160	40	-161	-160	-255	-65	160
7	-241	-240	-255	-98	160	41	-159	-157	-255	-64	160
8	-239	-237	-255	-97	160	42	-156	-155	-255	-63	160
9	-236	-235	-255	-96	160	43	-154	-153	-255	-62	160
10	-234	-232	-255	-95	160	44	-152	-150	-255	-61	160
11	-231	-230	-255	-94	160	45	-149	-148	-255	-60	160
12	-229	-227	-255	-93	160	46	-147	-145	-255	-59	160
13	-226	-225	-255	-92	160	47	-144	-143	-255	-58	160
14	-224	-223	-255	-91	160	48	-142	-141	-255	-57	160
15	-222	-220	-255	-90	160	49	-140	-138	-255	-56	160
16	-219	-218	-255	-89	160	50	-137	-136	-255	-55	160
17	-217	-215	-255	-88	160	51	-135	-133	-255	-54	160
18	-214	-213	-255	-87	160	52	-132	-131	-255	-53	160
19	-212	-211	-255	-86	160	53	-130	-128	-255	-52	160
20	-210	-208	-255	-85	160	54	-127	-126	-255	-51	160
21	-207	-206	-255	-84	160	55	-125	-124	-255	-50	160
22	-205	-203	-255	-83	160	56	-123	-121	-255	-49	160
23	-202	-201	-255	-82	160	57	-120	-119	-255	-48	160
24	-200	-198	-255	-81	160	58	-118	-116	-255	-47	160
25	-197	-196	-255	-80	160	59	-115	-114	-255	-46	160
26	-195	-194	-255	-79	160	60	-113	-112	-255	-45	160
27	-193	-191	-255	-78	160	61	-111	-109	-255	-44	160
28	-190	-189	-255	-77	160	62	-108	-107	-255	-43	160
29	-188	-186	-255	-76	160	63	-106	-106	-253	-43	160
30	-185	-184	-255	-75	160	64	-105	-105	-251	-43	160
31	-183	-182	-255	-74	160	65	-104	-104	-248	-42	160
32	-181	-179	-255	-73	160	66	-103	-103	-246	-42	160
33	-178	-177	-255	-72	160	67	-102	-102	-243	-41	160
34	-176	-174	-255	-71	160	68	-101	-101	-241	-41	160

Index	Ymax	Ymin	Xmax	Xmin	OG
69	-100	-100	-239	-41	160
70	-99	-99	-236	-40	160
71	-98	-98	-234	-40	160
72	-97	-97	-231	-39	160
73	-96	-96	-229	-39	160
74	-95	-95	-226	-38	160
75	-94	-94	-224	-38	160
76	-93	-93	-222	-38	160
77	-92	-92	-219	-37	160
78	-91	-91	-217	-37	160
79	-90	-90	-214	-36	160
80	-89	-89	-212	-36	160
81	-88	-88	-210	-36	160
82	-87	-87	-207	-35	160
83	-86	-86	-205	-35	160
84	-85	-85	-202	-34	160
85	-84	-84	-200	-34	160
86	-83	-83	-197	-33	160
87	-82	-82	-195	-33	160
88	-81	-81	-193	-33	160
89	-80	-80	-190	-32	160
90	-79	-79	-188	-32	160
91	-78	-78	-185	-31	160
92	-77	-77	-183	-31	160
93	-76	-76	-181	-31	160
94	-75	-75	-178	-30	160
95	-74	-74	-176	-30	160
96	-73	-73	-173	-29	160
97	-72	-72	-171	-29	160
98	-71	-71	-168	-28	160
99	-70	-70	-166	-28	160
100	-69	-69	-164	-28	160
101	-68	-68	-161	-27	160
102	-67	-67	-159	-27	160
103	-66	-66	-156	-26	160
104	-65	-65	-154	-26	160
105	-64	-64	-152	-26	160
106	-63	-63	-149	-25	160
107	-62	-62	-147	-25	160
108	-61	-61	-144	-24	160
109	-60	-60	-142	-24	160
110	-59	-59	-140	-24	160
111	-58	-58	-137	-23	160
112	-57	-57	-135	-23	160
113	-56	-56	-132	-22	160
114	-55	-55	-130	-22	160
115	-54	-54	-127	-21	160
116	-53	-53	-125	-21	160
117	-52	-52	-123	-21	160
118	-51	-51	-120	-20	160
119	-50	-50	-118	-20	160
120	-49	-49	-115	-19	160
121	-48	-48	-113	-19	160
122	-47	-47	-111	-19	160
123	-46	-46	-108	-18	160
124	-45	-45	-106	-18	160
125	-44	-44	-103	-17	160
126	-43	-43	-101	-17	160
127	-42	-42	-98	-16	160
128	-41	-41	-96	-16	160
129	-40	-40	-94	-16	160
130	-39	-39	-91	-15	160
131	-38	-38	-89	-15	160
132	-37	-37	-86	-14	160
133	-36	-36	-84	-14	160
134	-35	-35	-82	-14	160
135	-34	-34	-79	-13	160
136	-33	-33	-77	-13	160
137	-32	-32	-74	-12	160
138	-31	-31	-72	-12	160
139	-30	-30	-70	-12	160
140	-29	-29	-67	-11	160
141	-28	-28	-65	-11	160
142	-27	-27	-62	-10	160
143	-26	-26	-60	-10	160
144	-25	-25	-57	-9	160
145	-24	-24	-55	-9	160
146	-23	-23	-53	-9	160
147	-22	-22	-50	-8	160
148	-21	-21	-48	-8	160
149	-20	-20	-45	-7	160
150	-19	-19	-43	-7	160
151	-18	-18	-41	-7	160
152	-17	-17	-38	-6	160
153	-16	-16	-36	-6	160
154	-15	-15	-33	-5	160

Index	Ymax	Ymin	Xmax	Xmin	OG
155	-14	-14	-31	-5	160
156	-13	-13	-28	-4	160
157	-12	-12	-26	-4	160
158	-11	-11	-24	-4	160
159	-10	-10	-21	-3	160
160	-9	-9	-19	-3	160
161	-8	-8	-16	-2	160
162	-7	-7	-14	-2	160
163	-6	-6	-12	-2	160
164	-5	-5	-9	-1	160
165	-4	-4	-7	-1	160
166	-3	-3	-4	0	160
167	-2	-2	-2	0	160
168	-1	-1	-255	0	160
169	0	-256	-105	0	128
170	-255	-254	-104	0	128
171	-253	-252	-103	0	128
172	-251	-249	-102	0	128
173	-248	-247	-101	0	128
174	-246	-244	-100	0	128
175	-243	-242	-99	0	128
176	-241	-240	-98	0	128
177	-239	-237	-97	0	128
178	-236	-235	-96	0	128
179	-234	-232	-95	0	128
180	-231	-230	-94	0	128
181	-229	-227	-93	0	128
182	-226	-225	-92	0	128
183	-224	-223	-91	0	128
184	-222	-220	-90	0	128
185	-219	-218	-89	0	128
186	-217	-215	-88	0	128
187	-214	-213	-87	0	128
188	-212	-211	-86	0	128
189	-210	-208	-85	0	128
190	-207	-206	-84	0	128
191	-205	-203	-83	0	128
192	-202	-201	-82	0	128
193	-200	-198	-81	0	128
194	-197	-196	-80	0	128
195	-195	-194	-79	0	128
196	-193	-191	-78	0	128
197	-190	-189	-77	0	128

Index	Ymax	Ymin	Xmax	Xmin	OG
198	-188	-186	-76	0	128
199	-185	-184	-75	0	128
200	-183	-182	-74	0	128
201	-181	-179	-73	0	128
202	-178	-177	-72	0	128
203	-176	-174	-71	0	128
204	-173	-172	-70	0	128
205	-171	-169	-69	0	128
206	-168	-167	-68	0	128
207	-166	-165	-67	0	128
208	-164	-162	-66	0	128
209	-161	-160	-65	0	128
210	-159	-157	-64	0	128
211	-156	-155	-63	0	128
212	-154	-153	-62	0	128
213	-152	-150	-61	0	128
214	-149	-148	-60	0	128
215	-147	-145	-59	0	128
216	-144	-143	-58	0	128
217	-142	-141	-57	0	128
218	-140	-138	-56	0	128
219	-137	-136	-55	0	128
220	-135	-133	-54	0	128
221	-132	-131	-53	0	128
222	-130	-128	-52	0	128
223	-127	-126	-51	0	128
224	-125	-124	-50	0	128
225	-123	-121	-49	0	128
226	-120	-119	-48	0	128
227	-118	-116	-47	0	128
228	-115	-114	-46	0	128
229	-113	-112	-45	0	128
230	-111	-109	-44	0	128
231	-108	-107	-43	0	128
232	-106	-104	-42	0	128
233	-103	-102	-41	0	128
234	-101	-99	-40	0	128
235	-98	-97	-39	0	128
236	-96	-95	-38	0	128
237	-94	-92	-37	0	128
238	-91	-90	-36	0	128
239	-89	-87	-35	0	128
240	-86	-85	-34	0	128

Index	Ymax	Ymin	Xmax	Xmin	OG
241	-84	-83	-33	0	128
242	-82	-80	-32	0	128
243	-79	-78	-31	0	128
244	-77	-75	-30	0	128
245	-74	-73	-29	0	128
246	-72	-71	-28	0	128
247	-70	-68	-27	0	128
248	-67	-66	-26	0	128
249	-65	-63	-25	0	128
250	-62	-61	-24	0	128
251	-60	-58	-23	0	128
252	-57	-56	-22	0	128
253	-55	-54	-21	0	128
254	-53	-51	-20	0	128
255	-50	-49	-19	0	128
256	-48	-46	-18	0	128
257	-45	-44	-17	0	128
258	-43	-42	-16	0	128
259	-41	-39	-15	0	128
260	-38	-37	-14	0	128
261	-36	-34	-13	0	128
262	-33	-32	-12	0	128
263	-31	-29	-11	0	128
264	-28	-27	-10	0	128
265	-26	-25	-9	0	128
266	-24	-22	-8	0	128
267	-21	-20	-7	0	128
268	-19	-17	-6	0	128
269	-16	-15	-5	0	128
270	-14	-13	-4	0	128
271	-12	-10	-3	0	128
272	-9	-8	-2	0	128
273	-7	-5	-1	0	128
274	-4	-3	-255	0	128
275	-2	0	0	1	128
276	1	2	0	2	128
277	3	4	0	3	128
278	5	7	0	4	128
279	8	9	0	5	128
280	10	12	0	6	128
281	13	14	0	7	128
282	15	16	0	8	128
283	17	19	0	9	128

Index	Ymax	Ymin	Xmax	Xmin	OG
284	20	21	0	10	128
285	22	24	0	11	128
286	25	26	0	12	128
287	27	28	0	13	128
288	29	31	0	14	128
289	32	33	0	15	128
290	34	36	0	16	128
291	37	38	0	17	128
292	39	41	0	18	128
293	42	43	0	19	128
294	44	45	0	20	128
295	46	48	0	21	128
296	49	50	0	22	128
297	51	53	0	23	128
298	54	55	0	24	128
299	56	57	0	25	128
300	58	60	0	26	128
301	61	62	0	27	128
302	63	65	0	28	128
303	66	67	0	29	128
304	68	70	0	30	128
305	71	72	0	31	128
306	73	74	0	32	128
307	75	77	0	33	128
308	78	79	0	34	128
309	80	82	0	35	128
310	83	84	0	36	128
311	85	86	0	37	128
312	87	89	0	38	128
313	90	91	0	39	128
314	92	94	0	40	128
315	95	96	0	41	128
316	97	98	0	42	128
317	99	101	0	43	128
318	102	103	0	44	128
319	104	106	0	45	128
320	107	108	0	46	128
321	109	111	0	47	128
322	112	113	0	48	128
323	114	115	0	49	128
324	116	118	0	50	128
325	119	120	0	51	128
326	121	123	0	52	128

Index	Ymax	Ymin	Xmax	Xmin	OG
327	124	125	0	53	128
328	126	127	0	54	128
329	128	130	0	55	128
330	131	132	0	56	128
331	133	135	0	57	128
332	136	137	0	58	128
333	138	140	0	59	128
334	141	142	0	60	128
335	143	144	0	61	128
336	145	147	0	62	128
337	148	149	0	63	128
338	150	152	0	64	128
339	153	154	0	65	128
340	155	156	0	66	128
341	157	159	0	67	128
342	160	161	0	68	128
343	162	164	0	69	128
344	165	166	0	70	128
345	167	168	0	71	128
346	169	171	0	72	128
347	172	173	0	73	128
348	174	176	0	74	128
349	177	178	0	75	128
350	179	181	0	76	128
351	182	183	0	77	128
352	184	185	0	78	128
353	186	188	0	79	128
354	189	190	0	80	128
355	191	193	0	81	128
356	194	195	0	82	128
357	196	197	0	83	128
358	198	200	0	84	128
359	201	202	0	85	128
360	203	205	0	86	128
361	206	207	0	87	128
362	208	210	0	88	128
363	211	212	0	89	128
364	213	214	0	90	128
365	215	217	0	91	128
366	218	219	0	92	128
367	220	222	0	93	128
368	223	224	0	94	128
369	225	226	0	95	128

Index	Ymax	Ymin	Xmax	Xmin	OG
370	227	229	0	96	128
371	230	231	0	97	128
372	232	234	0	98	128
373	235	236	0	99	128
374	237	239	0	100	128
375	240	241	0	101	128
376	242	243	0	102	128
377	244	246	0	103	128
378	247	248	0	104	128
379	249	251	0	105	128
380	252	253	0	106	128
381	254	-256	0	106	0
382	-255	-254	0	105	0
383	-253	-252	0	104	0
384	-251	-249	0	103	0
385	-248	-247	0	102	0
386	-246	-244	0	101	0
387	-243	-242	0	100	0
388	-241	-240	0	99	0
389	-239	-237	0	98	0
390	-236	-235	0	97	0
391	-234	-232	0	96	0
392	-231	-230	0	95	0
393	-229	-227	0	94	0
394	-226	-225	0	93	0
395	-224	-223	0	92	0
396	-222	-220	0	91	0
397	-219	-218	0	90	0
398	-217	-215	0	89	0
399	-214	-213	0	88	0
400	-212	-211	0	87	0
401	-210	-208	0	86	0
402	-207	-206	0	85	0
403	-205	-203	0	84	0
404	-202	-201	0	83	0
405	-200	-198	0	82	0
406	-197	-196	0	81	0
407	-195	-194	0	80	0
408	-193	-191	0	79	0
409	-190	-189	0	78	0
410	-188	-186	0	77	0
411	-185	-184	0	76	0
412	-183	-182	0	75	0

Index	Ymax	Ymin	Xmax	Xmin	OG
413	-181	-179	0	74	0
414	-178	-177	0	73	0
415	-176	-174	0	72	0
416	-173	-172	0	71	0
417	-171	-169	0	70	0
418	-168	-167	0	69	0
419	-166	-165	0	68	0
420	-164	-162	0	67	0
421	-161	-160	0	66	0
422	-159	-157	0	65	0
423	-156	-155	0	64	0
424	-154	-153	0	63	0
425	-152	-150	0	62	0
426	-149	-148	0	61	0
427	-147	-145	0	60	0
428	-144	-143	0	59	0
429	-142	-141	0	58	0
430	-140	-138	0	57	0
431	-137	-136	0	56	0
432	-135	-133	0	55	0
433	-132	-131	0	54	0
434	-130	-128	0	53	0
435	-127	-126	0	52	0
436	-125	-124	0	51	0
437	-123	-121	0	50	0
438	-120	-119	0	49	0
439	-118	-116	0	48	0
440	-115	-114	0	47	0
441	-113	-112	0	46	0
442	-111	-109	0	45	0
443	-108	-107	0	44	0
444	-106	-104	0	43	0
445	-103	-102	0	42	0
446	-101	-99	0	41	0
447	-98	-97	0	40	0
448	-96	-95	0	39	0
449	-94	-92	0	38	0
450	-91	-90	0	37	0
451	-89	-87	0	36	0
452	-86	-85	0	35	0
453	-84	-83	0	34	0
454	-82	-80	0	33	0
455	-79	-78	0	32	0

Index	Ymax	Ymin	Xmax	Xmin	OG
456	-77	-75	0	31	0
457	-74	-73	0	30	0
458	-72	-71	0	29	0
459	-70	-68	0	28	0
460	-67	-66	0	27	0
461	-65	-63	0	26	0
462	-62	-61	0	25	0
463	-60	-58	0	24	0
464	-57	-56	0	23	0
465	-55	-54	0	22	0
466	-53	-51	0	21	0
467	-50	-49	0	20	0
468	-48	-46	0	19	0
469	-45	-44	0	18	0
470	-43	-42	0	17	0
471	-41	-39	0	16	0
472	-38	-37	0	15	0
473	-36	-34	0	14	0
474	-33	-32	0	13	0
475	-31	-29	0	12	0
476	-28	-27	0	11	0
477	-26	-25	0	10	0
478	-24	-22	0	9	0
479	-21	-20	0	8	0
480	-19	-17	0	7	0
481	-16	-15	0	6	0
482	-14	-13	0	5	0
483	-12	-10	0	4	0
484	-9	-8	0	3	0
485	-7	-5	0	2	0
486	-4	-3	0	1	0
487	-2	-1	-255	1	0
488	0	2	-1	0	0
489	3	4	-2	0	0
490	5	7	-3	0	0
491	8	9	-4	0	0
492	10	12	-5	0	0
493	13	14	-6	0	0
494	15	16	-7	0	0
495	17	19	-8	0	0
496	20	21	-9	0	0
497	22	24	-10	0	0
498	25	26	-11	0	0

Index	Ymax	Ymin	Xmax	Xmin	OG
499	27	28	-12	0	0
500	29	31	-13	0	0
501	32	33	-14	0	0
502	34	36	-15	0	0
503	37	38	-16	0	0
504	39	41	-17	0	0
505	42	43	-18	0	0
506	44	45	-19	0	0
507	46	48	-20	0	0
508	49	50	-21	0	0
509	51	53	-22	0	0
510	54	55	-23	0	0
511	56	57	-24	0	0
512	58	60	-25	0	0
513	61	62	-26	0	0
514	63	65	-27	0	0
515	66	67	-28	0	0
516	68	70	-29	0	0
517	71	72	-30	0	0
518	73	74	-31	0	0
519	75	77	-32	0	0
520	78	79	-33	0	0
521	80	82	-34	0	0
522	83	84	-35	0	0
523	85	86	-36	0	0
524	87	89	-37	0	0
525	90	91	-38	0	0
526	92	94	-39	0	0
527	95	96	-40	0	0
528	97	98	-41	0	0
529	99	101	-42	0	0
530	102	103	-43	0	0
531	104	106	-44	0	0
532	107	108	-45	0	0
533	109	111	-46	0	0
534	112	113	-47	0	0
535	114	115	-48	0	0
536	116	118	-49	0	0
537	119	120	-50	0	0
538	121	123	-51	0	0
539	124	125	-52	0	0
540	126	127	-53	0	0
541	128	130	-54	0	0
542	131	132	-55	0	0
543	133	135	-56	0	0
544	136	137	-57	0	0
545	138	140	-58	0	0
546	141	142	-59	0	0
547	143	144	-60	0	0
548	145	147	-61	0	0
549	148	149	-62	0	0
550	150	152	-63	0	0
551	153	154	-64	0	0
552	155	156	-65	0	0
553	157	159	-66	0	0
554	160	161	-67	0	0
555	162	164	-68	0	0
556	165	166	-69	0	0
557	167	168	-70	0	0
558	169	171	-71	0	0
559	172	173	-72	0	0
560	174	176	-73	0	0
561	177	178	-74	0	0
562	179	181	-75	0	0
563	182	183	-76	0	0
564	184	185	-77	0	0
565	186	188	-78	0	0
566	189	190	-79	0	0
567	191	193	-80	0	0
568	194	195	-81	0	0
569	196	197	-82	0	0
570	198	200	-83	0	0
571	201	202	-84	0	0
572	203	205	-85	0	0
573	206	207	-86	0	0
574	208	210	-87	0	0
575	211	212	-88	0	0
576	213	214	-89	0	0
577	215	217	-90	0	0
578	218	219	-91	0	0
579	220	222	-92	0	0
580	223	224	-93	0	0
581	225	226	-94	0	0
582	227	229	-95	0	0
583	230	231	-96	0	0
584	232	234	-97	0	0

Index	Ymax	Ymin	Xmax	Xmin	OG
585	235	236	-98	0	0
586	237	239	-99	0	0
587	240	241	-100	0	0
588	242	243	-101	0	0
589	244	246	-102	0	0
590	247	248	-103	0	0
591	249	251	-104	0	0
592	252	253	-105	0	0
593	254	-256	106	0	32
594	-255	-254	105	0	32
595	-253	-252	104	0	32
596	-251	-249	103	0	32
597	-248	-247	102	0	32
598	-246	-244	101	0	32
599	-243	-242	100	0	32
600	-241	-240	99	0	32
601	-239	-237	98	0	32
602	-236	-235	97	0	32
603	-234	-232	96	0	32
604	-231	-230	95	0	32
605	-229	-227	94	0	32
606	-226	-225	93	0	32
607	-224	-223	92	0	32
608	-222	-220	91	0	32
609	-219	-218	90	0	32
610	-217	-215	89	0	32
611	-214	-213	88	0	32
612	-212	-211	87	0	32
613	-210	-208	86	0	32
614	-207	-206	85	0	32
615	-205	-203	84	0	32
616	-202	-201	83	0	32
617	-200	-198	82	0	32
618	-197	-196	81	0	32
619	-195	-194	80	0	32
620	-193	-191	79	0	32
621	-190	-189	78	0	32
622	-188	-186	77	0	32
623	-185	-184	76	0	32
624	-183	-182	75	0	32
625	-181	-179	74	0	32
626	-178	-177	73	0	32

Index	Ymax	Ymin	Xmax	Xmin	OG
627	-176	-174	72	0	32
628	-173	-172	71	0	32
629	-171	-169	70	0	32
630	-168	-167	69	0	32
631	-166	-165	68	0	32
632	-164	-162	67	0	32
633	-161	-160	66	0	32
634	-159	-157	65	0	32
635	-156	-155	64	0	32
636	-154	-153	63	0	32
637	-152	-150	62	0	32
638	-149	-148	61	0	32
639	-147	-145	60	0	32
640	-144	-143	59	0	32
641	-142	-141	58	0	32
642	-140	-138	57	0	32
643	-137	-136	56	0	32
644	-135	-133	55	0	32
645	-132	-131	54	0	32
646	-130	-128	53	0	32
647	-127	-126	52	0	32
648	-125	-124	51	0	32
649	-123	-121	50	0	32
650	-120	-119	49	0	32
651	-118	-116	48	0	32
652	-115	-114	47	0	32
653	-113	-112	46	0	32
654	-111	-109	45	0	32
655	-108	-107	44	0	32
656	-106	-106	44	254	32
657	-105	-105	44	252	32
658	-104	-104	43	249	32
659	-103	-103	43	247	32
660	-102	-102	42	244	32
661	-101	-101	42	242	32
662	-100	-100	42	240	32
663	-99	-99	41	237	32
664	-98	-98	41	235	32
665	-97	-97	40	232	32
666	-96	-96	40	230	32
667	-95	-95	39	227	32
668	-94	-94	39	225	32
669	-93	-93	39	223	32

Index	Ymax	Ymin	Xmax	Xmin	OG
670	-92	-92	38	220	32
671	-91	-91	38	218	32
672	-90	-90	37	215	32
673	-89	-89	37	213	32
674	-88	-88	37	211	32
675	-87	-87	36	208	32
676	-86	-86	36	206	32
677	-85	-85	35	203	32
678	-84	-84	35	201	32
679	-83	-83	34	198	32
680	-82	-82	34	196	32
681	-81	-81	34	194	32
682	-80	-80	33	191	32
683	-79	-79	33	189	32
684	-78	-78	32	186	32
685	-77	-77	32	184	32
686	-76	-76	32	182	32
687	-75	-75	31	179	32
688	-74	-74	31	177	32
689	-73	-73	30	174	32
690	-72	-72	30	172	32
691	-71	-71	29	169	32
692	-70	-70	29	167	32
693	-69	-69	29	165	32
694	-68	-68	28	162	32
695	-67	-67	28	160	32
696	-66	-66	27	157	32
697	-65	-65	27	155	32
698	-64	-64	27	153	32
699	-63	-63	26	150	32
700	-62	-62	26	148	32
701	-61	-61	25	145	32
702	-60	-60	25	143	32
703	-59	-59	25	141	32
704	-58	-58	24	138	32
705	-57	-57	24	136	32
706	-56	-56	23	133	32
707	-55	-55	23	131	32
708	-54	-54	22	128	32
709	-53	-53	22	126	32
710	-52	-52	22	124	32
711	-51	-51	21	121	32
712	-50	-50	21	119	32
713	-49	-49	20	116	32
714	-48	-48	20	114	32
715	-47	-47	20	112	32
716	-46	-46	19	109	32
717	-45	-45	19	107	32
718	-44	-44	18	104	32
719	-43	-43	18	102	32
720	-42	-42	17	99	32
721	-41	-41	17	97	32
722	-40	-40	17	95	32
723	-39	-39	16	92	32
724	-38	-38	16	90	32
725	-37	-37	15	87	32
726	-36	-36	15	85	32
727	-35	-35	15	83	32
728	-34	-34	14	80	32
729	-33	-33	14	78	32
730	-32	-32	13	75	32
731	-31	-31	13	73	32
732	-30	-30	13	71	32
733	-29	-29	12	68	32
734	-28	-28	12	66	32
735	-27	-27	11	63	32
736	-26	-26	11	61	32
737	-25	-25	10	58	32
738	-24	-24	10	56	32
739	-23	-23	10	54	32
740	-22	-22	9	51	32
741	-21	-21	9	49	32
742	-20	-20	8	46	32
743	-19	-19	8	44	32
744	-18	-18	8	42	32
745	-17	-17	7	39	32
746	-16	-16	7	37	32
747	-15	-15	6	34	32
748	-14	-14	6	32	32
749	-13	-13	5	29	32
750	-12	-12	5	27	32
751	-11	-11	5	25	32
752	-10	-10	4	22	32
753	-9	-9	4	20	32
754	-8	-8	3	17	32
755	-7	-7	3	15	32

Index	Ymax	Ymin	Xmax	Xmin	OG
756	-6	-6	3	13	32
757	-5	-5	2	10	32
758	-4	-4	2	8	32
759	-3	-3	1	5	32
760	-2	-2	1	3	32
761	-1	-1	-255	3	32
762	0	-256	-255	3	192
763	-255	-106	-255	-253	192
764	-105	-105	-255	-251	192
765	-104	-104	-255	-248	192
766	-103	-103	-255	-246	192
767	-102	-102	-255	-243	192
768	-101	-101	-255	-241	192
769	-100	-100	-255	-239	192
770	-99	-99	-255	-236	192
771	-98	-98	-255	-234	192
772	-97	-97	-255	-231	192
773	-96	-96	-255	-229	192
774	-95	-95	-255	-226	192
775	-94	-94	-255	-224	192
776	-93	-93	-255	-222	192
777	-92	-92	-255	-219	192
778	-91	-91	-255	-217	192
779	-90	-90	-255	-214	192
780	-89	-89	-255	-212	192
781	-88	-88	-255	-210	192
782	-87	-87	-255	-207	192
783	-86	-86	-255	-205	192
784	-85	-85	-255	-202	192
785	-84	-84	-255	-200	192
786	-83	-83	-255	-197	192
787	-82	-82	-255	-195	192
788	-81	-81	-255	-193	192
789	-80	-80	-255	-190	192
790	-79	-79	-255	-188	192
791	-78	-78	-255	-185	192
792	-77	-77	-255	-183	192
793	-76	-76	-255	-181	192
794	-75	-75	-255	-178	192
795	-74	-74	-255	-176	192
796	-73	-73	-255	-173	192
797	-72	-72	-255	-171	192
798	-71	-71	-255	-168	192

Index	Ymax	Ymin	Xmax	Xmin	OG
799	-70	-70	-255	-166	192
800	-69	-69	-255	-164	192
I801	-68	-68	-255	-161	192
802	-67	-67	-255	-159	192
803	-66	-66	-255	-156	192
804	-65	-65	-255	-154	192
805	-64	-64	-255	-152	192
806	-63	-63	-255	-149	192
807	-62	-62	-255	-147	192
808	-61	-61	-255	-144	192
809	-60	-60	-255	-142	192
810	-59	-59	-255	-140	192
811	-58	-58	-255	-137	192
812	-57	-57	-255	-135	192
813	-56	-56	-255	-132	192
814	-55	-55	-255	-130	192
815	-54	-54	-255	-127	192
816	-53	-53	-255	-125	192
817	-52	-52	-255	-123	192
818	-51	-51	-255	-120	192
819	-50	-50	-255	-118	192
820	-49	-49	-255	-115	192
821	-48	-48	-255	-113	192
822	-47	-47	-255	-111	192
823	-46	-46	-255	-108	192
824	-45	-45	-255	-106	192
825	-44	-44	-255	-103	192
826	-43	-43	-255	-101	192
827	-42	-42	-255	-98	192
828	-41	-41	-255	-96	192
829	-40	-40	-255	-94	192
830	-39	-39	-255	-91	192
831	-38	-38	-255	-89	192
832	-37	-37	-255	-86	192
833	-36	-36	-255	-84	192
834	-35	-35	-255	-82	192
835	-34	-34	-255	-79	192
836	-33	-33	-255	-77	192
837	-32	-32	-255	-74	192
838	-31	-31	-255	-72	192
839	-30	-30	-255	-70	192
840	-29	-29	-255	-67	192
841	-28	-28	-255	-65	192

Index	Ymax	Ymin	Xmax	Xmin	OG
842	-27	-27	-255	-62	192
843	-26	-26	-255	-60	192
844	-25	-25	-255	-57	192
845	-24	-24	-255	-55	192
846	-23	-23	-255	-53	192
847	-22	-22	-255	-50	192
848	-21	-21	-255	-48	192
849	-20	-20	-255	-45	192
850	-19	-19	-255	-43	192
851	-18	-18	-255	-41	192
852	-17	-17	-255	-38	192
853	-16	-16	-255	-36	192
854	-15	-15	-255	-33	192
855	-14	-14	-255	-31	192
856	-13	-13	-255	-28	192
857	-12	-12	-255	-26	192
858	-11	-11	-255	-24	192
859	-10	-10	-255	-21	192
860	-9	-9	-255	-19	192
861	-8	-8	-255	-16	192
862	-7	-7	-255	-14	192
863	-6	-6	-255	-12	192
864	-5	-5	-255	-9	192
865	-4	-4	-255	-7	192
866	-3	-3	-255	-4	192
867	-2	-2	-255	-2	192
868	-1	-1	-255	0	192
869	0	0	-255	-2	192
870	1	1	-255	-4	192
871	2	2	-255	-7	192
872	3	3	-255	-9	192
873	4	4	-255	-12	192
874	5	5	-255	-14	192
875	6	6	-255	-16	192
876	7	7	-255	-19	192
877	8	8	-255	-21	192
878	9	9	-255	-24	192
879	10	10	-255	-26	192
880	11	11	-255	-28	192
881	12	12	-255	-31	192
882	13	13	-255	-33	192
883	14	14	-255	-36	192
884	15	15	-255	-38	192

Index	Ymax	Ymin	Xmax	Xmin	OG
885	16	16	-255	-41	192
886	17	17	-255	-43	192
887	18	18	-255	-45	192
888	19	19	-255	-48	192
889	20	20	-255	-50	192
890	21	21	-255	-53	192
891	22	22	-255	-55	192
892	23	23	-255	-57	192
893	24	24	-255	-60	192
894	25	25	-255	-62	192
895	26	26	-255	-65	192
896	27	27	-255	-67	192
897	28	28	-255	-70	192
898	29	29	-255	-72	192
899	30	30	-255	-74	192
900	31	31	-255	-77	192
901	32	32	-255	-79	192
902	33	33	-255	-82	192
903	34	34	-255	-84	192
904	35	35	-255	-86	192
905	36	36	-255	-89	192
906	37	37	-255	-91	192
907	38	38	-255	-94	192
908	39	39	-255	-96	192
909	40	40	-255	-98	192
910	41	41	-255	-101	192
911	42	42	-255	-103	192
912	43	43	-255	-106	192
913	44	44	-255	-108	192
914	45	45	-255	-111	192
915	46	46	-255	-113	192
916	47	47	-255	-115	192
917	48	48	-255	-118	192
918	49	49	-255	-120	192
919	50	50	-255	-123	192
920	51	51	-255	-125	192
921	52	52	-255	-127	192
922	53	53	-255	-130	192
923	54	54	-255	-132	192
924	55	55	-255	-135	192
925	56	56	-255	-137	192
926	57	57	-255	-140	192
927	58	58	-255	-142	192

Index	Ymax	Ymin	Xmax	Xmin	OG
928	59	59	-255	-144	192
929	60	60	-255	-147	192
930	61	61	-255	-149	192
931	62	62	-255	-152	192
932	63	63	-255	-154	192
933	64	64	-255	-156	192
934	65	65	-255	-159	192
935	66	66	-255	-161	192
936	67	67	-255	-164	192
937	68	68	-255	-166	192
938	69	69	-255	-168	192
939	70	70	-255	-171	192
940	71	71	-255	-173	192
941	72	72	-255	-176	192
942	73	73	-255	-178	192
943	74	74	-255	-181	192
944	75	75	-255	-183	192
945	76	76	-255	-185	192
946	77	77	-255	-188	192
947	78	78	-255	-190	192
948	79	79	-255	-193	192
949	80	80	-255	-195	192
950	81	81	-255	-197	192
951	82	82	-255	-200	192
952	83	83	-255	-202	192
953	84	84	-255	-205	192
954	85	85	-255	-207	192
955	86	86	-255	-210	192
956	87	87	-255	-212	192
957	88	88	-255	-214	192
958	89	89	-255	-217	192
959	90	90	-255	-219	192
960	91	91	-255	-222	192
961	92	92	-255	-224	192
962	93	93	-255	-226	192
963	94	94	-255	-229	192
964	95	95	-255	-231	192
965	96	96	-255	-234	192
966	97	97	-255	-236	192
967	98	98	-255	-239	192
968	99	99	-255	-241	192
969	100	100	-255	-243	192
970	101	101	-255	-246	192

Index	Ymax	Ymin	Xmax	Xmin	OG
971	102	102	-255	-248	192
972	103	103	-255	-251	192
973	104	104	-255	-253	192
974	105	-256	-255	-253	64
975	-255	-106	254	-253	64
976	-255	-106	252	-253	64
977	-104	-104	249	-253	64
978	-103	-103	247	-253	64
979	-102	-102	244	-253	64
980	-101	-101	242	-253	64
981	-100	-100	240	-253	64
982	-99	-99	237	-253	64
983	-98	-98	235	-253	64
984	-97	-97	232	-253	64
985	-96	-96	230	-253	64
986	-95	-95	227	-253	64
987	-94	-94	225	-253	64
988	-93	-93	223	-253	64
989	-92	-92	220	-253	64
990	-91	-91	218	-253	64
991	-90	-90	215	-253	64
992	-89	-89	213	-253	64
993	-88	-88	211	-253	64
994	-87	-87	208	-253	64
995	-86	-86	206	-253	64
996	-85	-85	203	-253	64
997	-84	-84	201	-253	64
998	-83	-83	198	-253	64
999	-82	-82	196	-253	64
1000	-81	-81	194	-253	64
1001	-80	-80	191	-253	64
1002	-79	-79	189	-253	64
1003	-78	-78	186	-253	64
1004	-77	-77	184	-253	64
1005	-76	-76	182	-253	64
1006	-75	-75	179	-253	64
1007	-74	-74	177	-253	64
1008	-73	-73	174	-253	64
1009	-72	-72	172	-253	64
1010	-71	-71	169	-253	64
1011	-70	-70	167	-253	64
1012	-69	-69	165	-253	64
1013	-68	-68	162	-253	64

Index	Ymax	Ymin	Xmax	Xmin	OG
1014	-67	-67	160	-253	64
1015	-66	-66	157	-253	64
1016	-65	-65	155	-253	64
1017	-64	-64	153	-253	64
1018	-63	-63	150	-253	64
1019	-62	-62	148	-253	64
1020	-61	-61	145	-253	64
1021	-60	-60	143	-253	64
1022	-59	-59	141	-253	64
1023	-58	-58	138	-253	64
1024	-57	-57	136	-253	64
1025	-56	-56	133	-253	64
1026	-55	-55	131	-253	64
1027	-54	-54	128	-253	64
1028	-53	-53	126	-253	64
1029	-52	-52	124	-253	64
1030	-51	-51	121	-253	64
1031	-50	-50	119	-253	64
1032	-49	-49	116	-253	64
1033	-48	-48	114	-253	64
1034	-47	-47	112	-253	64
1035	-46	-46	109	-253	64
1036	-45	-45	107	-253	64
1037	-44	-44	104	-253	64
1038	-43	-43	102	-253	64
1039	-42	-42	99	-253	64
1040	-41	-41	97	-253	64
1041	-40	-40	95	-253	64
1042	-39	-39	92	-253	64
1043	-38	-38	90	-253	64
1044	-37	-37	87	-253	64
1045	-36	-36	85	-253	64
1046	-35	-35	83	-253	64
1047	-34	-34	80	-253	64
1048	-33	-33	78	-253	64
1049	-32	-32	75	-253	64
1050	-31	-31	73	-253	64
1051	-30	-30	71	-253	64
1052	-29	-29	68	-253	64
1053	-28	-28	66	-253	64
1054	-27	-27	63	-253	64
1055	-26	-26	61	-253	64
1056	-25	-25	58	-253	64

Index	Ymax	Ymin	Xmax	Xmin	OG
1057	-24	-24	56	-253	64
1058	-23	-23	54	-253	64
1059	-22	-22	51	-253	64
1060	-21	-21	49	-253	64
1061	-20	-20	46	-253	64
1062	-19	-19	44	-253	64
1063	-18	-18	42	-253	64
1064	-17	-17	39	-253	64
1065	-16	-16	37	-253	64
1066	-15	-15	34	-253	64
1067	-14	-14	32	-253	64
1068	-13	-13	29	-253	64
1069	-12	-12	27	-253	64
1070	-11	-11	25	-253	64
1071	-10	-10	22	-253	64
1072	-9	-9	20	-253	64
1073	-8	-8	17	-253	64
1074	-7	-7	15	-253	64
1075	-6	-6	13	-253	64
1076	-5	-5	10	-253	64
1077	-4	-4	8	-253	64
1078	-3	-3	5	-253	64
1079	-2	-2	3	-253	64
1080	-1	-1	1	-253	64
1081	0	0	3	-253	64
1082	1	1	5	-253	64
1083	2	2	8	-253	64
1084	3	3	10	-253	64
1085	4	4	13	-253	64
1086	5	5	15	-253	64
1087	6	6	17	-253	64
1088	7	7	20	-253	64
1089	8	8	22	-253	64
1090	9	9	25	-253	64
1091	10	10	27	-253	64
1092	11	11	29	-253	64
1093	12	12	32	-253	64
1094	13	13	34	-253	64
1095	14	14	37	-253	64
1096	15	15	39	-253	64
1097	16	16	42	-253	64
1098	17	17	44	-253	64
1099	18	18	46	-253	64

Index	Ymax	Ymin	Xmax	Xmin	OG
1100	19	19	49	-253	64
1101	20	20	51	-253	64
1102	21	21	54	-253	64
1103	22	22	56	-253	64
1104	23	23	58	-253	64
1105	24	24	61	-253	64
1106	25	25	63	-253	64
1107	26	26	66	-253	64
1108	27	27	68	-253	64
1109	28	28	71	-253	64
1110	29	29	73	-253	64
1111	30	30	75	-253	64
1112	31	31	78	-253	64
1113	32	32	80	-253	64
1114	33	33	83	-253	64
1115	34	34	85	-253	64
1116	35	35	87	-253	64
1117	36	36	90	-253	64
1118	37	37	92	-253	64
1119	38	38	95	-253	64
1120	39	39	97	-253	64
1121	40	40	99	-253	64
1122	41	41	102	-253	64
1123	42	42	104	-253	64
1124	43	43	107	-253	64
1125	44	44	109	-253	64
1126	45	45	112	-253	64
1127	46	46	114	-253	64
1128	47	47	116	-253	64
1129	48	48	119	-253	64
1130	49	49	121	-253	64
1131	50	50	124	-253	64
1132	51	51	126	-253	64
1133	52	52	128	-253	64
1134	53	53	131	-253	64
1135	54	54	133	-253	64
1136	55	55	136	-253	64
1137	56	56	138	-253	64
1138	57	57	141	-253	64
1139	58	58	143	-253	64
1140	59	59	145	-253	64
1141	60	60	148	-253	64
1142	61	61	150	-253	64

Index	Ymax	Ymin	Xmax	Xmin	OG
1143	62	62	153	-253	64
1144	63	63	155	-253	64
1145	64	64	157	-253	64
1146	65	65	160	-253	64
1147	66	66	162	-253	64
1148	67	67	165	-253	64
1149	68	68	167	-253	64
1150	69	69	169	-253	64
1151	70	70	172	-253	64
1152	71	71	174	-253	64
1153	72	72	177	-253	64
1154	73	73	179	-253	64
1155	74	74	182	-253	64
1156	75	75	184	-253	64
1157	76	76	186	-253	64
1158	77	77	189	-253	64
1159	78	78	191	-253	64
1160	79	79	194	-253	64
1161	80	80	196	-253	64
1162	81	81	198	-253	64
1163	82	82	201	-253	64
1164	83	83	203	-253	64
1165	84	84	206	-253	64
1166	85	85	208	-253	64
1167	86	86	211	-253	64
1168	87	87	213	-253	64
1169	88	88	215	-253	64
1170	89	89	218	-253	64
1171	90	90	220	-253	64
1172	91	91	223	-253	64
1173	92	92	225	-253	64
1174	93	93	227	-253	64
1175	94	94	230	-253	64
1176	95	95	232	-253	64
1177	96	96	235	-253	64
1178	97	97	237	-253	64
1179	98	98	240	-253	64
1180	99	99	242	-253	64
1181	100	100	244	-253	64
1182	101	101	247	-253	64
1183	102	102	249	-253	64
1184	103	103	252	-253	64
1185	104	104	254	-253	64

Index	Ymax	Ymin	Xmax	Xmin	OG
1186	105	105	-255	-253	64
1187	106	-256	-255	-253	255
1188	-255	-1	0	1	255
1189	0	0	-255	1	255
1190	1	-256	-255	1	224
1191	-255	0	-2	0	224
1192	1	1	-4	0	224
1193	2	2	-7	-1	224
1194	3	3	-9	-1	224
1195	4	4	-12	-2	224
1196	5	5	-14	-2	224
1197	6	6	-16	-2	224
1198	7	7	-19	-3	224
1199	8	8	-21	-3	224
1200	9	9	-24	-4	224
1201	10	10	-26	-4	224
1202	11	11	-28	-4	224
1203	12	12	-31	-5	224
1204	13	13	-33	-5	224
1205	14	14	-36	-6	224
1206	15	15	-38	-6	224
1207	16	16	-41	-7	224
1208	17	17	-43	-7	224
1209	18	18	-45	-7	224
1210	19	19	-48	-8	224
1211	20	20	-50	-8	224
1212	21	21	-53	-9	224
1213	22	22	-55	-9	224
1214	23	23	-57	-9	224
1215	24	24	-60	-10	224
1216	25	25	-62	-10	224
1217	26	26	-65	-11	224
1218	27	27	-67	-11	224
1219	28	28	-70	-12	224
1220	29	29	-72	-12	224
1221	30	30	-74	-12	224
1222	31	31	-77	-13	224
1223	32	32	-79	-13	224
1224	33	33	-82	-14	224
1225	34	34	-84	-14	224
1226	35	35	-86	-14	224
1227	36	36	-89	-15	224
1228	37	37	-91	-15	224
1229	38	38	-94	-16	224
1230	39	39	-96	-16	224
1231	40	40	-98	-16	224
1232	41	41	-101	-17	224
1233	42	42	-103	-17	224
1234	43	43	-106	-18	224
1235	44	44	-108	-18	224
1236	45	45	-111	-19	224
1237	46	46	-113	-19	224
1238	47	47	-115	-19	224
1239	48	48	-118	-20	224
1240	49	49	-120	-20	224
1241	50	50	-123	-21	224
1242	51	51	-125	-21	224
1243	52	52	-127	-21	224
1244	53	53	-130	-22	224
1245	54	54	-132	-22	224
1246	55	55	-135	-23	224
1247	56	56	-137	-23	224
1248	57	57	-140	-24	224
1249	58	58	-142	-24	224
1250	59	59	-144	-24	224
1251	60	60	-147	-25	224
1252	61	61	-149	-25	224
1253	62	62	-152	-26	224
1254	63	63	-154	-26	224
1255	64	64	-156	-26	224
1256	65	65	-159	-27	224
1257	66	66	-161	-27	224
1258	67	67	-164	-28	224
1259	68	68	-166	-28	224
1260	69	69	-168	-28	224
1261	70	70	-171	-29	224
1262	71	71	-173	-29	224
1263	72	72	-176	-30	224
1264	73	73	-178	-30	224
1265	74	74	-181	-31	224
1266	75	75	-183	-31	224
1267	76	76	-185	-31	224
1268	77	77	-188	-32	224
1269	78	78	-190	-32	224
1270	79	79	-193	-33	224
1271	80	80	-195	-33	224

Index	Ymax	Ymin	Xmax	Xmin	OG
1272	81	81	-197	-33	224
1273	82	82	-200	-34	224
1274	83	83	-202	-34	224
1275	84	84	-205	-35	224
1276	85	85	-207	-35	224
1277	86	86	-210	-36	224
1278	87	87	-212	-36	224
1279	88	88	-214	-36	224
1280	89	89	-217	-37	224
1281	90	90	-219	-37	224
1282	91	91	-222	-38	224
1283	92	92	-224	-38	224
1284	93	93	-226	-38	224
1285	94	94	-229	-39	224
1286	95	95	-231	-39	224
1287	96	96	-234	-40	224
1288	97	97	-236	-40	224
1289	98	98	-239	-41	224
1290	99	99	-241	-41	224
1291	100	100	-243	-41	224
1292	101	101	-246	-42	224
1293	102	102	-248	-42	224
1294	103	103	-251	-43	224
1295	104	104	-253	-43	224
1296	105	105	-255	-43	224
1297	106	106	-255	-44	224
1298	107	108	-255	-45	224
1299	109	111	-255	-46	224
1300	112	113	-255	-47	224
1301	114	115	-255	-48	224
1302	116	118	-255	-49	224
1303	119	120	-255	-50	224
1304	121	123	-255	-51	224
1305	124	125	-255	-52	224
1306	126	127	-255	-53	224
1307	128	130	-255	-54	224
1308	131	132	-255	-55	224
1309	133	135	-255	-56	224
1310	136	137	-255	-57	224
1311	138	140	-255	-58	224
1312	141	142	-255	-59	224
1313	143	144	-255	-60	224
1314	145	147	-255	-61	224
1315	148	149	-255	-62	224
1316	150	152	-255	-63	224
1317	153	154	-255	-64	224
1318	155	156	-255	-65	224
1319	157	159	-255	-66	224
1320	160	161	-255	-67	224
1321	162	164	-255	-68	224
1322	165	166	-255	-69	224
1323	167	168	-255	-70	224
1324	169	171	-255	-71	224
1325	172	173	-255	-72	224
1326	174	176	-255	-73	224
1327	177	178	-255	-74	224
1328	179	181	-255	-75	224
1329	182	183	-255	-76	224
1330	184	185	-255	-77	224
1331	186	188	-255	-78	224
1332	189	190	-255	-79	224
1333	191	193	-255	-80	224
1334	194	195	-255	-81	224
1335	196	197	-255	-82	224
1336	198	200	-255	-83	224
1337	201	202	-255	-84	224
1338	203	205	-255	-85	224
1339	206	207	-255	-86	224
1340	208	210	-255	-87	224
1341	211	212	-255	-88	224
1342	213	214	-255	-89	224
1343	215	217	-255	-90	224
1344	218	219	-255	-91	224
1345	220	222	-255	-92	224
1346	223	224	-255	-93	224
1347	225	226	-255	-94	224
1348	227	229	-255	-95	224
1349	230	231	-255	-96	224
1350	232	234	-255	-97	224
1351	235	236	-255	-98	224
1352	237	239	-255	-99	224
1353	240	241	-255	-100	224
1354	242	243	-255	-101	224
1355	244	246	-255	-102	224
1356	247	248	-255	-103	224
1357	249	251	-255	-104	224

Index	Ymax	Ymin	Xmax	Xmin	OG
1358	252	253	-255	-105	224
1359	254	-256	-255	-105	96
1360	-255	0	1	3	96
1361	1	1	1	5	96
1362	2	2	2	8	96
1363	3	3	2	10	96
1364	4	4	3	13	96
1365	5	5	3	15	96
1366	6	6	3	17	96
1367	7	7	4	20	96
1368	8	8	4	22	96
1369	9	9	5	25	96
1370	10	10	5	27	96
1371	11	11	5	29	96
1372	12	12	6	32	96
1373	13	13	6	34	96
1374	14	14	7	37	96
1375	15	15	7	39	96
1376	16	16	8	42	96
1377	17	17	8	44	96
1378	18	18	8	46	96
1379	19	19	9	49	96
1380	20	20	9	51	96
1381	21	21	10	54	96
1382	22	22	10	56	96
1383	23	23	10	58	96
1384	24	24	11	61	96
1385	25	25	11	63	96
1386	26	26	12	66	96
1387	27	27	12	68	96
1388	28	28	13	71	96
1389	29	29	13	73	96
1390	30	30	13	75	96
1391	31	31	14	78	96
1392	32	32	14	80	96
1393	33	33	15	83	96
1394	34	34	15	85	96
1395	35	35	15	87	96
1396	36	36	16	90	96
1397	37	37	16	92	96
1398	38	38	17	95	96
1399	39	39	17	97	96
1400	40	40	17	99	96

Index	Ymax	Ymin	Xmax	Xmin	OG
1401	41	41	18	102	96
1402	42	42	18	104	96
1403	43	43	19	107	96
1404	44	44	19	109	96
1405	45	45	20	112	96
1406	46	46	20	114	96
1407	47	47	20	116	96
1408	48	48	21	119	96
1409	49	49	21	121	96
1410	50	50	22	124	96
1411	51	51	22	126	96
1412	52	52	22	128	96
1413	53	53	23	131	96
1414	54	54	23	133	96
1415	55	55	24	136	96
1416	56	56	24	138	96
1417	57	57	25	141	96
1418	58	58	25	143	96
1419	59	59	25	145	96
1420	60	60	26	148	96
1421	61	61	26	150	96
1422	62	62	27	153	96
1423	63	63	27	155	96
1424	64	64	27	157	96
1425	65	65	28	160	96
1426	66	66	28	162	96
1427	67	67	29	165	96
1428	68	68	29	167	96
1429	69	69	29	169	96
1430	70	70	30	172	96
1431	71	71	30	174	96
1432	72	72	31	177	96
1433	73	73	31	179	96
1434	74	74	32	182	96
1435	75	75	32	184	96
1436	76	76	32	186	96
1437	77	77	33	189	96
1438	78	78	33	191	96
1439	79	79	34	194	96
1440	80	80	34	196	96
1441	81	81	34	198	96
1442	82	82	35	201	96
1443	83	83	35	203	96

Index	Ymax	Ymin	Xmax	Xmin	OG
1444	84	84	36	206	96
1445	85	85	36	208	96
1446	86	86	37	211	96
1447	87	87	37	213	96
1448	88	88	37	215	96
1449	89	89	38	218	96
1450	90	90	38	220	96
1451	91	91	39	223	96
1452	92	92	39	225	96
1453	93	93	39	227	96
1454	94	94	40	230	96
1455	95	95	40	232	96
1456	96	96	41	235	96
1457	97	97	41	237	96
1458	98	98	42	240	96
1459	99	99	42	242	96
1460	100	100	42	244	96
1461	101	101	43	247	96
1462	102	102	43	249	96
1463	103	103	44	252	96
1464	104	104	44	254	96
1465	105	106	45	254	96
1466	107	108	46	254	96
1467	109	111	47	254	96
1468	112	113	48	254	96
1469	114	115	49	254	96
1470	116	118	50	254	96
1471	119	120	51	254	96
1472	121	123	52	254	96
1473	124	125	53	254	96
1474	126	127	54	254	96
1475	128	130	55	254	96
1476	131	132	56	254	96
1477	133	135	57	254	96
1478	136	137	58	254	96
1479	138	140	59	254	96
1480	141	142	60	254	96
1481	143	144	61	254	96
1482	145	147	62	254	96
1483	148	149	63	254	96
1484	150	152	64	254	96
1485	153	154	65	254	96
1486	155	156	66	254	96
1487	157	159	67	254	96
1488	160	161	68	254	96
1489	162	164	69	254	96
1490	165	166	70	254	96
1491	167	168	71	254	96
1492	169	171	72	254	96
1493	172	173	73	254	96
1494	174	176	74	254	96
1495	177	178	75	254	96
1496	179	181	76	254	96
1497	182	183	77	254	96
1498	184	185	78	254	96
1499	186	188	79	254	96
1500	189	190	80	254	96
1501	191	193	81	254	96
1502	194	195	82	254	96
1503	196	197	83	254	96
1504	198	200	84	254	96
1505	201	202	85	254	96
1506	203	205	86	254	96
1507	206	207	87	254	96
1508	208	210	88	254	96
1509	211	212	89	254	96
1510	213	214	90	254	96
1511	215	217	91	254	96
1512	218	219	92	254	96
1513	220	222	93	254	96
1514	223	224	94	254	96
1515	225	226	95	254	96
1516	227	229	96	254	96
1517	230	231	97	254	96
1518	232	234	98	254	96
1519	235	236	99	254	96
1520	237	239	100	254	96
1521	240	241	101	254	96
1522	242	243	102	254	96
1523	244	246	103	254	96
1524	247	248	104	254	96
1525	249	251	105	254	96
1526	252	253	106	254	96

REFERENCE

[And 87] Anderson, H.L., R. Bajcsy and M. Mintz, "A Modular Feedback System for Image Segmentation", Univ. Pennsylvania GRASP Lab., Tech. Rep. 110, 1987.

[Ani 90] Anil, K. J. and G.N. Sateesha, "MRF Model-Based Segmentation of Range Image", Proc. IEEE International Conf. on Computer Vision, 1990.

[Arn 87] Arnulfo, P. and R.C. Gonzalez, "An Iterative Thresholding Algorithm for Image Segmentation", IEEE Trans. Pattern Analysis and Machine Intelligence, vol. PAMI-9, no. 6, pp 742-751, 1987.

[Ber 87] Bertero, M., T. Poggio and V. Torre, "Ill-posed Problems in Early Vision," Tech. report, MIT AI Lab., AI Memo 924, 1987.

[Bev 89] Beveridge, I., J. Griffith, R. Kohler, A.R. Hanson and E.M. Riseman, "Segmenting Images Using Localized Histograms and Region Merging", International Journal of Computer Vision, vol. 2, pp 311-347, 1989.

[Bha 91] Bhanu, Bir, J. Ming and S. Lee, "Closed-Loop Adaptive Image Segmentation", IEEE Int. Conf. on Computer Vision and Pattern Recognition, pp 734-735, 1991.

[Bla 87] Blake, A. and A. Zisserman, "Visual Reconstruction", Cambridge, MA: MIT Press, 1987.

[Can 83] Canny, F.R., "Finding Edges and Lines in Images", Cambridge MA, Tech. Report 720, MIT AI Lab., June 1983.

[Che 87] Chen, J.S. and G. Medioni, " Estimation and Accurate Location of Edges", Institute for Robotics and Intelligenct Systems, Dept. of Electrical Engineering and Computer Science, University of Southern California, Los Angeles, CA, 1987.

[Cho 72.] Chow, C.K. and T.Kaneko, "Automatic Boundary Detection of the Left Vetricle from Cineangiograms", Comp. and Biomed. Res., vol. 5, pp 338-410, 1972.

[Dai 89] Daily, M. J., "Color Image Segmentation Using Markov Random Field," Proc. IEEE ICASSP, vol. 4, pp 304-312, 1989.

[Der 87] Derin, H., "Modeling and Segmentation of Noisy and Textured Image Using Gibbs Random Field", IEEE Trans. Pattern Analysis and Machine Intelligence, vol PAMI-9, no. 1 pp 39-55 Jan. 1987.

[Dud 73] Duda, R.O. and P.E. Hart, "Pattern Classification and Sense Analysis", New York, Wiley, 1973.

[Fre 77] Frei, W. and C.C. Chen, "Fast Boundary Detection: A Generalization and a New Algorithm", IEEE Trans. Computers, vol. C-26, no. 10, pp. 988-998, 1977.

[Fri 91] Friedman, R. J., D. S. Riegel, M. K. Silverman, A. W. Kopf, and K. A. Vosseart, "Malignant Melanoma in the 1990s: The Continued Importance of Early Detection and the Role of Physician Examination and Self Examination of the Skin", Ca--A Cancer Journal for Clinicians, vol. 41, no. 4, 1991.

[Fua 89] Fua, P. and A.J. Hanson, "Objective Functions for Feature Discrimination: Applications to Semiautomated and Automated Feature Extraction", Menlo Park, CA, Artificial Intelligence Center, SRI International, 1989.

[Gei 90] Geiger, D. and F. Girosi, "Mean Field Theory for Surface Reconstruction", Cambridge MA, MIT Press, AI Lab., 1990

[Gon 87] Gonzalez, R.C. and P. Wintz, " Digital Image Processing ", Reading, MA, Addison-Wesley, 1987.

[Gri 85] Grimson, W.E.L. and T. Pavlidis, "Discontinuity Detection for Visual Surface Reconstruction", Computer, Vision, Graphics, Image Processing, vol. 30 pp 316-330, 1985.

[Han 91] Hancock, E.R., "Adaptive Estimation of Hysteresis Thresholds", IEEE Int. Conf. on Computer Vision and Pattern Recognition, pp 196-201, 1991.

[Hor 74] Horowitz, S.L. and T. Pavlidis, "Picture Segmentation by a Direct Split and Merge Procedure", Proc. 2nd Int. Conf. on Pattern Recognition, pp 424-433, 1974.

[Hua 87] Huang, K., D. Lee, T. Pavlidis, "Edge Detection Through Two-Dimensional Regularization," Proc. IEEE ICASSP, vol. 7, pp 225-227, 1987.

[Jai 90] Jain, A.K. and S.G. Nadabar, "MRF Model-Based Segmentation of Range Image", IEEE, Int. Conf. on Computer Vision, pp 667-671, 1990.

[Kli 88] Klinger, J.W., C.L. Vaughan, T.D. Franker and L.T. Andrews, "Segmentation of Echocardiographic Images Using Mathematical Morphology", IEEE Trans. Biomedical Engineering, vol. 35, pp 925-934, 1988.

[Koh 88] Kohl, C.A., A.R. Hanson and E.M. Riseman, "Goal-Directed Control of Low-Level Processing for Image Interpretation", Dept. of Computer and Information Science, University of Massachusetts, Amherst, MA, 1988.

[Kol 91] Kolles, H. and K. Rememberger, "How to Build a Computer-Assisted Diagnosis Finding system", Arch. Pathol. Lab. Med-vol 115, 1991.

[Kun 89] Kundu, A., "Robust Edge Detection", IEEE Int. Conf. on Computer Vision and Pattern Recognition, pp 11-18, 1989.

[Lee 88] Lee, David, " Edge Detection through Residual Analysis", Int. Conf. CH2605-4, pp 215-222, 1988.

[Lee 91a] Lee, David, "Discontinuity Detection and Thresholding---A Stochastic Approach", Proc. IEEE International Conf. on Computer Vision, pp 208-214,1991.

[Lee 91b] Lee, David, "Residual Analysis for Feature Detection", IEEE Trans. Pattern Analysis and Machine Intelligence, vol. 13, no. 1 pp 30-40, 1991.

[Lev 85] Levine, M.D., "Dynamic Measurement of Computer Generated Image Segmentation", IEEE, Trans. Pattern Analysis and Machine Intelligence, vol. PAMI-7, no. 2, pp 155-164, 1985.

[Li 90] Li, S.Z., "Reconstruction Without Discontinuities", Proc. IEEE ICASSP, vol. 8 pp 709-712, 1990.

[Mar 80] Marr, D.C. and E.C. Hildreth, "Theory of Edge Detection", Proceedings of the Royal Society of London, B207, pp 187-217, 1980.

[Mic 89] Michael, D.J. and A.C. Nelson, "A Model-Based System for Automatic Segmentation of Bones from Digital Hand Radiographs", IEEE, Trans. Medical Imaging, vol. 8, no. 1, pp 64-69, 1989.

[Mor 89] Morris, D.T. and A. Narendra-Nathan, "A Rule-Based System for Dimensional Analysis of Glass Containers", Image and Vision Computing, vol. 7, no. 4, pp 274-280, 1989.

[Mur 87] Murray, D.W. and B.F. Buxton, "Scene Segmentation from Visial Motion Using Global Optimization", IEEE Trans. Pattern Analysis and Machine Intelligence, vol. PAMI-9, no. 2, pp 220-228, 1987.

[Nob 88] Noble, J.A., "Morphological Feature Detection", IEEE Int. Conf. on Computer Vision, pp 112-116, 1988.

[Nun 87] Nuncan, J.S., "Knowledge Directed Left Ventricular Boundary Detection in Equilibrium Radionuclide Angiocardiography", IEEE Trans. Medical Imaging, vol. MI-6, no. 4, pp 325-336, 1987.

[Per 87] Perez, Arnulfo, "An Iterative Thresholding Algorithm for Image Segmentation", IEEE, Trans. Pattern Analysis and Machine Intelligence, vol. PAMI-9, no. 6 1987.

[Pog 85] Poggio, T., V. Torre and C. Koch, "Computational Vision and Regularization Theory", Nature, vol. 317, pp 314-319, 1985.

[Pre 70] Prewitt, J.M.S., Object Enhancement and Extraction, in "Picture Processing and Psychopictorics", B.S. Lipkin and A. Rosenfeld, eds., New York, Academic Press, 1970.

[Ram 91] Raman, S.V., "Tissue Boundary Refinement in Magnetic Resonance Images Using Contour-Based Scale Matching", IEEE Trans. on Medical Imaging, vol. 10, no. 2, 1991.

[Ray 91] Raya, S.P., "Low-Level Segmentation of 3-D Magnetic Resonance Brain Images -- A Rule-Based System", IEEE Trans. Medical Imaging, vol. 9 no. 3, pp 327-337, 1991.

[Rei 67] Reinsch, C.H., "Smoothing by Spline Functions", Numer. Math., vol. 10, pp 177-183, 1967.

[Rob 65] Roberts, L.G. and J.T. Tippet, Machine Perception of Three-Dimensional Solids, in "Optical and Electro-Optical Information Processing", Cambridge, MA, MIT Press, 1965.

[Sal 91] Salembier, P., "Multiresolution Decomposition and Adaptive Filtering with Rank Order Based filters: Application to Detect Defection", IEEE, Int. Conf. on , pp 2389-2392, 1991.

[Sch 91] Schmitt, F. and X. Chen, "Fast Segmentation of Range Image into Planar Regions", IEEE Int. Conf. on Computer Vision and Pattern Recognition, pp 710-711, 1991.

[Sch 64] Schoenberg, I.J., "Spline Functions and the Problem of Graduation", Proc. Nat. Acad. Sci., vol. 52, pp 947-950, 1964.

[Ser 82] Serra, J., "Image Analysis and Mathematical Morphology", London, Academic Press Inc., 1982.

[Sha 93] Shao, S, J. Staudhammer and R. R. Grams, "Pixel-Feature-Controlling Edge Detection Based on Regularization (PEDBOR)" Proc. IEEE, SSST, 1993.

[Sim 88] Simchony, T., R.C. Chellappa and Z. Lichtenstein, "Pyramid Implementation of Optimal Step Conjugation Search Algorithm for Some Computer Vision Problem", Proc. IEEE Int. Conf. on Computer Vision, pp 580-590, 1988.

[Ste 86] Sternberg, S.R., "Grayscale Morphology", Computer Vision, Graphics and Image Processing, vol 35, pp 333-355, 1986.

[Suk 84] Suk, M and S. Hong, "An Edge Extraction Technique for Noise Image", London, Academic Press Inc., 1984.

[Tan 92] Tan, H.L., S.B. Gelfand and E.J. Delp, "A Cost Minimization Approach to Edge Detection Using Simulated Annealing", IEEE Trans. Pattern Analysis and Machine Intelligence, vol. 14 no. 1, pp 3-18, 1992.

[Ter 86] Terzopoulos, D., "Regularization of Inverse Problems Involving Discontinuities," IEEE Trans. Pattern Analysis and Machine Intell., vol. PAMI-8, pp 129-139, 1986.

[Tho 91] Thomas, J.G. and R.A. Peters II, "Automatic Segmentation of Ultrasound Image Using Morphological Operators", IEEE Trans. Medical Imaging, vol. 10, pp 180-186, June, 1991.

[Tik 77] Tikhonov, A.N. and V.A., Arsenin, "Solution of Ill-Posed Problems", Washington, D.C., Winston & Sons, 1977.

[Tor 86] Torre, V. and T.A. Poggio, "On Edge Detection", IEEE, Trans. Pattern Analysis and Machine Intelligence, vol. PAMI-8, no. 2, pp 147-163, 1986.

[Tou 77] Tou, J.T., "Pattern Recognition Principles", Reading, MA, Addison-Wesley Pub. Co., 1977.

[Tuc 91] Tuceryan, M. and A.T. Deborah, "Segmentation and Grouping of Object Boundaries Using Energy Minimization", IEEE Int. Conf. on Computer Vision and Pattern Recognition, pp 730-731, 1991.

[Wan 88] Wan, S.J., S. K. M. Wong and P. Prusinkiewicz, "An Algorithm for Multidimensional Data Clustering", ACM Trans. on Mathematical Software, vol. 14, no. 2, 1988.

[Wan 91] Wang, Y. and Sanjit K. Mitra, "Edge Detection Based On Orientation Distribution Of Gradient Image," Proc. IEEE ICASSP, vol. 7, pp 2569-2571, 1991.

[Wri 89] Wright, W.A. "A Markov Random Field Approach to Data Fusion and Color Image Segmentation", Image and Vision Computer, vol. 7, pp 144-149, 1989.

[Yu 91] Yu, X. and Y. Juha, "A New Algorithm for Image segmentation Based on Region Growing and Edge Detection", IEEE, Int. Conf. ICASSP, pp 156-519, 1991.

BIOGRAPHICAL SKETCH

Suyi Shao was born in Nanjing, People's Republic of China (P. R. C.), on June 24, 1957. She received a B.S. degree in electrical engineering from Nanjing Institute of Posts and Telecommunications, Nanjing, P. R. C. in 1982. She then served in the same university as assistant teacher and lecturer for eight years. In 1989, she came to Gainesville as a visiting scholar at the Center for Information Research, University of Florida. She started her graduate study for a master's degree in electrical engineering at University of Florida in May 1990 and received her M.S. degree in April 1992. Then she started her Ph.D. study at the same department in May 1992. Her current Ph.D. work is in the area of image processing, particularly in low-level image processing.

I certify that I have read this study and that in my opinion it conforms to acceptable standards of scholarly presentation and is fully adequate, in scope and quality, as a dissertation for the degree of Doctor of Philosophy.

John Staudhammer, Chairman
Professor of Electrical Engineering

I certify that I have read this study and that in my opinion it conforms to acceptable standards of scholarly presentation and is fully adequate, in scope and quality, as a dissertation for the degree of Doctor of Philosophy.

Stanley Y. Su
Professor of Electrical Engineering

I certify that I have read this study and that in my opinion it conforms to acceptable standards of scholarly presentation and is fully adequate, in scope and quality, as a dissertation for the degree of Doctor of Philosophy.

A. Antonio Arroyo
Associate Professor of Electrical Engineering

I certify that I have read this study and that in my opinion it conforms to acceptable standards of scholarly presentation and is fully adequate, in scope and quality, as a dissertation for the degree of Doctor of Philosophy.

Fazil T. Najafi
Associate Professor of Civil Engineering

I certify that I have read this study and that in my opinion it conforms to acceptable standards of scholarly presentation and is fully adequate, in scope and quality, as a dissertation for the degree of Doctor of Philosophy.

Ralph R. Grams
Professor of Pathology and Laboratory Medicine

This dissertation was submitted to the Graduate Faculty of the College of Engineering and to the Graduate School and was accepted as partial fulfillment of the requirements for the degree of Doctor of Philosophy.

April 1994

for Winfred M. Phillips
Dean, College of Engineering

Karen A. Holbrook
Dean, Graduate School